Error Correction and Opportunistic Scheduling Protocols in Random Wireless Networks

A THESIS
SUBMITTED TO THE FACULTY OF THE GRADUATE SCHOOL
OF THE UNIVERSITY OF MINNESOTA
BY

Amogh Rajanna

IN PARTIAL FULFILLMENT OF THE REQUIREMENTS
FOR THE DEGREE OF
DOCTOR OF PHILOSOPHY

Professor Mos Kaveh, Advisor

December, 2014

Acknowledgements

My time in graduate school at University of Minnesota have been the most memorable years of my life to date. Many people have earned my gratitude for their contribution to my graduate studies.

First and foremost, i would like to thank Prof Mos Kaveh for taking me under his wings as a PhD student. His support and encouragement during the course of my PhD research was a key ingredient for the successful completion of the thesis. Whenever the research pace slowed down because of my health issues, Prof Kaveh was very patient and tolerant. For this one aspect, i submit my deep gratitude to him.

I had the wonderful opportunity of working with Prof Itsik Bergel from Bar Ilan University, Israel during the last phase of my PhD research. He helped me fine tune my theoretical skills and improve my research presentation skills. His research expertise on information theoretic aspects of wireless communication is commendable. Hopefully i get more of these excellent collaborations in the subsequent chapters of my research career.

Dr Nihar Jindal (now with Google) was my first research supervisor at University of Minnesota. I thank him for patiently teaching me how to do research. His emphasis on clarity of system model, concepts and the research insights and take away messages have well shaped my research experience to date. His kind and timely help with my visa issues back in the $2010-11$ academic year helped me navigate through difficult circumstances in graduate school without getting into any trouble.

I thank Prof Soheil Mohager for proof reading the PhD thesis, making helpful comments and pointing out errors at the right places. I truly appreciate his time and energy to help me structure the thesis into a more readable and accessible form.

I sincerely acknowledge the efforts of Prof Georgios Giannakis and Prof Bill Cooper to serve on my PhD exam committee. I enjoyed being a student in their courses here at University of Minnesota. I am greatly indebted to the help offered by Prof Bill Robbins and Prof Keshab Parhi in regards to the administrative tasks of being a student in the Electrical Engineering Dept.

A word of thanks is necessary for Prof John Kieffer who hired me as an RA for a short term project on data compression when i was a first year graduate student and also for his remarkably well taught courses. Apart from the above mentioned faculty, i learned a great deal from the courses of Prof Tom Luo and Prof Ahmed Tewfik (now at University of Texas, Austin). I would like to thank Prof Anand Gopinath for being a good friend and offering guidance for my transition into a post doctoral researcher.

My current labmates Akshay, Swavyambhoo and Sirisha have been wonderful with timely help and well spaced humor and laughter. Having good colleagues really helps with the negative effects of stress one might encounter during PhD research. I would also like to thank my previous colleagues Dr Niranjay Ravindran and Bala for their valuable time and friendship.

Perhaps the most important people outside of professional circles are the following four people: my mother, Jodi Nyquist ND, Viktoria Sears DC and Christi Jergens CCH. When i got into some health related problems during my stay here at University of Minnesota, these four people healed me and equipped me to complete the PhD dissertation. Without their timely help, completion of the planned research by Dec 2014 would not have been possible.

In social circles, Bethany Mann is a friend who introduced me to the Hope Community church and helped build a good social support system. My good friends Hannah, Mickey and baby Lydia have been instrumental in maintaining a

positive social dimension in my life during my graduate school.

I thank my sister (and father) for being a good source of encouragement and compassion during my graduate school.

Dedication

To The Field

the invisible, conscious, intelligent and secret force of the Universe.

Abstract

Retransmission with error correction capability and opportunistic user scheduling are two of the cross layer protocols that hold promise to substantially improve the performance of wireless networks. In this thesis, we do a performance analysis of Hybrid Automatic Repeat reQuest (HARQ), a joint error correction and retransmission protocol, and downlink multiuser diversity opportunistic scheduling in both single hop and multihop wireless adhoc networks (WANETs).

In the first part of the thesis, we study the performance of rateless codes employed in the physical layer of a WANET. The nodes of the WANET are modeled by a homogeneous space time Poisson point process with Rayleigh fading, constant transmission power per node and pure ALOHA as the channel access protocol. The thesis considers 2 types of receivers, an ideal matched receiver and a practical nonmatched receiver. For such a WANET, the thesis quantifies the rate density and the dynamic variations of packet transmission time by deriving an upper bound to the CCDF of the packet transmission time. The thesis presents a WANET system model in which a packet transmission spans a single coherence time and it is shown that the rate density can be upto 70% of the ergodic rate density. This is good news, because the presented network does not require diversity, and transmits each message within one coherence time. Thus, the presented network nearly achieves the ERD, while requiring significantly shorter delays. From a rate density perspective, the thesis illustrates the advantage of power control in the form of channel thresholding. For both the rate density and the dynamic variations of packet transmission time, the analytical insights are supported by a

very good match with the simulation results.

In the second part of the thesis, we do a performance analysis of the cooperative HARQ protocol in a wireless adhoc multihop network employing spatial ALOHA. We model the nodes in such a network by a homogeneous 2-D Poisson point process. We study the tradeoff between the transport capacity submetrics inherent in the network by optimizing the transport capacity w.r.t the network design parameters, HARQ coding rate and medium access probability. Using stochastic geometirc approximations, we obtain an analytic expression for the expected progress of opportunistic routing and optimize the capacity approximation by convex optimization. By way of numerical results, we show that the network design parameters obtained by optimizing the analytic approximation of transport capacity closely follows that of Monte Carlo based exact transport capacity optimization. As a result of the analysis, we argue that the optimal HARQ coding rate and medium access probability are independent of the node density in the network.

In the final part of the thesis, we do a cost-benefit analysis of multiuser diversity in single antenna broadcast channels. It is well known that the multiuser diversity can be beneficial but there is a significant cost in terms of system resources, bandwidth and power associated with acquiring instantaneous CSI. We work out a cost-benefit analysis of multiuser diversity for 2 types of CSI feedback methods, dedicated feedback and SNR dependent feedback, quantifying how many users should feedback CSI i.e the amount of available multiuser diversity that should be used from a net throughput perspective. Dedicated feedback, in which orthogonal resources are allocated to each user, has significant feedback cost and this limits the amount of available multiuser diversity that can be used. SNR dependent feedback method, in which only users with SNR above a threshold attempt to feedback, has relatively much smaller feedback cost and this allows for all of the available multiuser diversity to be used. Next, we study the effect of single user multiantenna techniques, which reduce the SNR variation, on the number of feedback users. It is seen that a broadcast channel using single user multiantenna

techniques should reduce the number of feedback users with the spatial dimension.

Contents

List of Tables

List of Figures

Chapter 1

Introduction

Wireless Networks have seen a tremendous increase in their capability to support high data rates and provide wider coverage in the last decade or so. This is a result of breakthroughs in a number of research directions and technologies such as Multiple antenna transmission reception (MIMO), Space Time Block Coding (STBC), Hybrid Automatic Repeat reQuest (HARQ), Network Coding and Multiuser Diversity scheduling to name a few. While there has been a number of research efforts in each of these directions, the focus of this thesis is to study 2 of the above research topics namely HARQ and multiuser diversity in random wireless networks. The first two parts of the thesis focus on the performance of HARQ in single hop and multihop WANETs respectively while the final part of the thesis is dedicated to the study of multiuser diversity opportunistic scheduling in downlink wireless channels.

1.1 Background and Motivation

HARQ combines error correction coding and retransmission protocols to obtain capacity achieving performance in fading wireless channels. In the analysis and design of WANETs two commonly used performance metrics are outage rate density (ORD) and ergodic rate density (ERD). Although ergodic rate is higher than

the outage rate, its achievability entails substantial higher delays than the outage rate. The ORD metric is suited for delay constrained applications where information packets are either successfully decoded or discarded at the first attempt whereas the ERD metric is suited to delay tolerant applications with high data rates. However with the integration of sophisticated error correction coding techniques and protocols, achieving near ERD performance has become feasible even for delay constrained applications.

In the literature, a number of approaches to achieve ERD in the network have been studied. One simple approach involves spreading the codeword of an information packet either in time or frequency before transmission. For a large spreading, the time or frequency diversity order of the spread codeword will be high enough to achieve the ergodic rate. But in many practical scenarios, the channel coherence time and the channel coherence bandwidth are too large, and hence this approach requires very large delays. Second approach makes use of incremental redundancy(IR) based HARQ[1, 2]. Punctured parity symbols of a codeword are transmitted on a block by block basis in response to receiver's ACK/NACK. This method requires much less delay and is widely used in wireless standards, UMTS HSDPA/ HSUPA [3], mobile WiMAX [4, 5] and the 3GPP Long Term Evolution (LTE) [6].

Fountain codes take the concept of HARQ to its limit[7, 8, 9, 10] . Given an information bit vector, a transmitter incrementally generates and transmits the parity symbols. Using the received parity symbols, at periodic intervals the receiver attempts to decode a subset of the information bits. These periodic attempts continue until the receiver successfully decodes the complete information bit vector and sends an ACK. Since the number of parity symbols required to decode an information bit vector of fixed length is a random variable that depends on the instantaneous fading and interference conditions, fountain codes are also known as rateless codes.

Rateless codes offer a number of advantages over the widely used fixed rate codes[11, 12]. Rateless codes can achieve ergodic capacity over fading channels

with much shorter delay when compared to block level IR based HARQ. In a WANET, the network reaches ERD operating point much quicker relative to the 2 previous approaches. Rateless codes offer robustness to no CSIT transmission whereas the fixed rate codes have a higher outage under no CSIT. Since rateless codes have a better performance than fixed rate codes in terms of throughput delay reliability(TDR) in a WANET, there is a seamless integration of rateless codes into WANETs[13, 14].

In the second part of the thesis, we consider the HARQ protocol in the cooperative network scenario. The HARQ protocol for wireless multihop networks, termed cooperative HARQ, was introduced in [15]. It makes use of the broadcast nature of the wireless channel where the destination has access to different copies of the same packet received from different intermediate relay nodes. The destination combines the different copies of the same packet, thereby utilizing the inherent spatial and time diversity. Formally the cooperative HARQ protocol operates as described below. In a typical source-destination communication,

1) The source transmits the 1^{st} block of the codeword.

2) The 1^{st} relay transmits the 2^{nd} block of the codeword. From among the set of relays that are able to decode the data packet using 1^{st} block of the codeword and are ready to transmit the 2^{nd} block, the relay closest to the destination is selected opportunistically as the 1^{st} forwarding relay[16, 17]. Transmission of a block of the codeword from a relay corresponds to the retransmission round as per the standard HARQ terminology.

3) Similarly in every retransmission round, the set of potential relays combine the blocks of the codeword they have received till now and decode the data packet. From among the set of relays that can transmit the next block of the codeword, the relay closest to the destination is selected as the forwarding relay for the next retransmission round.

4) This process of relays transmitting the subsequent blocks of the codeword incrementally continues until either the destination decodes the packet or the delay constraints are violated.

Transport capacity[18](alternatively, progress rate density (PRD)[19]) captures the tradeoff between the submetrics like hop rate, density of transmissions and the transmission distance inherent in the network design. To illustrate the tradeoff between transport capacity submetrics, we note that interference is an inherent feature in wireless adhoc networks and the SINR at a receiving node is a building block measure for performance analysis[20]. If all the communication hops in the network are operating at a higher hop rate, then to achieve a sufficiently high SINR at receiver nodes, the density of transmissions and transmission distance affecting the interference power and desired signal power respectively have to be small. Similarly if the network has to maintain a higher density of transmissions, the increased interference limits the SINR at receiver nodes thereby restricting the rate and range of communication. Since the transmission distance in wireless networks is mostly fixed, this tradeoff between the transport capacity submetrics can be balanced by solving a basic network design problem of selecting the optimal hop rate and density of transmissions.

In broadcast wireless systems, where the channels to different users fade independently, it is well known that multiuser diversity can be beneficial [21, 22]. At any point in time, it is likely that at least one user will have a very good channel realization. If the base station (BS) is aware of the user channels, it can schedule data transmission to the user with the best instantaneous channel at a high rate, thereby achieving better performance. The quality of the selected channel increases with the number of users, and a very well known result is that the spectral efficiency increases double logarithmically in the number of users [23]. Multiuser diversity is a key component of contemporary cellular systems UMTS, LTE [24].

Although multiuser diversity can provide significant benefits, there is also a non-negligible cost associated with obtaining instantaneous channel state information (CSI) at the BS. Such CSI is obtained through explicit feedback of the instantaneous SNR from each of the users or through utilization of uplink pilots when the channel is reciprocal. Thus, the cost is in terms of the system resources bandwidth and power used to acquire CSI and it increases with the number of

users. Hence there is a cost-benefit tradeoff associated with multiuser diversity.

The feedback cost associated with obtaining CSI at the BS depends on the specific CSI feedback method used and the number of users who feedback. In this thesis, we consider 2 types of CSI feedback methods. The first method is dedicated feedback, where each user is allocated an orthogonal resource per coherence time i.e., a fixed number of uplink symbols to be used either for SNR feedback or for transmission of uplink pilots. For this method, the feedback resources increase *linearly* with the number of feedback users. The second method is SNR dependent feedback [23, 25, 26], where only users who have an instantaneous SNR above a threshold, attempt to feedback instead of having every user always feedback its SNR. This method utilizes the fact that only users with strong channels are likely to be scheduled, and thus feedback is not required from users with weak channels. Since only the users with strong channels feedback their SNR, the feedback consists of MS ID and SNR value, and must be performed on a shared random access channel (e.g., using slotted ALOHA or spread spectrum) [26, 27]. For this method, the feedback resources increase *logarithmically* with the number of users[28]. Another fundamental overhead common to both the feedback methods arises from the fact that the BS must signal which of the users has been selected for transmission. This overhead is *logarithmic* in the number of users.

Thus the cost of multiuser diversity scales *linearly* in the number of users for dedicated feedback and *logarithmically* for SNR dependent feedback where as the downlink spectral efficiency increases only *double-logarithmically*. Hence, it is clear that the cost-benefit tradeoff of multiuser diversity is nontrivial. An optimally designed system should make sure that the feedback cost does not outweigh the spectral efficiency benefit by achieveing a balance between the cost and benefit of multiuser diversity [29], and a basic design question is to determine how many users the BS should acquire CSI from or in other words, how much of the available multiuser diversity should be used.

1.2 Existing Literature

A recent work studying the achievability of ERD in WANETs can be found in [30, 31]. Accurate upper and lower bounds on the ergodic rate of a WANET are derived. Based on the bounds on ergodic rate, network density is optimized for operation at the optimal ERD point. The work of [32] studies the achievability of ergodic capacity in a multiple access channel using IR-HARQ protocol. The punctured blocks of the codeword are transmitted over IID coherence times. A closed form expression for the long run average rate/user is derived by applying Renewal reward theorem [33] and the asymptotic convergence to ergodic rate is shown. In [34], the ergodic rate of a WANET is achieved by employing frequency hopping diversity. Upper and lower bounds to the ERD are presented for the system model of multiple antenna nodes, fixed power and matched filter reception. Performance analysis of IR-HARQ protocol in a single hop WANET is presented in [35]. Novel upper and lower bounds for the outage probability of a packet transmission after k^{th} retransmission round are derived. In [36], the performance of IR-HARQ protocol in a heterogeneous WANET for the local (single hop) broadcast scenario is presented. For a broadcast node, the distribution of the number of successful neighbors and bounds on its mean are derived. In [37], the problem of optimizing the maximum number of retransmission rounds in HARQ to maximize the transmission capacity is considered. For a single hop WANET with fixed power and path loss only, the optimum number of maximum retransmission rounds is quantified for CSMA, slotted and unslotted ALOHA protocols. The IR-HARQ is considered in a cooperative WANET in [38], which studies the related progress rate density (PRD) metric, defined as the product of area spectral efficiency and expected forward progress per hop. The HARQ coding rate is optimized to maximize the PRD in the network. The paper of [39] studies the throughput of IR-HARQ protocol under statistical queuing constraints in terms of the buffer overflow probability.

The contributions in the second part of thesis can be considered as an extension of the work in [19]. The authors in [19] use the stochastic geometry model of [16] for a wireless adhoc network without HARQ and solve a network design problem of optimizing the transport capacity w.r.t the SINR threshold and MAP. We extend the work of [19] by incorporating the cooperative HARQ protocol into the stochastic geometry model of a wireless network and perform mathematical analysis to derive convex approximations to the transport capacity. We then optimize the capacity approximation w.r.t the HARQ coding rate and MAP following the tradeoff balancing ideas of [19]. A mathematical analysis of opportunistic relaying in a downlink cellular system is presented in [40], which analyzes the success probability of a two hop communication with the choosen relay having the best channel to the destinaton.

Recent research has studied the tradeoff between transport capacity submetrics when using spatial multiplexing with interference cancellation[41] and bandwidth partitioning[42]. The scaling laws of transmission capacity of wireless adhoc networks with single hop has been quantified when employing interference cancellation[43], SIMO transmission with interference cancellation[44], spatial multiplexing and beamforming with interference cancellation[45] and spatial multiplexing with MMSE receivers[46]. All of these works use the transmission capacity framework introduced in [18], which pictures the network at any instant of time as a number of simultaneous single hop transmissions spread out in space and measures the transport capacity accordingly.

Random access transport capacity (RATC) is another version of transport capacity recently introduced in [47] which measures the rate submetric in transport capacity from an end-end perspective i.e., from source to destination accounting for the loss in bandwidth at the source end when the relays are fowarding packets. Although the RATC metric is a more accurate measure of transport capacity, it is complex to analyze for a multihop adhoc network and the work in [47] is based on the assumption of equidistant relays along a line between the source and destination and asymptotic delay constraints. The work of [47] is extended in [48],

which characterizes the throughput delay reliability tradeoff in multihop adhoc networks by deriving a closed form expression for the random access transport capacity under finite delay/energy constraints.

Although a number of papers in the literature have appeared that seek to reduce the feedback cost [23, 25, 26, 27], very little work has addressed the basic question of how much of the available multiuser diversity should be used. A closely related work [49] focuses on finding the optimal number of feedback users with 2 objectives, to minimize the BER for a given total power constraint and minimize the total power consumption for a given BER constraint. However, the model in [49] considers only the power cost of the feedback process and does not account for the bandwidth cost. In [28] the authors study the asymptotic scaling of the sum rate in downlink OFDMA when using both the dedicated and SNR dependent feedback accounting for the feedback cost in the sum rate expressions.

1.3 Contribution of the Thesis

The first part of the thesis studies the performance of rateless codes in a WANET in the direction of non equilibrium information theoretic approach to analysis and design of WANETs as laid out by [50]. The thesis considers a WANET employing fountain codes in the physical layer in which the node locations are modeled by the commonly used Poisson Point Process (PPP). The presented WANET system model involves packet transmission within a single coherence time and it is shown by asymptotic regime analysis that the achievable rate density can be as high as 70% of the ERD. This result illustrates that near ERD performance in a WANET is attainable with significantly shorter delays. The thesis characterizes the dynamic variations of the instantaneous rate per user in a WANET employing fountain codes in the physical layer by studying the distribution of the packet transmission time. In this thesis, packet transmission time is defined as the number of channel uses to transmit a information packet of K bits. An accurate upper bound to the CCDF of the packet transmission time is derived.

The thesis considers two types of receivers in the WANET system model. One type of receiver has estimates of instantaneous interference and noise power and is termed the ideal matched receiver. The second receiver is a simple Gaussian receiver which has access to interference and noise power estimates but over a large time scale. For the sake of analytical clarity, we first present the Gaussian receiver and then extend the results to the case of matched receiver. It is shown that the Gaussian receiver with low decoding complexity achieves most of the rate density of the ideal matched receiver. While most of the thesis focuses on constant power per transmit node, we do discuss the concept of channel thresholding as a form of power control to achieve higher rate density. By numerical results, it is shown that channel thresholding can lead to substantial improvements in rate density relative to constant power transmission.

The work in the second part of the thesis is heavily motivated by the material in [15, 16, 19]. The main contribution is to incorporate the cooperative HARQ protocol[15] into a wireless adhoc multihop network and solve the resulting network design problem of choosing the optimal hop rate and density of transmissions. We make use of the stochastic geometry model of [16, 51], in which the nodes of a wireless network are modeled as a spatial point process. As in [16], the nodes follow the spatial reuse ALOHA protocol, in which a node accesses the medium and transmits with probability p, termed medium access probability (MAP), and receives with probability $1-p$. Coding rate of HARQ has a tradeoff with spatial density of transmissions and/or communication distance (alternatively, progress). Similarly a higher MAP, thereby higher spatial density of transmissions, cannot be maintained without sacrificing the coding rate and/or progress. Hence the network design problem is to optimize the transport capacity w.r.t the coding rate and MAP, and solve for the optimal coding rate and MAP.

The exact expression of transport capacity is optimized by Monte Carlo simulations. The contribution of the thesis is in developing an analysis framework to derive a convex approximation to the transport capacity and optimize the capacity

approximation by standard convex optimization methods yielding close approximations to the optimal coding rate and MAP. The analysis will be valuable in studying the scaling behavior of the optimal coding rate and MAP in terms of network design parameters, path loss exponent and node density. In this thesis, we study 2 types of cooperative HARQ techniques, incremental redundancy and repetition time diversity. For both techniques, we develop convex approximations to the transport capacity.

In this thesis, we consider both the FDD and TDD (reciprocal) systems. The FDD and TDD systems differ in how the uplink and downlink bandwidths are related. For each system, the cost-benefit tradeoff of multiuser diversity for both the dedicated and SNR dependent feedback methods is quantified in terms of the key system parameters like the average SNR and the blocklength. Also, wherever possible, the optimal number of feedback users is quantified.

Although the focus of the thesis is on single antenna broadcast channels, we also study the effect of single user multiantenna techniques on multiuser diversity, more specifically, how the single user multiantenna techniques, which reduce SNR or mutual information (MI) variation, affect the multiuser diversity order that needs to be used.

1.4 Organization of the Thesis

The main body of the thesis is organized into 3 chapters. Chapter 2 presents the study dealing with the performance of Rateless codes employed in the physical layer of single hop WANETs. Chapter 4 presents the study dealing with the performance of the IR-HARQ protocol in a cooperative multihop WANET. Chapter 3 presents the study dealing with the performance of multiuser diversity opportunistic scheduling in downlink channels.

Chapter 2

Rateless Codes in a Single hop WANET

Based on the foundational work of [7, 8], a rateless code represents a fundamentally new way of encoding information bits for transmission over noisy channels. Fountain codes are one class of rateless codes. For an information bit vector of length K, a rateless code can generate upto $2K$ codewords of infinite length. Fountain codes incorporate low complexity belief propagation decoding. It is shown to have capacity achieving or capacity-approaching performance for many types of discrete channel models [7, 8, 9, 10], Gaussian channels[14] and fading channels[11]. Fountain codes and more generally rateless codes offer robustness to no channel state information at transmitter (CSIT) transmission since they follow channel conditions accurately (see [52] for a treatment of rateless coding in uncertain DMC's).

In this chapter, we study the achievability of ergodic rate density (ERD) in the WANET using rateless codes. Rateless codes hold the promise of capacity achieving performance with significantly shorter delays. This property of rateless codes is the focus of this chapter. The achievable rate density of the WANET is quantified and compared to the ERD. As part of the performance analysis of rateless codes, a characterization of the dynamic variations of the instantaneous rate

in the WANET is presented. This is accomplished by studying the distribution of the packet transmission time, defined as the number of channel uses to transmit K information bits. Two types of receivers are considered for analysis, the Gaussian receiver and the ideal matched receiver. The impact of power control in the form of channel thresholding on the rate density is investigated. The material and results presented in this chapter appears in part in [53]. The full version of the paper can be found in [54].

The remainder of the chapter is organized as follows. Section 2.1 contains the system model. Section 2.2 outlines an analytically tractable framework for studying the distribution of packet transmission time. Section 2.3 presents the theoretical results for the Gaussian receiver. Section 2.4 extends the results to the matched receiver case. Section 2.5 contains a brief study of the channel thresholding policy. Section 2.6 contains the numerical results and discussions. Conclusion of the chapter is in section 4.5.

2.1 System Model

We assume a continuous time ALOHA WANET, in which the probability of starting a transmission at any place and any time is identical. For mathematical simplicity, the network is modeled as if each transmit node transmits only once from a given location. Thus, the transmitter process is a space time homogeneous PPP Ψ with intensity λ_s (this model is also known as the Poisson rain model[55]). We use the notation $\Psi = \{X_i, T_i\}$ where $X_i \in \mathbb{R}^2$ is the location of node i and T_i is the packet transmission start time. Each node $X_i \in \Psi$ has a receive node at Y_i at a distance of d m. Without loss of generality, in the following we assume that the model is normalized so that $d = 1$. The MAC state of node i at $t \in \mathbb{R}$ is given by $e_i(t) = 1\left(T_i \leq t \leq T_i + B_i\right)$, where B_i is the packet transmission time and is defined later.

Each transmitter encodes K information bits with a rateless code and sends

Gaussian symbols incrementally over the channel. Each receiver collects the channel output symbols for every L channel uses and attempts to decode a subset of K information bits. Fig.2.1 illustrates an example of transmission of information bits from transmitter to receiver employing rateless codes. In this example, the transmitter encodes an information bit packet of length $K = 75$. The parity symbols are incrementally generated and sent over the channel. At the receiver side, for every $L = 100$ symbols/channel uses, the receiver attempts belief propagation decoding to decode information bits. At every attempt, the receiver will be able to decode a subset of information bit packet. The periodic attempts of the receiver continue until all $K = 75$ bits are decoded.

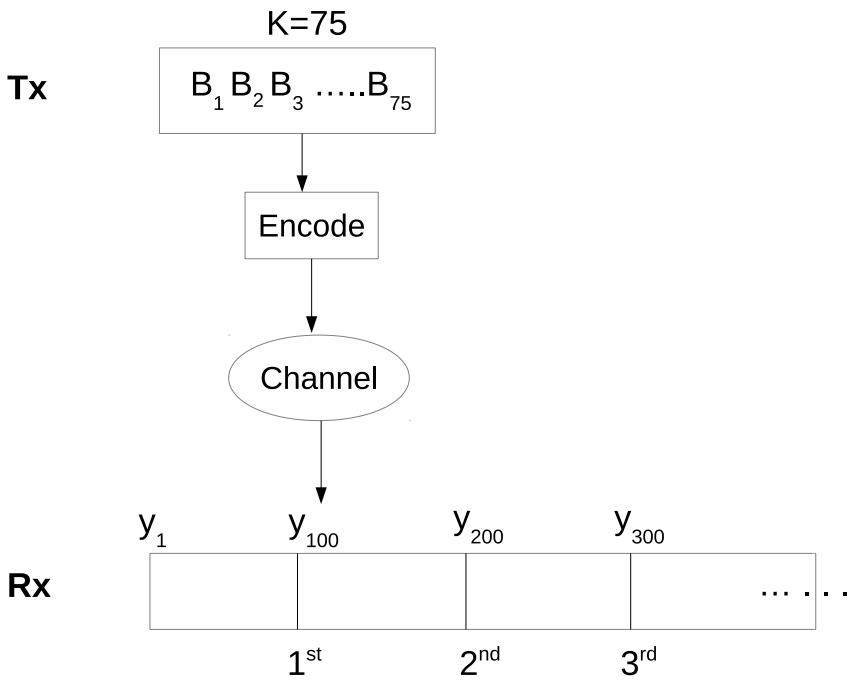

Figure 2.1: A typical example of rateless coded transmission of information bits from transmitter to receiver.

In the following, we consider a normalized model and assume that $L = 1$.

Varying L leads to a tradeoff between throughput performance and decoding complexity. The optimization of L is beyond the scope of our current work. The transmission of parity symbols continues until the receiver succeeds to decode the K information bits, and sends an ACK to the transmitter.

We assume that the fading coherence time T_c is large relative to packet transmission time and consider IID block fading. Thus the fading coefficient will be time invariant throughout any packet transmission time, but will be statistically independent of the fading coefficients for any other packet transmission.

2.1.1 Characterization of the packet transmission time

In this subsection, we define the packet transmission time for an arbitrary transmit node i. Transmitter i starts the packet transmission at T_i. During the packet transmission time B_i, transmissions from other transmit nodes $k \neq i$ may cause interference. The interference power at receiver i at time t is given by

$$I_i(t) = \sum_{k \neq i} \rho |h_{ki}|^2 |X_k - Y_i|^{-\alpha} e_k(t) \tag{2.1}$$

where ρ is the transmit SNR, $|h_{ki}|^2$ is the fading coefficient from transmitter k to receiver i and α is the path loss exponent.

Let $\hat{I}_i(t)$ represent the average interference upto time t where $t > T_i$. Assuming that the number of symbols is large enough, this average interference can be described by the integral

$$\hat{I}_i(t) = \frac{1}{t - T_i} \int_{T_i}^{t} I_i(\tau) \ \mathrm{d}\tau. \tag{2.2}$$

The SINR at receiver i based on the interference in (2.2) is given by

$$\hat{\mathrm{SINR}}_i(t) = \frac{\rho |h_{ii}|^2}{1 + \hat{I}_i(t)} \tag{2.3}$$

We assume that the receiver i uses a nearest neighbor decoder and is not capable of estimating the instantaneous interference and noise power during the

packet reception. The achievable rate of the nearest neighbor decoder at receiver i is given by [56]

$$C_i(t) = \log_2\left(1 + \hat{\mathrm{SINR}}_i\left(t\right)\right) \tag{2.4}$$

The time to decode K information bits, assuming that receiver i achieves $C_i(t)$ is defined as

$$\hat{B}_i = \min\left\{t : K < t \ \log_2\left(1 + \hat{\mathrm{SINR}}_i\left(t\right)\right)\right\} \tag{2.5}$$

Although we aim to achieve the ERD, this is not feasible for any finite delay, because we consider a slow fading scenario. We must also consider the occurrence of outage events, which are characterized by a delay constraint. Thus, each packet transmission of K bits is subject to a delay constraint of D. Whenever the packet transmission of transmitter i fails the delay constraint i.e., $\hat{B}_i > D$, an outage event is declared. In fact, without such a delay constraint, transmissions with poor fading states will result in unbounded packet times leading to network congestion. Thus, based on (2.5), the packet transmission time of receiver i is defined as

$$B_i = \min\left(D, \hat{B}_i\right) = \begin{cases} D, & \hat{B}_i > D \\ \hat{B}_i, & \hat{B}_i \leq D \end{cases} \tag{2.6}$$

The model in (2.1)-(2.6) is referred to as the exact model in the following since it takes into consideration the interference in (2.1) in its exact form.

Based on (2.6), the distribution of B_i is completely characterized by that of $\hat{B}_i$. From the RHS of (2.5), it is clear that $\hat{B}_i$ depends on all the other packet transmission times, which may interfere with the reception of the packet by receiver i. Similar to the definition in (2.5), it is straightforward to observe that each of the $\{B_j\}_{j\neq i}$ is again coupled to B_i. With such an interdependence the exact distribution of B_i is quite intractable. Hence in the next section, we define an independence model for the packet transmission times which provides a good approximation to the exact model (2.1)-(2.6).

2.2 Independence Model

In this section, we introduce an analytically tractable framework for characterizing the distribution of packet transmission times. By Slyvinak's theorem [55], the performance of the WANET can be quantified by studying a reference transmitter receiver pair. Without loss of generality, we choose node 0 to be the reference transmitter located at $X_0 = (d, 0)$. The corresponding receiver is located at the origin i.e., $Y_0 = (0, 0)$. We further assume that transmitter 0 starts the packet transmission at $T_0 = 0$.

Let $\bar{B}_1, \bar{B}_2, \bar{B}_3 \cdots$ represent the interferer packet transmission times. In order to quantify the dependence of packet transmission time on interference via mathematical analysis, we make an independence approximation to the distribution of interferer packet times. More precisely, we assume that $\bar{B}_1, \bar{B}_2, \bar{B}_3 \cdots$ are IID and are also statistically independent of $\tilde{B}_0$, the packet transmission time of transmitter 0. We further assume that $\{\bar{B}_j\}_{j\neq 0}$ have the same distribution as $\tilde{B}_0$, which will be specified later. With $\bar{B}_1, \bar{B}_2, \bar{B}_3 \cdots$ replacing the exact transmission times $B_1, B_2, B_3 \cdots$ in (2.1)-(2.6), the resulting expressions for average interference, SINR, achievable rate and packet transmission time of the reference pair under the independence model are given below.

$$\begin{aligned}
\tilde{e}_k(t) &= 1\left(T_k \leq t \leq T_k + \bar{B}_k\right) \\
\tilde{I}_0\left(t\right) &= \sum_{k\in\Psi} \rho |h_k|^2 |X_k|^{-\alpha} \tilde{e}_k(t) \\
\tilde{I}_a\left(t\right) &= \frac{1}{t}\int_0^t \tilde{I}_0(\tau)\ \mathrm{d}\tau = \sum_{k\in\Psi} \rho |h_k|^2 |X_k|^{-\alpha} \eta_k(t) \qquad (2.7) \\
\eta_k(t) &= \frac{1}{t}\int_0^t \tilde{e}_k(\tau)\ \mathrm{d}\tau \qquad (2.8) \\
\tilde{\mathrm{SINR}}_a\left(t\right) &= \frac{\rho |h_0|^2}{1 + \tilde{I}_a(t)} \\
\tilde{C}_0(t) &= \log_2\left(1 + \tilde{\mathrm{SINR}}_a\left(t\right)\right) \\
\tilde{B}_0 &= \min\left\{t : K < t\ \tilde{C}_0(t)\right\} \qquad (2.9)
\end{aligned}$$

From now onwards, without any ambiguity we refer to $\tilde{B}_0$ as $\tilde{B}$. Similar to (2.6), the packet transmission of transmitter 0 is subject to a delay constraint D in the independence model and the truncated version of (2.9) is defined as

$$\bar{B} = \min\left(D, \tilde{B}\right) = \begin{cases} D, & \tilde{B} > D \\ \tilde{B}, & \tilde{B} \leq D \end{cases} \tag{2.10}$$

Whenever the packet transmission of transmitter 0 fails the delay constraint i.e., $\tilde{B} > D$, an outage event is declared. Note that the distribution of interferer packet times $\{\bar{B}_j\}_{j\neq 0}$ is identical to the distribution of $\bar{B}$ in (2.10).

2.3 Performance Analysis

In this section, we characterize the distribution of the packet transmission time and the achievable rate density in the WANET. Since the reference pair packet transmission time $\tilde{B}$ and the interferer packet times $\{\bar{B}_j\}_{j\neq 0}$ have identical distribution, $\tilde{B}$ is said to have implicit distribution[1] . Hence the distribution of $\tilde{B}$ is characterized in 2 stages. In the following, we first give an expression for an upper bound on the distribution, and then illustrate the implicit nature of the distribution upper bound and the procedure for studying its behavior is outlined.

2.3.1 CCDF of $\tilde{B}$

Based on the definition of $\tilde{B}$ in (2.9), the CCDF is written as

$$\mathrm{P}\left(\tilde{B} > b\right) = \mathrm{P}\left(\int_0^b 1\left(\frac{K}{u} < \tilde{C}(u)\right) \mathrm{d}u < 1\right) \tag{2.11}$$

The exact CCDF of $\tilde{B}$ in (2.11) is complex to analyse. A novel and tractable upper bound on the CCDF of $\tilde{B}$ is given in the following theorem.

[1] One or more terms in the distribution expression are functions of the distribution itself.

Theorem 1. *An upper bound on the CCDF of the packet transmission time of the Gaussian receiver, $\tilde{B}$ in (2.9), is given by*

$$\mathrm{P}\left(\tilde{B} > b\right) \leq 1 - \exp\left(- \frac{2^{K/b} - 1}{\rho} - \pi \lambda_s \left(2^{K/b} - 1\right)^{\delta} \right.$$
$$\left. \Gamma\left(1-\delta\right)\Gamma\left(1+\delta\right) \ \frac{\hat{g}\left(b\right)}{b^{\delta}} \right) \tag{2.12}$$
$$\triangleq \mathrm{P}_u\left(b\right) \tag{2.13}$$
$$\hat{g}\left(b\right) = b^{\delta} \ \mu^{\delta} \max\left(b,\mu\right)^{1-\delta} + \frac{1-\delta}{1+\delta} \min\left(b,\mu\right)^{1+\delta} \tag{2.14}$$
$$\mu : \int_0^D \mathrm{P}_u\left(b\right) \ \ \mathrm{d}b - \mu = 0 \tag{2.15}$$

where $\delta = 2/\alpha$ and the bound in (2.12) is valid only if (2.15) is satisfied.

As can be noted, the bound of Theorem 1 is an implicit bound, as the value of $\mu = \mathbb{E}[\bar{B}]$ cannot be determined in advance. To evaluate the bound, one needs to guess the value of μ and then evaluate the CCDF and reevaluate $\mathbb{E}[\bar{B}]$. Fortunately, the result after reevaluation is monotonically increasing with the initial guess, and hence the tuning procedure in (2.15) is quite efficient.

The bound reveals the nature of the distribution of the packet transmission time, and also allows to evaluate an upper bound on the expected packet time. As a sidestep from the proof, we also show that replacing (2.14) with

$$\hat{g}\left(b\right) = \mu \ b^{\delta} \left(1 + \frac{1-\delta}{1+\delta} \frac{b}{D}\right) \tag{2.16}$$

results in a very useful approximation to the CCDF.

Proof: The complete proof of Theorem 1 is presented in Appendix 2.8.1. ■

The analytical bound presented in Theorem 1 will be useful in studying the dynamic variations of the packet transmission time and also in evaluating the performance of the WANET. The WANET performance is well described by its achievable rate density which is discussed in the following.

Corollary 1. *The CCDF upper bound P_u in (2.12) has a heavy tail distribution with parameter 'δ'.*

$$\mathrm{P}_u(b) = 1 - \exp\left(O\left(\frac{1}{b^{\delta}}\right)\right) \tag{2.17}$$

Proof: For a proof of Corollary 1, please refer to Appendix 2.8.3. ■

2.3.2 Achievable Rate Density

In this subsection, we quantify the rate density of the WANET system model considered in this chapter and compare it to the maximal achievable performance, which is the ERD. Considering a time space volume of area A and duration τ, the rate density over this volume is defined as the sum of bits that were generated within the volume and were received successfully divided by the volume. In mathematical terms, the rate density is

$$\mathrm{RD}(A,\tau) = \frac{1}{\tau A} \sum_{i \in \mathcal{M}} q_i K_i \tag{2.18}$$

where K_i is the number of bits in the i-th packet, $q_i \in \{0,1\}$ indicates the packet reception success or failure and $\mathcal{M}$ is the set of all packets that are generated within the considered volume.

Applying the asymptotic limits to the area A and time duration τ, the limiting rate density is given by

$$\mathrm{RD} = \lim_{A,\tau\to\infty} \mathrm{RD}(A,\tau) \tag{2.19}$$

A slotted ALOHA WANET, as in [30], using time (frequency) diversity or IR-HARQ is shown to achieve the ergodic rate density (ERD):

$$\mathrm{ERD}(\lambda) = \lambda\, \mathbb{E}\left[\log_2(1+\mathrm{SINR})\right] \tag{2.20}$$

where

$$\mathrm{SINR} = \frac{\rho|h_0|^2}{1+\sum_{j\in\Phi,\neq 0}\rho|h_j|^2|X_j|^{-\alpha}},$$

λ is the density of active transmitters and Φ is a homogeneous spatial PPP with density λ $/m^2$.

Based on the definition in (2.18) and (2.19), the rate density for our WANET system model is expressed as

$$\begin{aligned} \mathrm{RD} &= \lambda_s \, K\,(1-\epsilon) \\ \epsilon &= \mathrm{P}\left(\tilde{B} > D\right) \end{aligned} \tag{2.21}$$

where ϵ is the outage in packet transmission.

To compare the rate density in (2.21) to the network ERD in (2.20), note that at any given time, the density of active transmitters in our system model is given by:

$$\lambda = \lambda_s \, \mathbb{E}[\tilde{B}] \tag{2.22}$$

Comparison of RD **to** ERD

Defining $C\,(\lambda) = \mathbb{E}\left[\log_2\left(1+\mathrm{SINR}\right)\right]$ and using the relation in (2.22), the ratio of RD to ERD is expressed as

$$\begin{aligned} \frac{\mathrm{RD}}{\mathrm{ERD}} &= \frac{\lambda \; K\,(1-\epsilon)}{\lambda \; C\,(\lambda)\,\mathbb{E}[\tilde{B}]} \\ &= \frac{K/C\,(\lambda)}{\mathbb{E}[\tilde{B}]}\,(1-\epsilon) \qquad (2.23) \\ &\triangleq \upsilon\,(1-\epsilon) \qquad (2.24) \end{aligned}$$

where υ denotes the loss in RD due to lack of diversity since $K/C\,(\lambda)$ represents the expected packet time with diversity and $\mathbb{E}[\tilde{B}]$ represents the expected packet time with no diversity.

For the WANET system model of section 2.1, the deviation of RD from ERD can be accounted for by 2 factors, *primarily* by lack of fading and interference diversity in the channel[2] and *nominally* by the choice of receiver. The Gaussian receiver presented in (2.4) does not have estimates of instantaneous interference and noise power, which causes rate density loss in the interference limited regime.

[2] Meaning no IID realizations of fading and almost no variation in interference during packet transmission.

The effect of the choice of receiver vanishes as $\lambda \to 0$ i.e., as interference decreases. Thus, a basic limit in terms of the achievability of ERD can be obtained by applying $\lambda \to 0$ in (2.23) and is given by

$$\frac{\text{RD}}{\text{ERD}} \xrightarrow{\lambda \to 0} \frac{\ln 2 \; K \; \exp\left(-\frac{2^{K/D}}{\rho}\right)}{E_1\left(\frac{1}{\rho}\right)\left(D - e^{\frac{1}{\rho}} \int_0^D \exp\left(-\frac{2^{K/b}}{\rho}\right) \, \mathrm{d}b\right)} \tag{2.25}$$

where the limiting success probability is given by $1 - \epsilon \to \exp\left(-\frac{2^{K/D}-1}{\rho}\right)$ and $E_1(x) = \int_1^\infty \frac{e^{-xt}}{t} \, \mathrm{d}t$ is the exponential integral function. The ratio in (2.25) can be upper bounded based on the following lower bound [57] $E_1(x) > \frac{1}{2} e^{-x} \log\left(1 + \frac{2}{x}\right)$. It is interesting to note that the ratio in (2.25) approaches zero as $D \to 0$ and $D \to \infty$.

The loss in rate density due to the Gaussian receiver can be addressed by considering a receiver which tracks instantaneous interference and noise power. Since a matched receiver has estimates of the instantaneous interference and noise power, the successful packet transmissions in the WANET will increase leading to a higher rate density relative to the receiver in (2.4). This concept is addressed in section 2.4.

2.4 Matched Receiver

In section 2.3, the analysis was based on a receiver that is incapable of estimating the instantaneous interference and noise power. In this section, the performance analysis of a receiver matched to the instantaneous interference and noise power is presented. Similar to the Gaussian receiver, the analysis of matched receiver requires the framework of exact and independence model as in sections 2.1 and 2.2. But since the only difference is in the choice of the receiver, we skip the exact model and present only the independence model. Assuming the receiver 0

is employing a matched receiver, the achievable rate upto time t is given by [3]

$$\tilde{C}(t) = \frac{1}{t}\int_0^t \log_2\left(1+\tilde{\mathrm{SINR}}\left(\tau\right)\right)\ \mathrm{d}\tau \tag{2.26}$$

$$\tilde{\mathrm{SINR}}\left(t\right) = \frac{\rho|h_0|^2}{1+\tilde{I}(t)} \tag{2.27}$$

The corresponding packet transmission time $\tilde{B}$ is defined as

$$\begin{aligned}\tilde{B} &= \min\left\{t : K < t\ \tilde{C}(t)\right\}\\ &= \int_0^\infty 1\left(K \geq t\ \tilde{C}(t)\right)\ \mathrm{d}t\end{aligned} \tag{2.28}$$

2.4.1 CCDF of $\tilde{B}$

The CCDF of $\tilde{B}$ in (2.28) is given by

$$\mathrm{P}\left(\tilde{B} > b\right) = \mathrm{P}\left(K \geq \int_0^b \log_2\left(1+\tilde{\mathrm{SINR}}(\tau)\right)\ \mathrm{d}\tau\right) \tag{2.29}$$

The above CCDF is dependent on the distribution of $\tilde{C}(b)$ in (2.26). From (2.26) and (2.27), it is clear that $\tilde{C}(b)$ is an integral function of time invariant random variable $|h_0|^2$ and a time varying one $\tilde{I}(\tau),\ \tau \in (0,b)$. As such there is no conceptual way of determining the distribution of $\tilde{C}(b)$ directly. Instead a lower bound to $\tilde{C}(b)$ is developed using interference bounding techniques [30]. Based on Jensen's inequality for convex functions and upper bounding the strongest interference at receiver 0 in the interval $(0,b)$ by a threshold $\gamma_{th} > 0$, we develop a lower bound to $\tilde{C}(b)$ and present the corresponding upper bound on the CCDF of $\tilde{B}$ in the following theorem.

[3] We assume that K is large enough so that an integral can replace the mutual information sum over channel uses.

Theorem 2. *For any $\gamma_{th} > 0$, an upper bound on the CCDF of the packet transmission time of the matched receiver, $\tilde{B}$ in (2.28), is given by*

$$\mathrm{P}\left(\tilde{B} > b\right) \leq 1 - \exp\left(- \frac{2^{K'/b} - 1}{\rho} - \pi\lambda_s \left(2^{K'/b} - 1\right)^{\delta} \right.$$
$$\left. G\left(\gamma_{th}\right)\ \Gamma\left(1+\delta\right)\ \frac{\hat{g}\left(\bar{B}\right)}{b^{\delta}} \right) \tag{2.30}$$

$$\triangleq \mathrm{P}_u \tag{2.31}$$

$$K' = K\ \exp\left(\pi\lambda_s \left(b+\mu\right)\Gamma\left(1+\delta\right)\left(\tfrac{\rho}{\gamma_{th}}\right)^{\delta}\right) \tag{2.32}$$

$$G\left(\gamma_{th}\right) = \int_{\frac{\gamma_{th}}{\rho}\left(2^{K'/b}-1\right)}^{0} \left(1 - e^{-t}\right)\ \mathrm{d}t^{-\delta} \tag{2.33}$$

$$\hat{g}\left(\bar{B}\right) = b^{\delta}\ \mu^{\delta} \max\left(b,\mu\right)^{1-\delta} + \frac{1-\delta}{1+\delta} \min\left(b,\mu\right)^{1+\delta} \tag{2.34}$$

$$\int_0^D \mathrm{P}_u\ \mathrm{d}b - \mu = 0 \tag{2.35}$$

Similiar to Theorem 1, the upper bound in (2.30) and (2.34) is implicit in nature and is computed by the tuning procedure. The solution to the tuning equation (2.35) yields the expected packet time $\mu = E[\bar{B}]$. A very accurate approximation to the CCDF is obtained using (2.16) in place of (2.34). The parameter γ_{th} in (2.32) and (2.33) is the interference threshold which limits the strongest interference at receiver 0. The expected packet time μ from (2.35) is a function of γ_{th}. The best CCDF bound (approximation) is obtained by optimizing γ_{th} to yield the minimal expected packet time,

$$\gamma_{th}^{*} = \arg\min_{\gamma_{th}}\ \mu\left(\gamma_{th}\right) \tag{2.36}$$

It is important to note that letting $\gamma_{th} = \infty$ reduces the CCDF upper bound in Theorem 2 to the bound presented in Theorem 1. Thus, Theorem 2 is always tighter than Theorem 1 (which obviously is also valid for the matched receiver).

Proof: Refer to Appendix 2.8.4 for the full proof of Theorem 2. ■

Since a transmitter with poor fading coefficient will likely transmit for a long duration, it will cascade the effect of interference in the WANET and thus increase

the outage probability. By allowing only the transmitters with fading coefficients above a certain threshold to transmit, interference from poor transmitters can be reduced. By suitably choosing the threshold, the WANET can experience a higher success probability of packet transmission. The effect of such a power control scheme is studied in section 2.5.

2.5 Channel Thresholding

In this section, we consider a WANET system model in which each transmit receive pair employs a Gaussian receiver for reception and a form of power control known as channel thresholding for transmission. The transmit SNR is a function of the instantaneous fading coefficient from the transmit to receive node. Mathematically, the transmit SNR from transmitter i to the WANET is given by

$$\rho_i = \begin{cases} \rho, & |h_{ii}|^2 \geq \beta \\ 0, & |h_{ii}|^2 < \beta \end{cases} \tag{2.37}$$

where β is a threshold on the fading coefficient. Since the transmit nodes with $|h|^2 < \beta$ are off, the decreased interference in the WANET increases the success probability of transmission leading to a higher rate density relative to the constant power transmission discussed in section 2.3.

The rate density and transmit density for a WANET with channel thresholding are defined as

$$\mathrm{RD} = \lambda_s p \; K\left(1-\epsilon\right) \tag{2.38}$$

$$\lambda = \lambda_s p \; \mathbb{E}\left[\tilde{B}\right] \tag{2.39}$$

where $p = \mathrm{P}\left(|h|^2 \geq \beta\right)$ is the transmission probability[4] . Similar to section 2.2, considering a reference transmitter receiver pair, the achievable rate upto time t

[4] The PPP Ψ can be split into 2 independent PPPs Ψ_1 and Ψ_0 of densities $\lambda_s p$ and $\lambda_s\left(1-p\right)$ respectively.

is defined as

$$\tilde{C}(t) = \begin{cases} \log_2\left(1 + \frac{\rho|h|^2}{1+\tilde{I}_a(t)}\right), & |h|^2 \geq \beta \\ 0, & |h|^2 \leq \beta \end{cases} \tag{2.40}$$

where in the expression for $\tilde{I}_a(t)$ given in (2.7), ρ is replaced by ρ_i defined in (2.37). The packet transmission time $\tilde{B}$ has the same definition as in (2.9). The CCDF of $\tilde{B}$ is upper bounded as

$$\mathrm{P}\left(\tilde{B} > b\right) \leq \mathrm{P}\left(\frac{\rho|h|^2}{1+\tilde{I}_a(b)} \leq 2^{K/b} - 1 \middle| |h|^2 \geq \beta\right) \tag{2.41}$$

For the case $\beta = 0$, channel thresholding reduces to constant transmission power and the CCDF is upper bounded by the results of Theorem 1. Unfortunately for $\beta > 0$ due to the conditioning event $|h|^2 \geq \beta$, the CCDF bound is analytically intractable and does not admit a simple expression similar to the one given in Theorem 1. Due to space limitations, we omit the analytic bounds and present only the numerical results illustrating the benefit of using channel thresholding [5]

.

2.6 Numerical Results

In this section, we present numerical results that demonstrate the performance of the systems discussed above. First we detail the key aspects of the simulation model. The transmit nodes $\{X_i\}$ are realized as points of a homogeneous space time PPP Ψ of density λ_s in a square $\mathcal{S}$ of side $\ell = 100$ with wrap around edges. The receive nodes are positioned on circles of radii $d = 1$ centered around $\{X_i\}$. The operating transmit SNR is $\rho = 15$ dB. The length of each information bit packet is $K = 75$. The corresponding delay constraint on the packet transmission time is $D = 500$ channel uses. The WANET simulation is implemented in 2 stages.

[5] For $\beta > 0$, a closed form upper bound can be obtained for the CCDF using a different technique than that in Theorem 1 which involves bounding the tail probability of the additive shot noise $\tilde{I}_a(b)$ and is a subject of future work.

In the first stage, the exact model of section 2.1 is simulated. The WANET is run for a total duration of 50000 channel uses. All transmit nodes with packet start times T_i within the above time frame are allowed to transmit packets. The samples for computing the packet time statistics empirically are obtained only from the steady state region of the network operating time which is observed after the first $20 - 25\%$ of the channel uses.

In the second stage, the independence model of section 2.2 is simulated. The WANET performance is measured by simulating only transmitter 0, which starts its transmission at time $T_0 = 0$. The reference receiver is located at the origin. The network is run for a total duration of $2D$ channel uses centred around T_0. Under the independence model, the interferer packet durations are obtained based on the empirical distribution derived from the simulation of exact model in the first stage. For the independence model, the network is simulated for 10000 iterations. The corresponding packet time samples of the reference pair are used for computing the statistics.

Edge effect: The edge effect is eliminated for the transmitter receiver pairs near the edges of the simulation square $\mathcal{S}$ by considering 8 virtual squares of same dimension around $\mathcal{S}$. The nodes of $\mathcal{S}$ are replicated in the 8 virtual squares. For each Rx node $y_i \in \mathcal{S}$, every interferer $X_j \in \mathcal{S}$ has 8 virtual interferers in the 8 virtual squares. At y_i, the interference contribution from only the nearest of the 9 interferers (1 + 8 virtual) will be considered for simulation. This method of computing interference contribution at each Rx node $y_i \in \mathcal{S}$ from every interferer X_j eliminates the edge effect. Mathematically, the above operation can be expressed in the following form. Given an Rx node $y_i \in \mathcal{S}$ and an interfering node $X_j \in \mathcal{S}$, the distance vector from y_i to the nearest interferer of the set of 9 interferers corresponding to X_j is given by

$$\Delta\left(y_i, X_j\right) = \mod\left(y_i - X_j + \frac{N}{2}, N\right) - \frac{N}{2} \tag{2.42}$$

2.6.1 Rate Density

In this subsection, we illustrate the performance of the Gaussian and matched receivers of sections 2.3 and 2.4 by studying the achievable rate density. Fig.2.2 shows a plot of the ERD in (2.20) and rate density RD in (2.21) for both the Gaussian and matched receivers as a function of the transmit density λ for $\alpha = 3$ and a delay constraint $D = 500$. It is observed that the RD and ERD curves achieve their maximum values around transmit density $\lambda = 0.2$. As $\lambda \to 0$, the network operates in noise limited regime and the effect of interference is negligible. But the WANET system model in this chapter cannot use diversity, and is required to transmit each packet within a single coherence time. Thus, whenever the channel gain is poor, the transmitter must spend a long transmission time to transfer the message in spite of the channel conditions. As a result, the network spends longer times in transmitting over poor channels, and the throughput decreases compared to the ERD. It is also interesting to note that for any finite delay constraint, the outage probability is strictly positive even in the absence of interference. Analytically the ratio of RD to ERD as $\lambda \to 0$ is given by (2.25). Plugging in the network parameter values into (2.25), the asymptotic ratio is given by

$$\frac{\text{RD}}{\text{ERD}} \xrightarrow{\lambda \to 0} 0.7 \tag{2.43}$$

From the simulation curves in Fig.1, the ratio is evaluated to equal 0.71 which is accurate with the prediction in (2.43). For higher transmission densities, the interference also starts to play a role increasing the packet transmission time. The cascading effect of longer packet times of the transmit nodes causes the network to experience more delay outage. As a result, the difference between the RD and the ERD grows monotonically. This difference between the RD and the ERD curves is even more pronounced for smaller values of α.

The values of rate density and transmit density on the curve are obtained based on (2.21) and (2.22). Since the ideal receiver of (2.26) is matched to the instantaneous interference and noise power, its achievable rate is higher than that of the Gaussian receiver in (2.4). Hence the ideal matched receiver has a lower

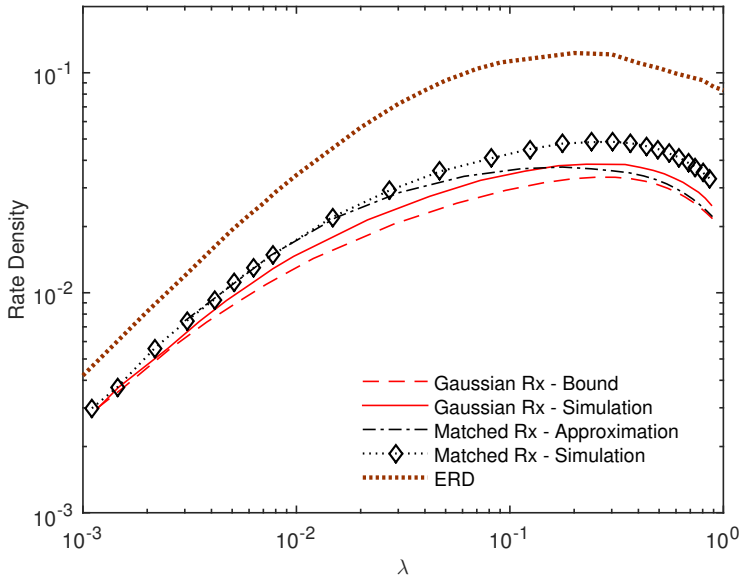

Figure 2.2: A plot of the ERD and RD from (2.20) and (2.21) respectively as a function of the transmit density λ for $\alpha = 3$ and a delay constraint $D = 500$. For both the Gaussian and matched receivers, the curves based on simulation and theoretical analysis are shown.

outage and smaller expected packet transmission time. From (2.21) and (2.22), it immediately follows that the matched receiver has a higher RD curve relative to the Gaussian receiver. However the performance of the ideal receiver is based on the assumption that the receiver will be able to track the instantaneous interferer activity even while receiving a packet. This is quite complicated in a practical WANET. On the other hand, from Fig.2.2, it is observed that the maximal RD value of the Gaussian receiver is almost 75% of that of the ideal matched receiver. *This is good news for a practical WANET since the Gaussian receiver achieves most of the rate density of the ideal receiver with low decoding complexity.* The analysis curves for both the Gaussian and ideal receivers based on Theorems 1 and 2 describe the system performance pretty well.

Fig.2.3 shows a plot of the success probability $1 - \epsilon$ against the space time density λ_s for the Gaussian receiver at $\alpha = 3$ and a delay constraint $D = 500$. The curves corresponding to both the exact model and the independence model are shown and it is found that the independence model closely follows the exact model over a wide range of densities λ_s. Note that any decrease in the success probability also reduces the RD and takes it further away from the ERD (see (2.21) for the exact formula).

Fig.2.3 also shows two analysis curves. The first is the lower bound that results from the CCDF bound of Theorem 1. This bound gives a performance guarantee, and good characterization of the performance. But, as can be seen, the bound is not tight. A better characterization of the network performance is obtained by the approximation that results from plugging (2.16) in (2.12).

2.6.2 Dynamic Variations of Packet time

In this subsection, we present the dynamic variations of the packet transmission time for the Gaussian receiver. The analysis results of section 2.3 are compared against the Monte carlo simulation results corresponding to (2.5) and (2.9). The

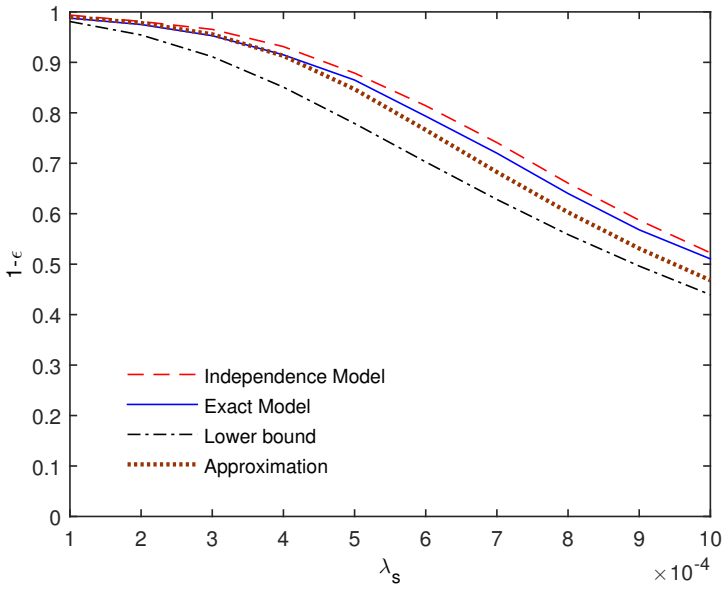

Figure 2.3: A plot of the success probability $1-\epsilon$ as a function of the space time density λ_s for the Gaussian receiver at $\alpha = 3$ and a delay constraint $D = 500$.

instantaneous rate in the WANET is given by

$$R = \frac{K}{\tilde{B}} \, 1\left(\tilde{B} \leq D\right) \tag{2.44}$$

and the distribution of R is characterized by the CCDF of $\tilde{B}$. A characterization of the dynamic variations of instantaneous rate is useful in studying the queue sizes and network congestion.

Fig.2.4 shows a plot of the CCDF of packet transmission time $\tilde{B}$ for the Gaussian receiver for 3 different values of λ_s. The values of λ_s correspond to noise limited regime, moderate interference regime and interference limited regime respectively. For all 3 values of λ_s, the analysis curves from Theorem 1 accurately describe the nature of CCDF behavior observed in the simulation curves (the gap between the analysis and simulation widens as λ_s increases). As mentioned above, in all cases the distributions have 'heavy' tails, and there is a small but non negligible probability to get very long packet times. Nevertheless, in the noise limited regime ($\lambda_s = 1 \cdot 10^{-4}$) the variations of the packet time is quite small, and most

packets are transmitted over few tens of symbols. As the interference increases, we see that the variations increase, and we get a significant probability to require any packet time in the range (0,D].

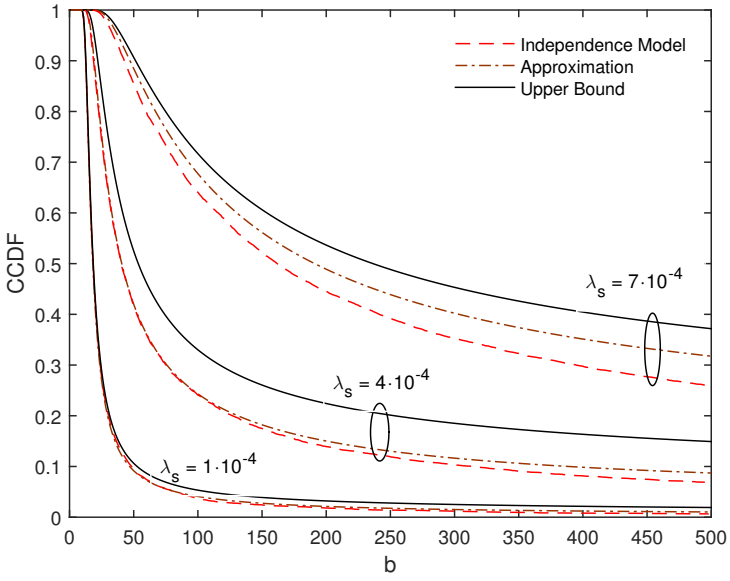

Figure 2.4: A plot of the CCDF of packet transmission time $\tilde{B}$ for the Gaussian receiver for $\lambda_s = \{1, 4, 7\} \cdot 10^{-4}$ at $\alpha = 3$.

To illustrate the dynamics of the packet time variations as a function of λ_s, Figs.2.5 and 2.6 contain plots of the expectation $\mathbb{E}\left[\bar{B}\right]$ and the standard deviation $\mathrm{SD}\left[\bar{B}\right]$ as a function of λ_s for both the exact model and the independence model at $\alpha = 3$. As λ_s increases, the higher interference increases the outage probability and the expected packet time, with $\mathbb{E}\left[\bar{B}\right]$ getting quite close to D. The exact model and independence model have very accurate match in terms of the expected packet time.

In terms of the $\mathrm{SD}\left[\bar{B}\right]$, in low to moderate interference regime, as λ_s increases the additional interferers cause monotonic increase in packet time deviation around the mean, as expected. However in the high interference regime, for a choice of $K = 75$ and $D = 500$, the expected packet time approaching towards

D and the increased fraction of packets in outage reduce the absolute measure of packet time deviation around the mean. To have a monotonic increase in packet time deviation in the interference limited regime, the delay constraint D needs to increase with λ_s accordingly.

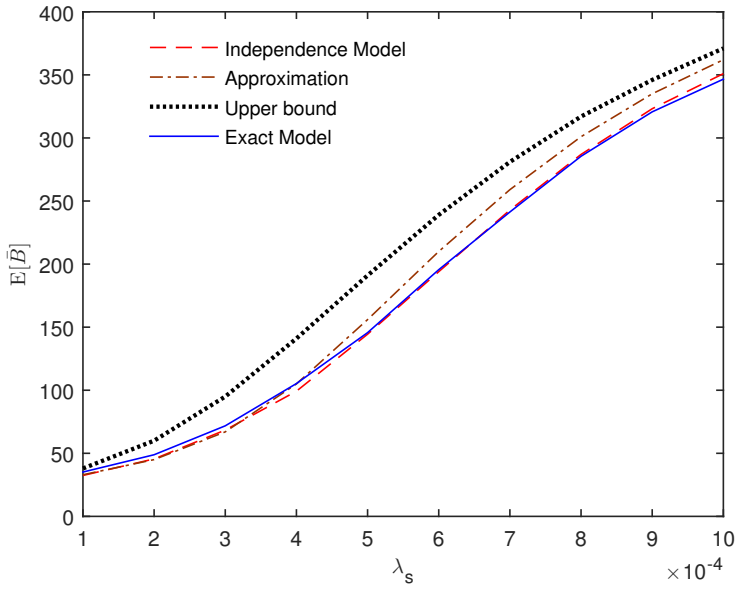

Figure 2.5: A plot of average packet transmission time $\mathbb{E}\left[\bar{B}\right]$ derived from (2.12) as a function of network density λ_s for $\alpha = 3$.

2.6.3 Channel Thresholding

This subsection presents the numerical results corresponding to the channel thresholding approach of section 2.5. For $\beta = 0$, all transmit nodes in the WANET are allowed to transmit and the performance is described by Fig.2.2. First we illustrate the effect of a channel threshold β on the rate density. Fig.2.7 plots the rate density RD from (2.38), normalized by $\lambda_s K$, as a function of the channel threshold β for the nonmatched receiver at $\lambda_s = 5 \cdot 10^{-4}$, $\alpha = 3$ and delay constraint $D = 500$. Initially as β increases above 0, the transmit nodes with poor fading are turned off and this reduces the effective interference in the WANET leading to a

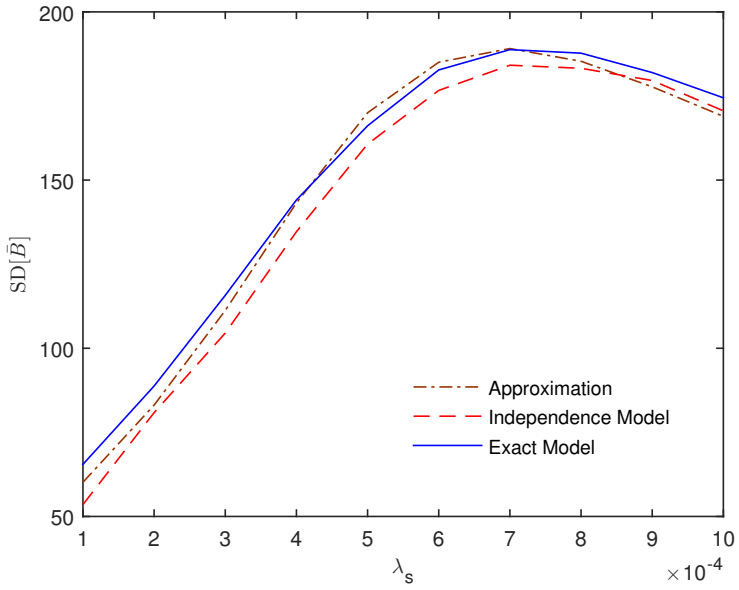

Figure 2.6: A plot of standard deviation of the packet transmission time SD $\left[\bar{B}\right]$ as a function of network density λ_s for $\alpha = 3$.

higher rate density. This nature of rate density increase continues upto a certain β, at which the maximal rate density is attained. Increasing β beyond this point causes p, the fraction of the transmit nodes in the WANET that actually transmit, to be too small and this is not compensated by the gain in the $1 - \epsilon$ term leading to a effective decrease in the rate density.

In the following, we denote by β_D^* the value of β at which the maximal rate density is attained for a delay constraint of D. Fig.2.8 contains a plot of the rate density (RD) as a function of the transmit density λ for both constant power transmission $\beta = 0$ and channel thresholding with $\beta = \beta_D^*$ at $\alpha = 3$. The figure depicts the RD for delay constraints of $D = \{500, 125, 25\}$ and the corresponding optimal threshold values where found to be $\beta_D^* = \{0.4, 0.525, 0.65\}$. While the packet success probability is monotonically increasing with D, this is not the case for the rate density. This difference results from the increase in the expected packet time as D increases (as mentioned above, the expected packet time actually

diverges if D grows to infinity). Thus, a wise choice of D can significantly increase the rate density. As can be seen, in the setup of Fig.2.8, a delay constraint of $D = 125$ is better than the two other alternatives. Note however that in general, decreasing D will increase the packet delay[6] in the network because more packets will fail and will need to wait for the next transmission attempt.

The figure shows that channel thresholding can increase the rate density by $70 - 90\%$ relative to constant power transmission. Note that the gain of channel thresholding is larger for smaller values of D. This is because for smaller values of D, the network has a higher outage and channel thresholding avoids many of these unsuccessful transmissions, and hence reduces the effective interference, thereby increasing the successful transmission of packets and thus, the rate density. In Fig.2.8, we observe that the WANET at $D = 25$ and $D = 125$ has a 90% and 76% increase in rate density from channel thresholding compared to the WANET at $D = 500$ which has a 72% increase.

2.7 Conclusion

In this chapter, we study the achievability of network ERD in a WANET employing fountain codes in the physical layer. The nodes in the WANET are modeled by a homogeneous space time Poisson Point process. The WANET operates under Rayleigh fading, constant power transmission and utilizes pure ALOHA as the medium access protocol. The chapter presents a rateless coding setup in which a packet is transmitted within a single coherence time and it was shown that the achievable rate density can be upto 70% of the ERD. We derive an accurate upper bound to the CCDF of the packet transmission time of a reference receiver and study its behavior. The analysis provides insights into the dynamic variations of packet time and is observed to have a good match with simulation results of WANET performance over a wide range of network parameters.

[6] Packet Delay is defined as the time spent by the packet in the queue (buffer) of a transmit node.

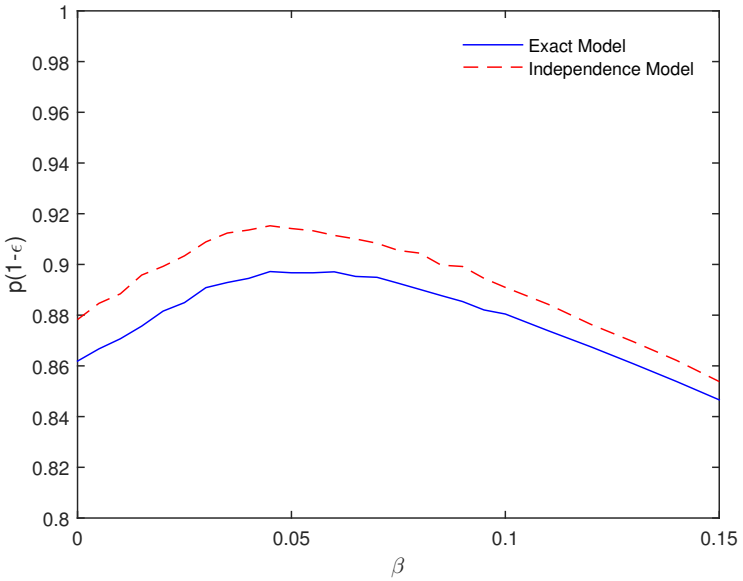

Figure 2.7: A plot of success probability $p\,(1-\epsilon)$ as a function of the channel threshold β for the Gaussian receiver at $\lambda_s = 5 \cdot 10^{-4}$, $\alpha = 3$ and delay constraint $D = 500$.

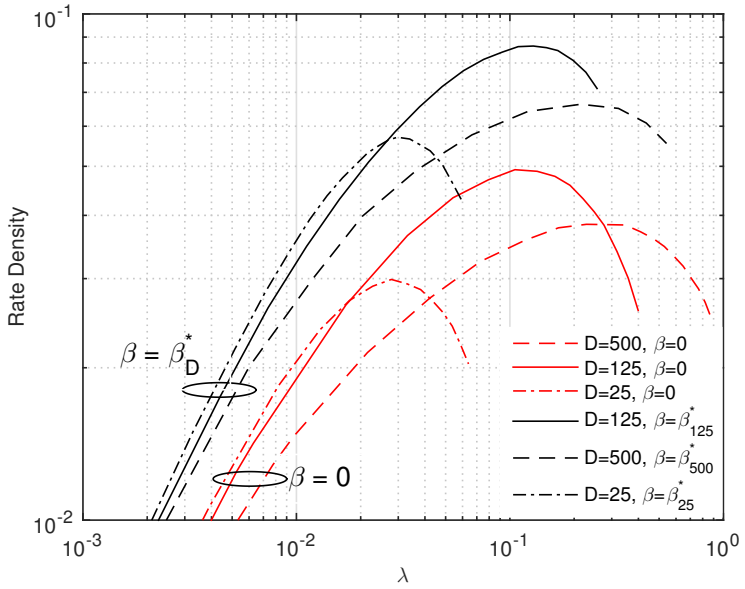

Figure 2.8: A plot of rate density RD as a function of the transmit density λ for both constant transmission power $\beta = 0$ and channel thresholding with $\beta = \beta_D^*$ at $\alpha = 3$ and delay constraint $D = \{500, 125, 25\}$.

The chapter analyzes the performance of both Gaussian and ideal matched receivers. It was shown that the low complexity Gaussian receiver achieves most of the rate density of the ideal matched receiver. Towards improving the rate density in the network, the chapter illustrates that employing power control in the form of channel thresholding can lead to tangible gains relative to constant power transmission.

Based on the results from this chapter, it is known that the rate density loss is caused by packet transmissions over poor fading states and by the presence of interference. Since multiple antenna transmission reception techniques tackle these issues, it is expected that the dynamic variations of packet time tend to cease with the spatial dimension. Hence an interesting future direction would be to investigate the effect of multiple antenna techniques on the achievability of ERD and the variations of packet time in the WANET. Also an addition to the current line of work would be the optimization of rate density for a given outage constraint yielding the optimal operating point for the WANET in terms of the network parameters balancing the rate outage tradeoff.

2.8 Mathematical Proofs

2.8.1 Proof of Theorem 1

An upper bound for P $\left(\tilde{B} > b\right)$ can be obtained based on the observation that for a given b, the event $\tilde{B} > b \Rightarrow$ i.e., necessarily implies the event $K \geq b \log_2 \left(1 + \tilde{\text{SINR}}_a(b)\right)$ and the converse is not true. This fact can be alternatively stated as '$b \log_2 \left(1 + \tilde{\text{SINR}}_a(b)\right)$' is a lower bound to the total number of info bits accumulated upto time b for the

receiver in (2.9) [7] . Thus

$$\begin{aligned} \mathrm{P}\left(\tilde{B} > b\right) &\leq \mathrm{P}\left(K \geq b \log_2\left(1 + \tilde{\mathrm{SINR}}_a(b)\right)\right) \\ &= \mathrm{P}\left(\tilde{\mathrm{SINR}}_a(b) \leq 2^{K/b} - 1\right) \end{aligned} \tag{2.45}$$

Now let $v = 2^{K/b} - 1$. For Rayleigh fading, (2.45) can be written out as

$$\begin{aligned} \mathrm{P}\left(\tilde{\mathrm{SINR}}_a(b) \leq v\right) &= 1 - \mathrm{P}\left(\frac{\rho|h|^2}{1+\tilde{I}_a(b)} \geq v\right) \\ &= 1 - \mathbb{E}\left[\exp\left(-\frac{v}{\rho}\left(1+\tilde{I}_a(b)\right)\right)\right] \\ &= 1 - \exp\left(-\frac{v}{\rho}\right)\ \mathcal{L}_{\tilde{I}_a(b)}\left(\frac{v}{\rho}\right) \end{aligned} \tag{2.46}$$

where $\mathcal{L}_Y(s) = \mathbb{E}\left[e^{-sY}\right]$ is the Laplace transform (LT) of R.V Y.

An expression for $\tilde{I}_a(b)$ the average interference upto time b is given in (2.7). It is in the form of a standard additive shot noise of the spatial PPP Ψ with intensity λ. Hence the LT of $\tilde{I}_a(b)$ is given by [58]

$$\begin{aligned} \mathcal{L}_{\tilde{I}_a(b)}(s) &= \exp\left(-\pi\lambda\mathbb{E}\left[\int_0^\infty \left(1 - e^{-s\rho r^{-\alpha}|h|^2\eta(b)}\right)\ \mathrm{d}r^2\right]\right) \\ \eta(b) &= \frac{1}{b}\int_0^b \tilde{e}(\tau)\ \mathrm{d}\tau = \frac{1}{b}\int_0^b 1\left(T \leq \tau \leq T + \bar{B}\right)\ \mathrm{d}\tau \end{aligned} \tag{2.47}$$

Define $\nu = |h|^2\eta(b)$ and $\delta = 2/\alpha$. From [59], (2.47) can be further simplified as

$$\begin{aligned} \mathcal{L}_{\tilde{I}_a(b)}(s) &= \exp\left(-\pi\lambda\left(s\rho\right)^\delta \Gamma\left(1-\delta\right)\mathbb{E}\left[\nu^\delta\right]\right) \\ &\overset{(a)}{=} \exp\left(-\pi\lambda\left(s\rho\right)^\delta \Gamma\left(1-\delta\right)\mathbb{E}\left[|h|^{2\delta}\right]\mathbb{E}\left[\eta(b)^\delta\right]\right) \end{aligned} \tag{2.48}$$

where (a) follows from the fact that $|h|^2$ and $\eta(b)$ are independent.

For Rayleigh fading, we obtain

$$\mathbb{E}\left[|h|^{2\delta}\right] = \Gamma\left(1+\delta\right) \tag{2.49}$$

[7] The nature of monotonic variation of '$b\log_2\left(1+\tilde{\mathrm{SINR}}_a(b)\right)$' depends on the particular realization of the PPP Ψ.

Combining (2.46)-(2.49) in (2.45) and substituting $\lambda = \lambda_s \; 2N_T$, where $2N_T$ is the length of the interval centred around $T_0 = 0$ over which the interferers transmit packets , the distribution of $\tilde{B}$ can be bounded as

$$\mathrm{P}\left(\tilde{B} > b\right) \leq 1 - \exp\left(- \frac{2^{K/b} - 1}{\rho} - \pi\lambda_s \left(2^{K/b} - 1\right)^{\delta} \right.$$
$$\left. \Gamma\left(1-\delta\right)\Gamma\left(1+\delta\right) \; 2N_T \; \mathbb{E}\left[\eta(b)^{\delta}\right] \right) \tag{2.50}$$

To evaluate the distribution, we need an expression that relates the 'δ' moment of $\eta(b)$ to the distribution of $\tilde{B}$. In Appendix 2.8.6, we show that

$$\mathbb{E}\left[\eta(b)^{\delta}\right] = \frac{1}{2N_T b^{\delta}} \left[\left(b \int_0^b \bar{b}^{\delta} + \frac{1-\delta}{1+\delta} \int_0^b \bar{b}^{1+\delta} + b^{\delta} \int_b^D \bar{b} \right.\right.$$
$$\left.\left. + \frac{1-\delta}{1+\delta} \; b^{1+\delta} \int_b^D \right) \; \mathrm{d}F_{\bar{b}} \right] \tag{2.51}$$
$$F_{\bar{b}} = \mathrm{P}\left(\bar{B} \leq \bar{b}\right)$$

However, the joint solution of (2.50) and (2.51) is still complicated, as we need to tune the whole CCDF. We need another significant step in order to simplify it to the single parameter tuning of Theorem 1. To illustrate the concept, consider the case $\delta = 1$. From (2.51), it is easy to check that

$$\mathbb{E}\left[\eta(b)\right] = \mathbb{E}\left[\bar{B}\right] / 2N_T \tag{2.52}$$

The expected interferer packet time $\mathbb{E}\left[\bar{B}\right]$ is given by

$$\mathbb{E}\left[\bar{B}\right] = \int_0^D \mathrm{P}\left(\tilde{B} > b\right) \; \mathrm{d}b \tag{2.53}$$

Let's define a parameter $\mu = \mathbb{E}\left[\bar{B}\right]$. The parameter μ is plugged into the bound in (2.50) and tuned to match the upper bound into a distribution. The tuned parameter μ^* is obtained as a solution to the equation (2.15) and is easily obtained by numerical integration methods.

Unfortunately the expression for $\mathbb{E}\left[\eta(b)^{\delta}\right]$ in (2.51) does not involve explicit moments of $\bar{B}$, except for special cases of b and δ. To simplify our bound for the general case, we next derive an upper bound on $\mathbb{E}\left[\eta(b)^{\delta}\right]$. This bound is obtained by rewriting (2.51) as an $\mathbb{E}[\cdot]$ operation over a function of $\bar{B}$,

$$\begin{aligned}\mathbb{E}\left[\eta(b)^{\delta}\right] &= \frac{1}{2N_T b^{\delta}}\,\mathbb{E}\Bigg[b\;\bar{B}^{\delta}\;1\left(\bar{B}<b\right)+b^{\delta}\;\bar{B}\;1\left(\bar{B}>b\right)\\ &\qquad+\frac{1-\delta}{1+\delta}\left(\bar{B}^{1+\delta}\;1\left(\bar{B}<b\right)+b^{1+\delta}\;1\left(\bar{B}>b\right)\right)\Bigg]\\ &\equiv \frac{1}{2N_T b^{\delta}}\,\mathbb{E}\left[g\left(\bar{B}\right)\right] \end{aligned} \tag{2.54}$$

In Appendix 2.8.2, we show that the function $g\left(\bar{B}\right)$ in (2.54) is concave in $\bar{B}$. Thus the upper bound on $\mathbb{E}\left[g\left(\bar{B}\right)\right]$, given in (2.14), follows from Jensen's inequality for concave functions. This bound completes the proof of Theorem 1 and allows the evaluation of the CCDF upper bound using single parameter tuning μ.

A concave function can also be lower bounded by a linear function between the edges of the considered region. This lower bound,which is given in (2.16), leads to a good approximation of the CCDF.

2.8.2 Concavity of $g\left(\bar{B}\right)$

From (2.54), the function $g\left(\bar{B}\right)$ is written out as

$$g\left(\bar{B}\right)=\begin{cases} b\;\bar{B}^{\delta}+\frac{1-\delta}{1+\delta}\bar{B}^{1+\delta}, & \bar{B}\le b\\ b^{\delta}\;\bar{B}+\frac{1-\delta}{1+\delta}b^{1+\delta}, & \bar{B}>b\end{cases} \tag{2.55}$$

The concavity can be verified easily by checking the 2^{nd} derivative of $g\left(\bar{B}\right)$. It is given by

$$\frac{\mathrm{d}^2 g}{\mathrm{d}\bar{B}^2}=\begin{cases} b\;\delta\left(\delta-1\right)\;\bar{B}^{\delta-2}+\left(1-\delta\right)\delta\;\bar{B}^{\delta-1}, & \bar{B}\le b\\ 0, & \bar{B}>b\end{cases} \tag{2.56}$$

The 2^{nd} derivative in (2.56) is simplified as

$$\frac{\mathrm{d}^2 g}{\mathrm{d}\bar{B}^2} = \begin{cases} \delta\,(1-\delta)\;\; \bar{B}^{\delta-1}\left(1-\frac{b}{\bar{B}}\right), & \bar{B} \le b \\ 0, & \bar{B} > b \end{cases} \tag{2.57}$$

From (2.57), it is easy to check that $\frac{\mathrm{d}^2 g}{\mathrm{d}\bar{B}^2} \le 0$ for $0 \le \bar{B} \le D$.

Concavity of $g\left(\bar{B}\right)$ leads to the following upper and lower bounds on $\mathbb{E}\left[g\left(\bar{B}\right)\right]$.

Lower Bound

Since $g\left(\bar{B}\right)$ is concave in $\bar{B}$ over $(0, D)$, a linear lower bound is given as

$$g\left(\bar{B}\right) \ge \left(1-\frac{\bar{B}}{D}\right) g\,(0) + \frac{\bar{B}}{D}\; g\,(D) \tag{2.58}$$

$$g\,(0) = 0 \tag{2.59}$$

$$g\,(D) = b^{\delta} D + \frac{1-\delta}{1+\delta}\; b^{1+\delta} \tag{2.60}$$

$$\begin{aligned} \mathbb{E}\left[g\left(\bar{B}\right)\right] &\ge \mathbb{E}\left[\bar{B}\right] \frac{g\,(D)}{D} \\ &= \mathbb{E}\left[\bar{B}\right]\;\; b^{\delta}\left(1+\frac{1-\delta}{1+\delta}\frac{b}{D}\right) \end{aligned} \tag{2.61}$$

Upper Bound

Using Jensen's inequality for concave functions, an upper bound for $\mathbb{E}\left[g\left(\bar{B}\right)\right]$ is given as

$$\begin{aligned}\mathbb{E}\left[g\left(\bar{B}\right)\right] &\leq g\left(\mathbb{E}\left[\bar{B}\right]\right) \\ &= \Bigg[b\ \mathbb{E}\left[\bar{B}\right]^{\delta}\ 1\left(\mathbb{E}\left[\bar{B}\right] < b\right) + b^{\delta}\ \mathbb{E}\left[\bar{B}\right] \\ &\quad 1\left(\mathbb{E}\left[\bar{B}\right] < b\right) + \frac{1-\delta}{1+\delta}\left(\mathbb{E}\left[\bar{B}\right]^{\delta}\ 1\left(\mathbb{E}\left[\bar{B}\right] < b\right)\right. \\ &\quad \left. + b^{1+\delta}\ 1\left(\mathbb{E}\left[\bar{B}\right] > b\right)\right)\Bigg] \\ &= b^{\delta}\ \mathbb{E}\left[\bar{B}\right]^{\delta} \max\left(b, \mathbb{E}\left[\bar{B}\right]\right)^{1-\delta} + \frac{1-\delta}{1+\delta} \\ &\quad \min\left(b, \mathbb{E}\left[\bar{B}\right]\right)^{1+\delta} \end{aligned} \tag{2.62}$$

2.8.3 Heavy Tail of CCDF upper bound

We observe the scaling of P_u in (2.12) as $b \to \infty$. Based on (2.54) and (2.61), the lower bound for $\mathbb{E}\left[\eta(b)^{\delta}\right]$ is $O(1)$. This result along with the definition of $\eta(b)$ in (2.8) indicates that $\mathbb{E}\left[\eta(b)^{\delta}\right] = O(1)$. Now the function $2^{K/b}$ is given a Taylors series expansion as $b \to \infty$

$$2^{K/b} = 1 + \frac{K}{b}\log 2 + \left(\log 2\ \frac{K}{b}\right)^{2} + O\left(\frac{1}{b^{3}}\right) \tag{2.63}$$

Using (2.63) in (2.12) for both the noise and interference terms, the asymptotic scaling of P_u as $b \to \infty$ is given as

$$P_u = 1 - \exp\left(O\left(\frac{1}{b^{\delta}}\right)\right) \tag{2.64}$$

Since $1 - \exp\left(-ax\right) = ax + O\left(x^{2}\right)$ as $x \to 0$, it is observed from (2.64) that P_u has a heavy tail distribution with parameter 'δ'[8] .

[8] Such a heavy tail nature is reported for the distribution of session duration in [60] which performs an empirical study of the distribution and dependence structure of session size, duration

2.8.4 Proof of Theorem 2

As mentioned in section 2.4.1, the CCDF of $\tilde{B}$ depends on the distribution of the achievable rate $\tilde{C}(b)$. So we proceed by first developing a novel lower bound for the achievable rate $\tilde{C}(b)$. In that direction, let us define an event $\mathcal{E}$ as

$$\begin{aligned}\mathcal{E} : &\text{ Strongest interference at } \mathrm{Rx}_0 \text{ in the interval} \\ &(0, b) < \gamma_{th}\end{aligned} \tag{2.65}$$

where γ_{th} is the interference threshold.

A lower bound on the achievable rate $\tilde{C}(b)$ is derived as follows

$$\tilde{C}(b) = \mathrm{P}\left(\mathcal{E}\right)\tilde{C}(b)\big|\mathcal{E} + \mathrm{P}\left(\mathcal{E}_c\right)\tilde{C}(b)\big|\mathcal{E}_c \tag{2.66}$$

$$\begin{aligned}\tilde{C}(b) &\geq \mathrm{P}\left(\mathcal{E}\right)\tilde{C}(b)\big|\mathcal{E} \\ \tilde{C}(b) &\geq \mathrm{P}\left(\mathcal{E}\right)\log_2\left(1 + \tilde{\mathrm{SINR}}_a\left(b\right)\big|\mathcal{E}\right)\end{aligned} \tag{2.67}$$

where (2.67) follows by noting that the spectral efficiency term $\log_2\left(1 + \tilde{\mathrm{SINR}}\left(b\right)\right)$ is a convex function of $\tilde{I}(b)$ and subsequently applying Jensen's inequality for convex functions to $\tilde{C}(b)\big|\mathcal{E}$.

In Appendix 2.8.5, the following expression for $\mathrm{P}\left(\mathcal{E}\right)$ is derived.

$$\begin{aligned}\mathrm{P}\left(\mathcal{E}\right) &= \exp\left(-\pi\lambda_s\left(\frac{\rho}{\gamma_{th}}\right)^{\delta}\Gamma\left(1+\delta\right)\left(b + \mathbb{E}\left[\bar{B}\right]\right)\right) \\ &\triangleq \exp(-\mu)\end{aligned} \tag{2.68}$$

---

and rate.

An upper bound on the CCDF of packet transmission time $\tilde{B}$ is derived below.

$$\begin{aligned}
\mathrm{P}\left(\tilde{B} > b\right) &= \mathrm{P}\left(\frac{K}{b} \geq \tilde{C}(b)\right) \\
&\leq \mathrm{P}\left(\frac{K}{b} \geq \mathrm{P}\left(\mathcal{E}\right) \log_2\left(1 + \mathrm{S\tilde{I}\tilde{N}R}_a\left(b\right) \middle| \mathcal{E}\right)\right) \\
&\overset{(a)}{=} \mathrm{P}\left(\frac{Ke^{\mu}}{b} \geq \log_2\left(1 + \mathrm{S\tilde{I}\tilde{N}R}_a\left(b\right) \middle| \mathcal{E}\right)\right) \\
&\overset{(b)}{=} \mathrm{P}\left(2^{\frac{K'}{b}} - 1 \geq \mathrm{S\tilde{I}\tilde{N}R}_a\left(b\right) \middle| \mathcal{E}\right) \\
&\overset{(c)}{=} 1 - e^{-\frac{v'}{\rho}}\ \mathcal{L}_{\tilde{I}_a(b)}\left(\frac{v'}{\rho}\right) \middle| \mathcal{E}
\end{aligned} \tag{2.69}$$

where (a) follows from the expression for $\mathrm{P}\left(\mathcal{E}\right)$ in Appendix 2.8.5, substituting $K' = Ke^{\mu}$ leads to (b) and applying (2.46) to (b) with the substitution $v' = 2^{\frac{K'}{b}} - 1$ yields (c).

The Laplace transform of $\tilde{I}_a(b)\big|\mathcal{E}$ is given by [61, 62]

$$\begin{aligned}
\mathcal{L}_{\tilde{I}_a(b)}\left(s\right) \big| \mathcal{E} &= \exp\Bigg(- \lambda\pi\mathbb{E}\Bigg[\int_{\left(\frac{\rho|h|^2\eta(b)}{\gamma_{th}}\right)^{\frac{1}{\alpha}}}^{\infty} \Big(1 - \\
&\qquad e^{-s\rho r^{-\alpha}|h|^2\eta(b)}\Big)\ \mathrm{d}r^2 \Bigg]\Bigg)
\end{aligned} \tag{2.70}$$

$$\begin{aligned}
&= \exp\Bigg(- \lambda\pi\mathbb{E}\Bigg[\int_{s\gamma_{th}}^{0} \left(1 - e^{-u}\right) \\
&\qquad \mathrm{d}\left(s\rho|h|^2\eta(b)u^{-1}\right)^{\delta} \Bigg]\Bigg)
\end{aligned} \tag{2.71}$$

where (2.71) follows from (2.70) using the substitution $u = s\rho|h|^2\eta(b)r^{-\alpha}$. Further (2.71) can be simplified as

$$\begin{aligned}
\mathcal{L}_{\tilde{I}_a(b)}\left(s\right) \big| \mathcal{E} = \exp\Bigg[&- \lambda_s\pi\left(s\rho\right)^{\delta} \mathbb{E}\left[|h|^{2\delta}\right] 2N_T\mathbb{E}\left[\eta(b)^{\delta}\right] \\
&\int_{s\gamma_{th}}^{0} \left(1 - e^{-u}\right)\ \mathrm{d}u^{-\delta} \Bigg]
\end{aligned} \tag{2.72}$$

Defining the integral in the exponent of (2.72) as a function $G\left(\gamma_{th}\right)$, the LT is written as

$$\mathcal{L}_{\tilde{I}_{a(b)}}\left(s\right)\left|\mathcal{E}=\exp\left[-\lambda_s\pi\left(s\rho\right)^{\delta}\Gamma\left(1+\delta\right)G\left(\gamma_{th}\right)\right.\right.$$
$$\left.\left.2N_T\mathbb{E}\left[\eta(b)^{\delta}\right]\right]\right. \tag{2.73}$$

$$G\left(\gamma_{th}\right)=\int_{s\gamma_{th}}^{0}\left(1-e^{-t}\right)\ \mathrm{d}t^{-\delta}$$
$$=\int_{0}^{s\gamma_{th}}t^{-\delta}e^{-t}\ \mathrm{d}t-\frac{1-e^{-s\gamma_{th}}}{\left(s\gamma_{th}\right)^{\delta}} \tag{2.74}$$

Plugging (2.73) back in (2.69), the CCDF upper bound can be written as

$$\mathrm{P}\left(\tilde{B}>b\right)\leq 1-\exp\left(-\frac{2^{K'/b}-1}{\rho}-\pi\lambda_s\left(2^{K'/b}-1\right)^{\delta}\right.$$
$$\left.G\left(\gamma_{th}\right)\Gamma\left(1+\delta\right)\ 2N_T\ \mathbb{E}\left[\eta(b)^{\delta}\right]\right) \tag{2.75}$$

The bound in (2.75) is similar to (2.50) in Theorem 1. The remainder of the proof follows the same arguments as in Appendix 2.8.1 after (2.50).

2.8.5 An expression for $\mathrm{P}\left(\mathcal{E}\right)$

An expression for the $\mathrm{P}\left(\mathcal{E}\right)$ term is derived now. The interference power from transmitter i at receiver 0 in the interval $(0,b)$ is given by

$$\gamma_i=\rho|h_i|^2|X_i|^{-\alpha}S_i \tag{2.76}$$

where

$$S_i=1\left(-\bar{B}_i\leq T_i\leq b\right) \tag{2.77}$$

measures the presence of an interferer 'i' during the interval $(0, b)$. Now

$$\begin{aligned} \mathrm{P}\left(\mathcal{E}\right) &= \mathrm{P}\left(\max_{i\in\Psi}\gamma_i \leq \gamma_{th}\right) \\ &= \prod_{i\in\Psi}\mathrm{P}\left(\gamma_i \leq \gamma_{th}\right) \\ &= \mathbb{E}\left[\prod_{i\in\Psi} 1\left(\gamma_i \leq \gamma_{th}\right)\right] \end{aligned} \tag{2.78}$$

The RHS of (2.78) takes on the form of a standard PGFL of PPP Ψ. The PGFL of a PPP Ψ with density λ and a function $v(X_i)$ is given by [59]

$$\mathbb{E}\left[\prod_{i\in\Psi} v(X_i)\right] = \exp\left(-\lambda\ \mathbb{E}\left[\int_{\mathbb{R}^2}\left(1-v(x)\right)\ \mathrm{d}x\right]\right) \tag{2.79}$$

Combining (2.76)-(2.79), the expression for $\mathrm{P}\left(\mathcal{E}\right)$ in (2.78) is written as

$$\begin{aligned} \mathrm{P}\left(\mathcal{E}\right) &= \exp\left(-\lambda\ \mathbb{E}\left[\int_{\mathbb{R}^2} 1\left(\rho|h|^2|x|^{-\alpha}S \geq \gamma_{th}\right)\ \mathrm{d}x\right]\right) \\ &= \exp\left(-\lambda\ \mathbb{E}\left[\int_0^\infty 1\left(\rho|h|^2 r^{-\alpha}S \geq \gamma_{th}\right)\pi\ \mathrm{d}r^2\right]\right) \end{aligned} \tag{2.80}$$

Let us define $A = \left(\rho|h|^2 S/\gamma_{th}\right)^{1/\alpha}$, then (2.80) can be simplified as

$$\begin{aligned} \mathrm{P}\left(\mathcal{E}\right) &= \exp\left(-\lambda\pi\ \mathbb{E}\left[\int_0^A \mathrm{d}r^2\right]\right) \\ &= \exp\left(-\lambda\pi\left(\frac{\rho}{\gamma_{th}}\right)^{\delta}\ \mathbb{E}\left[|h|^{2\delta}\right]\mathbb{E}\left[S^{\delta}\right]\right) \end{aligned} \tag{2.81}$$

Now the 'δ' moment of S is expressed as

$$\begin{aligned} \mathbb{E}\left[S^{\delta}\right] &= \mathbb{E}\left[1\left(-\bar{B} \leq T \leq b\right)\right] \\ &= \iint 1\left(-\bar{b} \leq t \leq b\right)\ \mathrm{d}F_t\ \mathrm{d}F_{\bar{b}} \\ &= \int\int_{-\bar{b}}^{b} \frac{1}{2N_T}\,\mathrm{d}t\ \mathrm{d}F_{\bar{b}} \\ &= \frac{b+\mathbb{E}\left[\bar{B}\right]}{2N_T} \end{aligned} \tag{2.82}$$

Using (2.82) in (2.81), $\mathrm{P}\left(\mathcal{E}\right)$ can be expressed as

$$\mathrm{P}\left(\mathcal{E}\right) = \exp\left(-\lambda_s \pi \left(\frac{\rho}{\gamma_{th}}\right)^{\delta} \Gamma\left(1+\delta\right)\left(b + \mathbb{E}\left[\bar{B}\right]\right)\right) \tag{2.83}$$

2.8.6 Proof of (2.51)

An expression for $\mathbb{E}\left[\eta(b)^{\delta}\right]$ is derived.

$$\mathbb{E}\left[\eta(b)^{\delta}\right] = \frac{1}{b^{\delta}}\mathbb{E}\left[\left(\int_0^b 1\left(T \le \tau \le T + \bar{B}\right)\ \mathrm{d}\tau\right)^{\delta}\right] \tag{2.84}$$

$\eta(b)$ is a function of r.v's T and $\bar{B}$. For the PPP Ψ, it is assumed that $T \sim \mathrm{Unif}\left[-N_T, N_T\right]$. Defining $F_{\bar{b}} = \mathrm{P}\left(\bar{B} \le \bar{b}\right)$, the $\mathbb{E}[\cdot]$ in (2.84) can be evaluated as

$$\begin{aligned}
\mathbb{E}\left[\eta(b)^{\delta}\right] = \frac{1}{2N_T b^{\delta}}\Bigg[\Bigg(&\iint_{t\ge 0, t+\bar{b}\le b} \bar{b}^{\delta} + \iint_{t\ge 0, t+\bar{b}\ge b} \\
&(b-t)^{\delta} + \iint_{-\bar{b}\le t\le 0, t+\bar{b}\le b} \left(t+\bar{b}\right)^{\delta} + \\
&\iint_{-\bar{b}\le t\le 0, t+\bar{b}\ge b} b^{\delta}\Bigg)\ \mathrm{d}t\ \ \mathrm{d}F_{\bar{b}}\Bigg] \qquad (2.85)\\
\overset{(a)}{=} \frac{1}{2N_T b^{\delta}}\Bigg[\Bigg(&\int_0^b \int_0^{b-\bar{b}} \bar{b}^{\delta} + \int_0^b \int_{b-\bar{b}}^b (b-t)^{\delta} + \\
&\int_b^D \int_0^b (b-t)^{\delta} + \int_b^D \int_{b-\bar{b}}^0 b^{\delta} + \int_0^b \int_{-\bar{b}}^0 \\
&\left(t+\bar{b}\right)^{\delta} + \int_b^D \int_{-\bar{b}}^{-\bar{b}+b} \left(t+\bar{b}\right)^{\delta}\Bigg)\ \mathrm{d}t\ \ \mathrm{d}F_{\bar{b}}\Bigg] \qquad (2.86)
\end{aligned}$$

where (a) follows by translating the integral regions in (2.85) into explicit ranges on t and $\bar{b}$. Now (2.86) can be further simplified as

$$\begin{aligned}
\mathbb{E}\left[\eta(b)^{\delta}\right] = \frac{1}{2N_T b^{\delta}}\Bigg[\Bigg(&\int_0^b \bar{b}^{\delta}\left(b-\bar{b}\right) + \int_0^b \frac{\bar{b}^{1+\delta}}{1+\delta} + \int_b^D \frac{b^{1+\delta}}{1+\delta} \\
&+ \int_b^D b^{\delta}\left(\bar{b}-b\right) + \int_0^b \frac{\bar{b}^{1+\delta}}{1+\delta} + \int_b^D \frac{b^{1+\delta}}{1+\delta}\Bigg)\ \mathrm{d}F_{\bar{b}}\Bigg]
\end{aligned} \tag{2.87}$$

$$= \frac{1}{2N_T b^{\delta}} \left[\left(b \int_0^b \bar{b}^{\delta} + \frac{1-\delta}{1+\delta} \int_0^b \bar{b}^{1+\delta} + b^{\delta} \int_b^D \bar{b} \right. \right.$$
$$\left. \left. + \frac{1-\delta}{1+\delta}\, b^{1+\delta} \int_b^D \right) \, \mathrm{d}F_{\bar{b}} \right] \tag{2.88}$$

Chapter 3

HARQ in a Cooperative Multihop WANET

In this chapter, we present a study on the performance of the HARQ protocol in a cooperative multihop WANET. In a multihop WANET, the information is transported from source node to the destination node via a set of intermediate relay nodes. In the HARQ protocol considered in this chapter, the different parts of the codeword of an information packet are jointly transmitted by the source and relay(s) nodes, hence the term cooperative WANET. The performance of a multihop WANET is characterized by the transport capacity metric defined as the number of information bits per second communicated reliably over a distance per unit area of the network. The parameters of the HARQ protocol are tuned to balance the tradeoff between the different components of transport capacity and operate the cooperative multihop WANET at maximal transport capacity point. The chapter studies two types of HARQ mechanisms namely the incremental redundancy and repetition time diversity. A partial set of results and material presented in this chapter has been published in [38]. The full material and results presented in this chapter appears in [63].

The organization of the rest of the chapter is outlined below. In Section 3.1, the system model and assumptions are presented. Section 3.2 studies the

transport capacity optimization for both incremental redundancy and repetition time diversity. Section 3.3 presents the numerical results. Section 3.4 contains the conclusions.

3.1 System Model

We consider a wireless adhoc multihop network in which nodes are modeled as a 2-D homogeneous Poisson point process (PPP) $\Phi = \{X_i\}$ of intensity $\lambda\ m^{-2}$, where X_i denotes the i^{th} node coordinates. Due to the homogeneous PPP assumption, the performance of the entire network can be quantified by the analysis of a typical source-destination communication. Without loss of generality, we assume that the source node is located at the origin and the destination is located at an asymptotic distance along the X-axis (See Fig.**??**). Conditioning on the source node at the origin does not affect the distribution of the homogeneous PPP Φ (See Slivnyak's theorem [64] for more details).

The MAC layer uses the spatial reuse ALOHA protocol[16]. The physical communication resource consists of orthogonal discrete time slots. In every time slot, a node either transmits data with MAP p or receives data with probability $1-p$. The decision process to either transmit or receive data is independent from slot to slot and across users. The parent PPP Φ can be split into 2 independent PPP's Φ^t and Φ^r of intensities $\lambda p\ m^{-2}$ and $\lambda(1-p)\ m^{-2}$ respectively.

Each slot period is split into 2 phases,
1) In the 1^{st} phase, a node $\in \Phi^t$ transmits either its own data packet or a data packet of another source node.
2) In the 2^{nd} phase, a distributed relay selection process selects one node $\in \Phi^r$ as the forwarding relay for the next hop communication. The relay selection process makes use of a signalling burst period[16]. A node $\in \Phi^r$ that can be a potential relay encodes its progress into a bit sequence of fixed length. During the signalling burst period, a node listens to the medium for every 0 bit in the encoded sequence and if it detects a 1 bit broadcast from another node, then quits

the relay selection process. On the other hand, if a node gets to broadcast a 1 bit during the signalling burst period, then it will be selected as the forwarding relay since it has the most progress towards destination. More details about the relay selection procedure can be found in the section VIII.B of [16].

It is beyond the scope of this chapter to give a detailed traffic model description. From [16], we use the basic traffic model assumptions of a mean value of τ fresh packets per slot per source-destination pair and a service rate of p per node.

The received signal at a receive node $v \in \mathbb{R}^2$ w.r.t the transmit node at origin is given by

$$\mathrm{y} = h_0|v|^{-\alpha/2}\mathrm{x}_0 + \sum_{k\in\Phi^t} h_k|v - X_k|^{-\alpha/2}\mathrm{x}_k + \mathrm{z} \tag{3.1}$$

where $h_k \sim \mathcal{CN}(0,1)$ is the Rayleigh fading coefficient, x_k is the message symbol and α is the path loss exponent. In (3.1), 1^{st} term represents the desired signal, 2^{nd} term represents the interference and z is the additive Gaussian noise.

The instantaneous SINR at receive node $v \in \mathbb{R}^2$ w.r.t the transmit node at origin is given by

$$\mathrm{SINR}_{v,0} = \frac{\rho|h_0|^2|v|^{-\alpha}}{\sum_{k\in\Phi^t}\rho|h_k|^2|v - X_k|^{-\alpha} + \sigma^2}, \tag{3.2}$$

where σ^2 is the noise power and ρ is the transmit power. In this chapter, we perform analysis in the interference limited regime i.e., $\sigma^2 = 0$. The effect of noise on the performance analysis is discussed later in the chapter.[1]

In this chapter, we study 2 types of HARQ mechanisms namely, incremental redundancy and repetition time diversity. In the next 2 subsections, we present the analysis framework for incremental redundancy and repetition time diversity respectively.

3.1.1 Incremental Redundancy

Each source node which has a data packet to transmit, encodes b information bits into a N-symbol codeword. Based on a puncturing process, the codeword is split

[1] Throughout the chapter, the R.V. $\mathrm{SIR}_{v,0}$ refers to (3.2) with $\sigma^2 = 0$.

into $M = 2$ non-overlapping blocks of length $L = \frac{N}{M}$. The source transmits the 1^{st} block at code rate $R = \frac{b}{L}$. An important property of the puncturing process to note is that the 1^{st} block of the codeword is sufficient to decode the information bit vector.

From among the nodes $\in \Phi^r$ that decode the data packet after receiving the 1^{st} block from the source, the node which offers the most progress towards the destination node is selected opportunistically as the forwarding relay. The progress achieved during the 1^{st} hop communication is given by [16]

$$\mathrm{D}_1\left(\Phi, R, p\right) = \max_{i \in \Phi^r} \left[\mathbf{1}\big(I_{i,0} \geq R | \Phi^t\big) \ |X_i| \cos\left(\theta\left(X_i\right)\right) \right] \tag{3.3}$$

where $I_{i,0} = \log_2\left(1 + \mathrm{SIR}_{i,0}\right)$ is the mutual information (MI) achieved by receive node i during 1^{st} hop communication from the source node at origin and $\mathbf{1}\left(\cdot\right)$ is the indicator function. As mentioned earlier, the destination node is at an asymptotic distance along the X-axis and the expression for 1^{st} hop progress in (3.3) considers the progress offered by each relay node in the X-axis direction as measured by the $|X_i| \cos\left(\theta\left(X_i\right)\right)$ term.

Since the forwarding relay n_1 is able to decode the data packet, it can re-generate the 2^{nd} block of the codeword. During the 2^{nd} hop communication, the forwarding relay n_1 transmits the 2^{nd} block of the codeword at rate R and the total progress upto the 2^{nd} hop is given by

$$\begin{aligned} \mathrm{F}_{ir}\left(\Phi, R, p\right) = \max_{i \in \Phi^r} \Bigg[& \mathbf{1}\Bigg(I_{i,0} + I_{i,Y_1} \geq R | \Phi^t, Y_1 \Bigg) \\ & |X_i| \cos\left(\theta\left(X_i\right)\right) \Bigg] \end{aligned} \tag{3.4}$$

where $Y_1 \sim \mathrm{D}_1$ in (3.3) and $I_{i,Y_1} = \log_2\left(1 + \mathrm{SIR}_{i,Y_1}\right)$ is the MI achieved by receive node i during 2^{nd} hop communication from the forwarding relay n_1. In SIR_{i,Y_1}, Y_1 denotes the x-coordinate of the forwarding relay n_1 and we assume the y-coordinate to be 0 for the sake of analytical tractability. The conditioning inside the $1\left(\right)$ function is for keeping the individual terms of the max operator a pure

function of the PPP Φ^r, so that RHS of (3.3 represents a extremal shot noise of the PPP Φ^r.

The progress achieved during the 2^{nd} hop communication is

$$\mathrm{D}_{ir}\left(\Phi, R, p\right) = \mathrm{F}_{ir}\left(\Phi, R, p\right) - \mathrm{D}_1\left(\Phi, R, p\right) \tag{3.5}$$

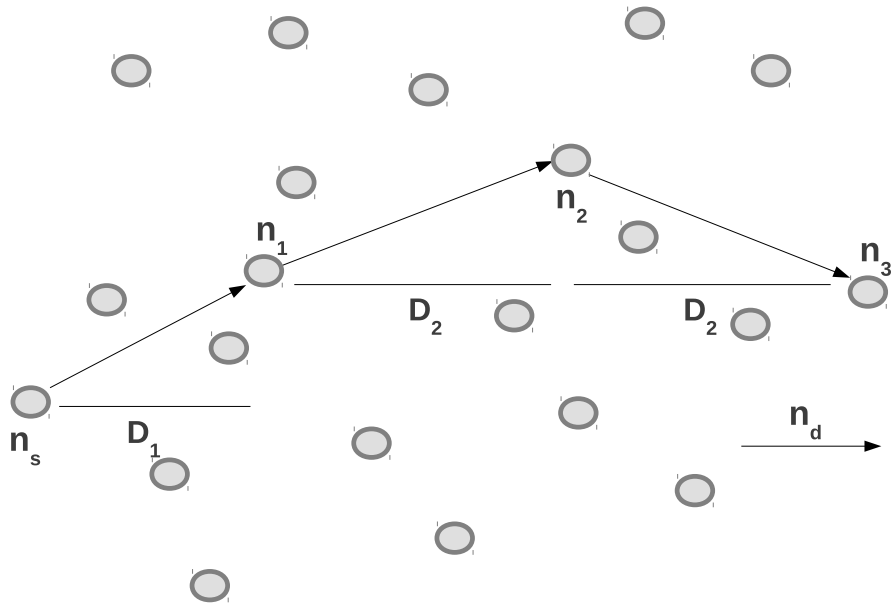

Figure 3.1: Source node n_s transmits the 1^{st} block of the codeword. Relay n_1 decodes the data packet using the 1^{st} block from n_s and offers the most progress D_1 towards destination n_d, which is at an asymptotic distance from n_s along the x-axis. Relays n_2 and n_3 decode the data packet using the blocks from $\{n_s, n_1\}$ and $\{n_1, n_2\}$ respectively and offer the progress D_2 in the direction of the destination. ($\{n_s, n_1, n_2, n_3, n_d\}$ are symbols used for illustration only and do not carry mathematical definition.)

Fig.3.1 shows a typical source-destination communication route for $M = 2$. The hop $n_s - n_1$ uses 1 block of the codeword to decode the data packet and its

progress is D_1 given in (3.3). The hops $n_1 - n_2$ and $n_2 - n_3$ use 2 blocks of the codeword to decode the data packet with progress D_{ir} given in (3.5). Intermediate relays selected for forwarding the packets transmit one block of the codeword at the same code rate R.

To measure the transport capacity as per [18], we consider a typical snapshot of the network at any point of time and measure the progress rate density. Every hop in the network has a fixed rate R bps/Hz. The spatial density of transmissions is $\lambda p\ m^{-2}$. The spatial expected progress is

$$d_{ir}\left(R,p\right)=\mathbb{E}_{\Phi,Y_1,|h|^2}\Big[\mathrm{D}_{ir}\left(\Phi,R,p\right)\Big] \tag{3.6}$$

where the $\mathbb{E}\left[\cdot\right]$ is taken w.r.t PPP Φ, forwarding relay location Y_1 and fading $|h|^2$. (The exact spatial expected progress is $q\ d_{ir}\left(R,p\right)+\left(1-q\right)\ d_1\left(R,p\right)$, where q is the spatial probability of a receiving node of an arbitrary hop using 2 blocks of a codeword to decode the data packet and

$$d_1\left(R,p\right)=\mathbb{E}_{\Phi,|h|^2}\left[\mathrm{D}_1\left(\Phi,R,p\right)\right] \tag{3.7}$$

But for the purpose of analytical tractability, we focus only on the upper bound $d_{ir}\left(R,p\right)$.)

Hence the transport capacity of the network C_{ir} is given by

$$C_{ir}=R\ \lambda p\ d_{ir}\left(R,p\right) \tag{3.8}$$

The tradeoff between the transport capacity submetrics in (3.8) is captured by the network design problem of optimizing the transport capacity w.r.t the MAP p and coding rate R.

3.1.2 Repetition Time Diversity

Each source node which has a data packet to transmit, encodes b information bits into a N-symbol packet. The source and the intermediate relays selected for forwarding the packets transmit the N-symbol packet at the code rate $R=\frac{b}{N}$.

During the 1^{st} hop communication from source to forwarding relay n_1, the progress achieved is D_1 in (3.3). During the 2^{nd} hop communication, the forwarding relay n_1 transmits the same N-symbol packet as the source at rate R and the total progress upto the 2^{nd} hop is given by

$$\mathrm{F}_{rtd}\left(\Phi, R, p\right) = \max_{i \in \Phi^r} \Bigg[\mathbf{1}\Big(\mathrm{SIR}_{i,0} + \mathrm{SIR}_{i,Y_1} \geq 2^R - 1 | \Phi^t, Y_1 \Big) \\ |X_i| \cos\left(\theta\left(X_i\right)\right) \Bigg] \tag{3.9}$$

The progress achieved during the 2^{nd} hop communication is $\mathrm{D}_{rtd} = \mathrm{F}_{rtd} - \mathrm{D}_1$. The transport capacity of the network C_{rtd} is given by

$$\begin{aligned} C_{rtd} &= R\ \lambda p\ \mathbb{E}_{\Phi, Y_1, |h|^2}\Big[\mathrm{D}_{rtd}\left(\Phi, R, p\right) \Big] \\ &\equiv R\ \lambda p\ d_{rtd}\left(R, p\right) \end{aligned} \tag{3.10}$$

3.2 Capacity Optimization

In this section, we study the optimization of transport capacity for both the incremental redundancy and repetition time diversity techniques respectively.

3.2.1 Incremental Redundancy

The optimal MAP p_{ir} and coding rate R_{ir} are given by

$$\langle R, p \rangle_{ir} = \arg\max_{R,p} \Big[R\ \lambda p\ d_{ir}\left(R, p\right) \Big] \tag{3.11}$$

Both R_{ir} and p_{ir} are solved by Monte Carlo simulation and the numerical results are presented in section 3.3. In an effort towards obtaining an analytic expression for the objective function in (3.11) and subsequently employ convex optimization methods, we now derive an approximate expression for $d_{ir}\left(R, p\right)$ using the idea of decoding cells, initially introduced in [64] and extended in [19, 38].

Decoding Cell for Incremental Redundancy

A decoding cell Σ_{ir} is defined as

$$\begin{aligned}
\Sigma_{ir} &= \left\{ v \in \mathbb{R}^2 : \; I_{v,0} + I_{v,\eta_1} \geq R \right\} \\
I_{v,0} &= \log_2 \left(1 + \mathrm{SIR}_{v,0}\right), \\
I_{v,\eta_1} &= \log_2 \left(1 + \mathrm{SIR}_{v,\eta_1}\right) \\
\eta_1 &= (d_1, 0)
\end{aligned} \tag{3.12}$$

where η_1 is the expected location of the forwarding relay n_1. The cell Σ_{ir} contains all $v \in \mathbb{R}^2$ that decode the data packet using 2 blocks of the codeword from origin and η_1. The definition of cell Σ_{ir} in (3.12) considers the average location of the forwarding relay n_1 instead of the instantaneous random location as in (3.4), but this relaxation is essential for tractability issues in the further analysis involving Σ_{ir} and also we demonstrate by numerical results in section 3.3 that the relaxation does not undermine the analysis resuts. The homogeneous assumption of PPP Φ facilitates to use the cell area to derive an approximate expression for $d_{ir}\left(R, p\right)$ as shown below.

The average cell area is given by

$$\mathbb{E}\left[|\Sigma_{ir}|\right] = \int_{\mathbb{R}^2} \mathbb{P}_{\Phi^t} \left(I_{v,0} + I_{v,\eta_1} \geq R\right) \; \mathrm{d}v \tag{3.13}$$

Proposition 1. *The average area of the decoding cell for incremental redundancy*

$\mathbb{E}\left[|\Sigma_{ir}|\right]$ *is given as*

$$\mathbb{E}\left[|\Sigma_{ir}|\right] = \frac{\pi}{\lambda p G(\alpha)}\Bigg[\frac{2}{(2^R-1)^\delta} - \frac{e^{-\lambda p G(\alpha)\left(2^R-1\right)^\delta d_1^2/\left(1+\left(2^R-1\right)^\delta\right)}}{1+(2^R-1)^\delta} + \frac{e^{-\lambda p G(\alpha)\left(2^R/2-1\right)^\delta d_1^2/\left(1+\left(2^R/2-1\right)^\delta\right)}}{1+(2^R/2-1)^\delta} - \frac{e^{-\lambda p G(\alpha)\left(2^R/2-1\right)^\delta\left(2^R-1\right)^\delta d_1^2/\left(\left(2^R-1\right)^\delta+\left(2^R/2-1\right)^\delta\right)}}{(2^R-1)^\delta+(2^R/2-1)^\delta}\Bigg]$$

$$G(\alpha) = \pi\delta\Gamma(\delta)\Gamma(1-\delta),\ \Gamma(x) = \int_0^\infty t^{x-1}e^{-t}dt,\ \delta = 2/\alpha \tag{3.14}$$

Proof: The derivation of the $\mathbb{E}\left[|\Sigma_{ir}|\right]$ expression is presented in Appendix 3.5.1. ■

Theorem 3. *The expected progress for incremental redundancy* $d_{ir}(R,p)$ *is approximated by* $\tilde{d}_{ir}(R,p)$*, given as*

$$\tilde{d}_{ir}(R,p) = \frac{\sqrt{|W_{ir}|}+d_1}{2}\left(1-\frac{1-e^{-c_1}}{c_1}\right) - d_1 \tag{3.15}$$

$$|W_{ir}| = \mathbb{E}\left[|\Sigma_{ir}|\right],\ c_1 = \lambda(1-p)|W_{ir}^+|,$$

$$|W_{ir}^+| = \frac{|W_{ir}|+d_1\sqrt{|W_{ir}|}}{2}.$$

Proof: The proof is based on the extension of initial ideas of cells approximation from [19]. Fig.3.2 shows a square W_{ir} centered around the 2 points origin and η_1 such that $|W_{ir}| = \mathbb{E}\left[|\Sigma_{ir}|\right]$. Now $\Phi^r\left(W_{ir}^+\right)$, the nodes of Φ^r in the positive portion of W_{ir}, is Poisson distributed with parameter $c_1 = \lambda(1-p)|W_{ir}^+|$. The nodes of Φ^r in W_{ir}^+ offer a maximum progress of $\left(\sqrt{|W_{ir}|}+d_1\right)/2$. Hence based on the above mentioned properties, an approximate expression for $\mathbb{E}\left[\mathrm{F}_{ir}\right]$ is given

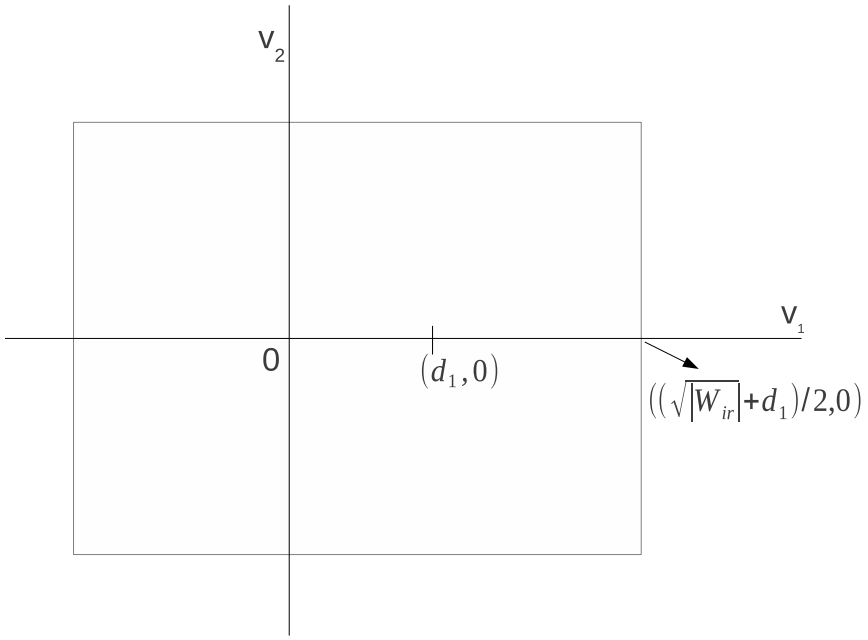

Figure 3.2: A square W_{ir} centered around the 2 points origin and $\eta_1 = (d_1, 0)$ approximates the decoding cell Σ_{ir}. The center of the square is $(d_1/2, 0)$. The maximum progress offered by nodes of Φ^r in W_{ir}^+, the portion of W_{ir} in the positive v_1 axis, is $\left(\sqrt{|W_{ir}|} + d_1\right)/2$.

as

$$\mathbb{E}\big[\mathrm{F}_{ir}\big] \approx \sum_{k=0}^{\infty} \mathbb{E}\Big[\max_{i\leq k}\ U_{i,v_1}\big|\Phi^r\left(W_{ir}^{+}\right)=k\Big]\ \mathbb{P}\big(\Phi^r\left(W_{ir}^{+}\right)=k\big)$$
$$= \frac{\sqrt{|W_{ir}|}+d_1}{2}\ \left(1-\frac{1-e^{-c_1}}{c_1}\right) \tag{3.16}$$

Using (3.5),(3.6) and (3.16), $d_{ir}\left(R,p\right)$ is approximated as

$$\tilde{d}_{ir}\left(R,p\right) = \frac{\sqrt{|W_{ir}|}+d_1}{2}\ \left(1-\frac{1-e^{-c_1}}{c_1}\right) - d_1 \tag{3.17}$$

■

Corollary 2. *The scaling of the approximation to expected progress for incremental redundancy $\tilde{d}_{ir}\left(R,p\right)$ w.r.t the density λ is given as*

$$\tilde{d}_{ir}\left(R,p\right) = O\left(\frac{1}{\sqrt{\lambda}}\right) \tag{3.18}$$

Proof: The following expression for d_1 is derived in [19].

$$d_1 = \frac{\sqrt{|W_1|}}{2}\ \left(1-\frac{1-e^{-c}}{c}\right) \tag{3.19}$$
$$c = \lambda(1-p)|W_1|/2,\ \ |W_1| = \frac{\pi}{\lambda p G\left(\alpha\right)\left(2^R-1\right)^{\delta}}$$

Using (3.19) in (3.17), it is straightforward to rewrite $\tilde{d}_{ir}\left(R,p\right)$ as

$$\tilde{d}_{ir}\left(R,p\right) = \frac{1}{\sqrt{\lambda}}\ J\left(R,p,\alpha\right) \tag{3.20}$$

where $J(\cdot)$ is a function of R,p and α. ■

Based on (3.17), an approximate analytic expression to the transport capacity in (3.8) is given by

$$\tilde{C}_{ir} = R\ \lambda p\ \left[\frac{\sqrt{|W_{ir}|}+d_1}{2}\ \left(1-\frac{1-e^{-c_1}}{c_1}\right) - d_1\right] \tag{3.21}$$

The tradeoff between the submetrics of transport capacity C_{ir} in (3.8) is also captured by its analytic approximation $\tilde{C}_{ir}$. Optimizing the approximation $\tilde{C}_{ir}$

w.r.t coding rate R and MAP p balances the tradeoff between the submetrics without relying on prohibitive Monte Carlo simulations as in (3.11). From (3.18), it is apparent that the transport capacity approximation $\tilde{C}_{ir}$ does not have a tradeoff w.r.t the node density λ and has a scaling of $O\left(\sqrt{\lambda}\right)$.

The coding rate $\tilde{R}_{ir}$ and MAP $\tilde{p}_{ir}$ that optimize the approximation $\tilde{C}_{ir}$ are given by

$$\langle \tilde{R}, \tilde{p} \rangle_{ir} = \arg\max_{R,p} \ \tilde{C}_{ir} \tag{3.22}$$

The objective function $\tilde{C}_{ir}$ is concave and the KKT points are given by

$$\left[\frac{\partial \tilde{C}_{ir}}{\partial R} \ \frac{\partial \tilde{C}_{ir}}{\partial p} \right] = 0 \tag{3.23}$$

which can be solved by gradient descent methods.

3.2.2 Repetition Time Diversity

For repetition time diversity, the optimal MAP p_{rtd} and coding rate R_{rtd} are given by

$$\langle R, p \rangle_{rtd} = \arg\max_{R,p} \left[R \ \lambda p \ d_{rtd}\left(R, p\right) \right] \tag{3.24}$$

Similiar to incremental redundancy in section 3.2.1, we now derive an approximate expression for $d_{rtd}\left(R, p\right)$ and optimize the convex approximation to transport capacity and compare the results with the Monte Carlo based optimization in (3.24).

Decoding Cell for Repetition Time Diversity

A decoding cell Σ_{rtd} is defined as

$$\begin{aligned} \Sigma_{rtd} &= \left\{ v \in \mathbb{R}^2 : \ \mathrm{SIR}_{v,0} + \mathrm{SIR}_{v,\eta_1} \geq 2^R - 1 \right\} \\ \eta_1 &= (d_1, 0) \end{aligned} \tag{3.25}$$

The cell Σ_{rtd} contains all $v \in \mathbb{R}^2$ that decode the data packet using the packet transmissions from origin and η_1.

The average cell area is given by

$$\mathbb{E}\big[|\Sigma_{rtd}|\big] = \int_{\mathbb{R}^2} \mathbb{P}_{\Phi^t}\left(\mathrm{SIR}_{v,0} + \mathrm{SIR}_{v,\eta_1} \geq 2^R - 1\right) \ \mathrm{d}v \tag{3.26}$$

Proposition 2. *The average area of the decoding cell for repetition time diversity* $\mathbb{E}\big[|\Sigma_{rtd}|\big]$ *is given as*

$$\mathbb{E}\big[|\Sigma_{rtd}|\big] = \frac{\pi}{\lambda p G\left(\alpha\right)\left(2^R-1\right)^{\delta}}\left[2 - \frac{e^{-\lambda p G(\alpha)\left(2^R-1\right)^{\delta} d_1^2/2}}{2}\right] \tag{3.27}$$

Proof: Refer to Appendix 3.5.2 for the derivation. ■

Theorem 4. *The expected progress for repetition time diversity* $d_{rtd}\left(R,p\right)$ *is approximated by* $\tilde{d}_{rtd}\left(R,p\right)$*, given as*

$$\begin{aligned}
\tilde{d}_{rtd}\left(R,p\right) &= \frac{\sqrt{|W_{rtd}|}+d_1}{2}\left(1-\frac{1-e^{-c_2}}{c_2}\right) - d_1 \\
|W_{rtd}| &= \mathbb{E}\big[|\Sigma_{rtd}|\big],\ c_2 = \lambda(1-p)|W^{+}_{rtd}|, \\
|W^{+}_{rtd}| &= \frac{|W_{rtd}| + d_1\sqrt{|W_{rtd}|}}{2}.
\end{aligned} \tag{3.28}$$

Proof: The proof of theorem 2 follows the same ideas as in theorem 3. Let W_{rtd} be a square similiar in definition and properties to W_{ir} in theorem 3. Similiar to (3.16), an approximate expression for $\mathbb{E}\big[\mathrm{F}_{rtd}\big]$ is given as

$$\mathbb{E}\big[\mathrm{F}_{rtd}\big] \approx \frac{\sqrt{|W_{rtd}|}+d_1}{2}\left(1-\frac{1-e^{-c_2}}{c_2}\right) \tag{3.29}$$

Using (3.10) and (3.29) along with the fact that $\mathrm{D}_{rtd} = \mathrm{F}_{rtd} - \mathrm{D}_1$, the expected progress $d_{rtd}\left(R,p\right)$ is approximated as

$$\tilde{d}_{rtd}\left(R,p\right) = \frac{\sqrt{|W_{rtd}|}+d_1}{2}\left(1-\frac{1-e^{-c_2}}{c_2}\right) - d_1 \tag{3.30}$$

■

Based on (3.30), an approximate analytic expression to the transport capacity in (3.10) is given by

$$\tilde{C}_{rtd} = R\ \lambda p\ \left[\frac{\sqrt{|W_{rtd}|}+d_1}{2}\left(1-\frac{1-e^{-c_2}}{c_2}\right) - d_1\right] \tag{3.31}$$

Similiar to incremental redundancy, the analytic expression based approximation $\tilde{C}_{rtd}$ allows to study the tradeoff nature of C_{rtd} w.r.t coding rate R and MAP p without relying on Monte Carlo simulations as in (3.24).

The coding rate $\tilde{R}_{rtd}$ and MAP $\tilde{p}_{rtd}$ that optimize the approximation $\tilde{C}_{rtd}$ are given by

$$\langle \tilde{R}, \tilde{p} \rangle_{rtd} = \arg\max_{R,p} \ \tilde{C}_{rtd} \tag{3.32}$$

By the concavity of objective function $\tilde{C}_{rtd}$, the gradient descent methods yield the KKT points

$$\left[\frac{\partial \tilde{C}_{rtd}}{\partial R} \ \frac{\partial \tilde{C}_{rtd}}{\partial p} \right] = 0 \tag{3.33}$$

3.3 Numerical Results

In this section, we present the numerical results for the optimization problems proposed in the incremental redundancy and reptition time diversity sections respectively. A wireless adhoc multihop network where nodes are distributed according to a 2-D homogeneous PPP of intensity λ m^{-2} was simulated[65, 66]. Nodes experience IID Rayleigh fading. The $\mathbb{E}[\cdot]$ operation for obtaining $d_{ir}(R,p)$ and $d_{rtd}(R,p)$ in (3.6) and (3.10) respectively is computed by Monte Carlo averaging. Values of the network parameters used in the simulation were $\lambda = 1$ and $\alpha = [2.5, 4]$, the path loss exponent.

Fig.3.3 shows a plot of the transport capacity C_{ir} in (3.8) and its approximation $\tilde{C}_{ir}$ in (3.21), both normalized by R, against the MAP p for $R = \{1, 3\}$ at $\alpha = 3$. In the low p region, C increases due to the linearity of spatial density λp, but beyond the extremal region of p, for further increase in density, the decrease in progress $d_{ir}(R,p)$ dominates leading to smaller values of C_{ir}. Although the numerical values of C_{ir} and $\tilde{C}_{ir}$ as a function of p differ, the extremal regions of C_{ir} and $\tilde{C}_{ir}$ w.r.t p is very similiar and thus optimizing $\tilde{C}_{ir}$ yields valuable system design insights. In an identical manner, a plot of C_{ir} and $\tilde{C}_{ir}$ against coding rate R for a fixed MAP illustrates a similiar tradeoff of C_{ir} and $\tilde{C}_{ir}$ w.r.t R and is

omitted due to space limitations.

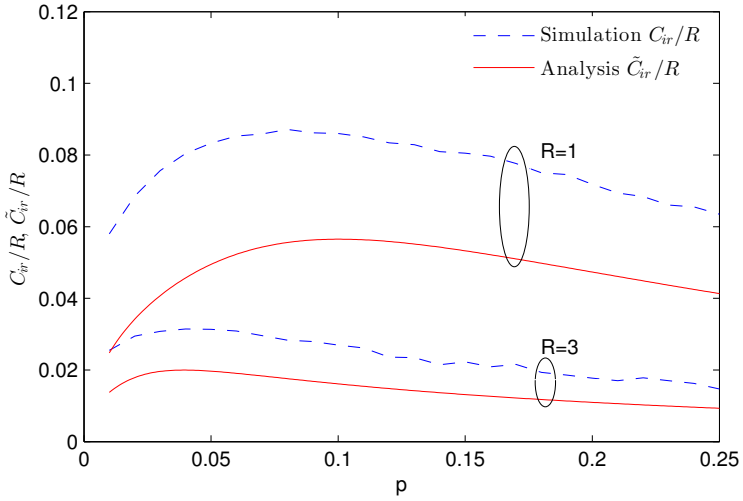

Figure 3.3: Transport capacity C_{ir} and its approximation $\tilde{C}_{ir}$, both normalized by R, plotted against the MAP p for different values of $R = \{1, 3\}$ at $\alpha = 3$.

3.3.1 Variation w.r.t path loss exponent α

The optimization in (3.11) was solved numerically by Monte Carlo simulation. The convex optimization problem in (3.22) is solved by gradient descent algorithms. Figs. 3.4 and 3.5 show plots of the optimal R_{ir} and p_{ir} from (3.11) against the path loss exponent α. Also shown are the approximations $\tilde{R}_{ir}$ and $\tilde{p}_{ir}$ from (3.22). As the path loss exponent α increases, the interference contribution from far away interferers drops off and thus increases the SIR at receiver nodes. Due to the increased SIR, the optimization increases both R and p w.r.t α. The scaling of $\langle \tilde{R}, \tilde{p} \rangle_{ir}$ w.r.t α very closely matches that of $\langle R, p \rangle_{ir}$ and thus facilitates to find close to optimal coding rate R_{ir} and MAP p_{ir} by solving the convex optimization problem in (3.22) than the prohibitively complex Monte Carlo simulation based optimization in (3.11).

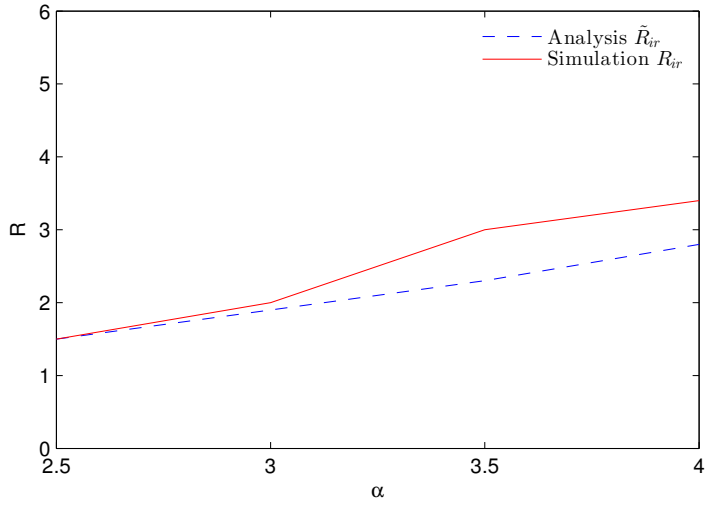

Figure 3.4: The optimal R_{ir} and its approximation $\tilde{R}_{ir}$ from (3.11) and (3.22) respectively plotted against the path loss exponent α at $\lambda = 1$.

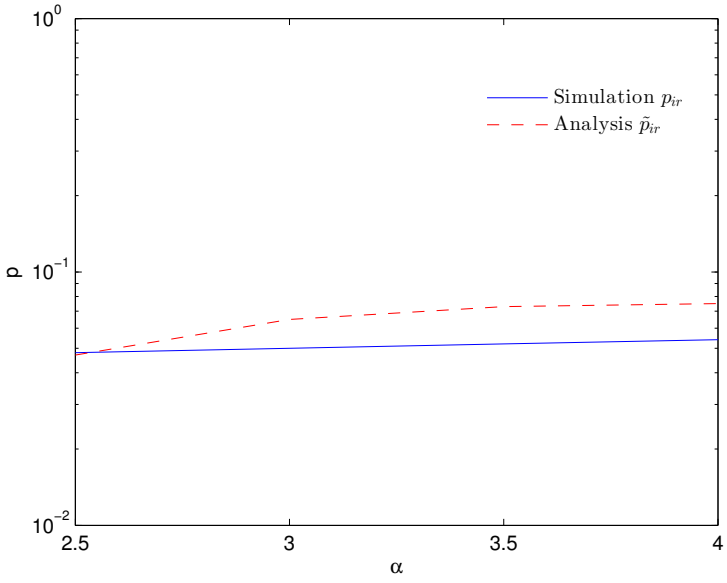

Figure 3.5: The optimal p_{ir} and its approximation $\tilde{p}_{ir}$ from (3.11) and (3.22) respectively plotted against the path loss exponent α at $\lambda = 1$.

3.3.2 Variation w.r.t node density λ

As mentioned in corollary 1, d_{ir} scales w.r.t λ as $O\left(1/\sqrt{\lambda}\right)$. Immediately it is apparent that the approximations $\tilde{R}_{ir}$ and $\tilde{p}_{ir}$ are $O(1)$ w.r.t λ. This has implications for the optimal values R_{ir} and p_{ir}. Fig. 3.6 shows a plot of the optimal R_{ir} and its approximation $\tilde{R}_{ir}$ against the density λ. When the density λ increases, the interference in the network increases and subsequently decreases the SIR at a receiver node. Although the SIR decreases, the coding rate R has a linear scaling component in the transport capacity expression and as a result, the optimization maintains a constant R as λ increases. Similiar observation holds true to Fig. 3.7, which shows a plot of the optimal p_{ir} and its approximation $\tilde{p}_{ir}$ against the density λ.

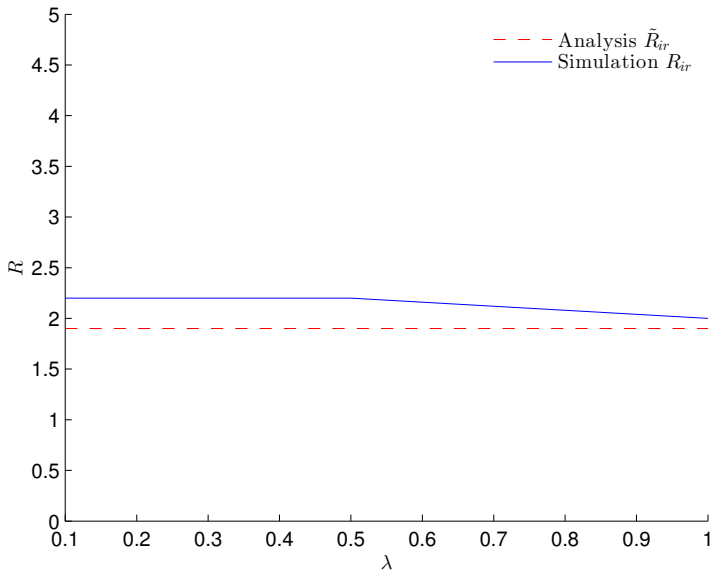

Figure 3.6: The optimal R_{ir} and its approximation $\tilde{R}_{ir}$ from (3.11) and (3.22) respectively plotted against the density λ for $\alpha = 3$.

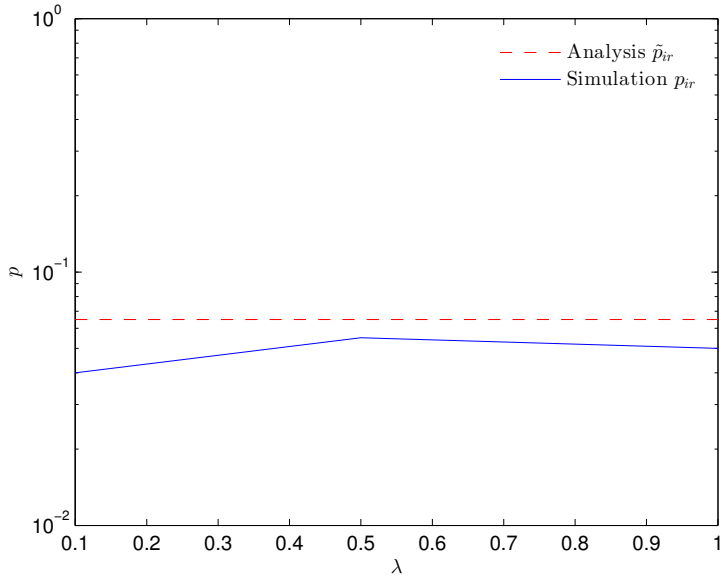

Figure 3.7: The optimal p_{ir} and its approximation $\tilde{p}_{ir}$ from (3.11) and (3.22) respectively plotted against the density λ for $\alpha = 3$.

3.3.3 Effect of Noise

In [47], it is shown that multihop communication is more beneficial in power limited regime(noise is not negligible) relative to interference limited regime. From [16], the success probability of a receiver node at $y \in \mathbb{R}^2$ w.r.t the transmit node at origin is given by

$$\mathbb{P}_{\Phi^t}\left(\mathrm{SINR}_{y,0} \geq T\right) = e^{-\lambda p G(\alpha)|y|^2 T^{\delta} + \sigma^2 |y|^{\alpha} T/\rho} \tag{3.34}$$

where $G(\alpha)$ is defined in (3.14) and T is the SINR threshold. From appendices 3.5.1 and 3.5.2, it is clear that (3.34) with $\sigma^2 = 0$ is the basis for all analysis in this chapter. Hence by making use of (3.34), the analysis framework developed in this chapter for the interference limited regime using the concept of decoding cells, pointwise decoding probability and average cell area can be extended in a straightforward manner to study the performance in the power limited regime.

3.3.4 Repetition Time Diversity

All of the above intuition and observations from incremental redundancy apply in a straightforward manner to the repetition time diversity mechanism. For illustration, plots of the optimal $\langle R, p \rangle_{rtd}$ and their approximations $\langle \tilde{R}, \tilde{p} \rangle_{rtd}$ from (3.24) and (3.32) respectively against the path loss exponent α are shown in Figs. 3.8 and 3.9. Results of analysis and simulation match very closely for repetition time diversity mechanism. The optimal values of HARQ coding rate and MAP for repetition time diversity are smaller than that of incremental redundancy since the decoding MI at a receiver node for incremental redundancy is higher than that of repetition time diversity due to the increased diversity extraction.[2]

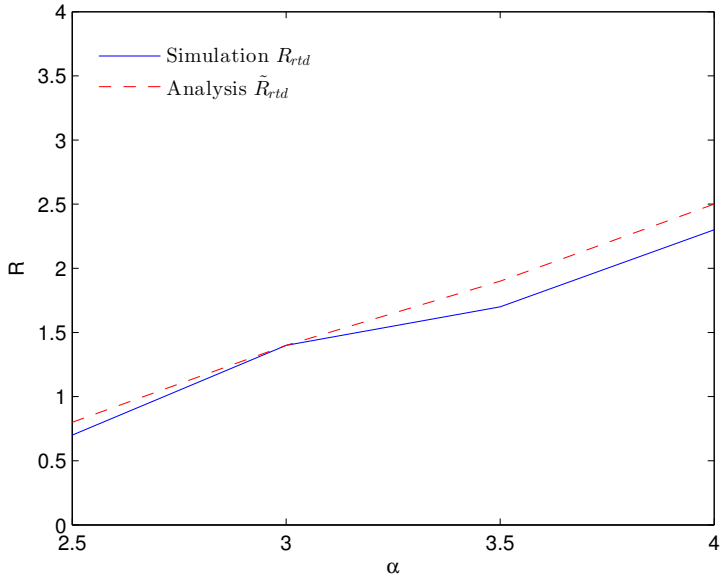

Figure 3.8: The optimal R_{rtd} and its approximation $\tilde{R}_{rtd}$ from (3.24) and (3.32) respectively plotted against the path loss exponent α at $\lambda = 1$.

[2] $\sum_{i=1}^{2} \log_2 (1 + a_i) \geq \log_2 (1 + a_1 + a_2)$, $a_i \geq 0$.

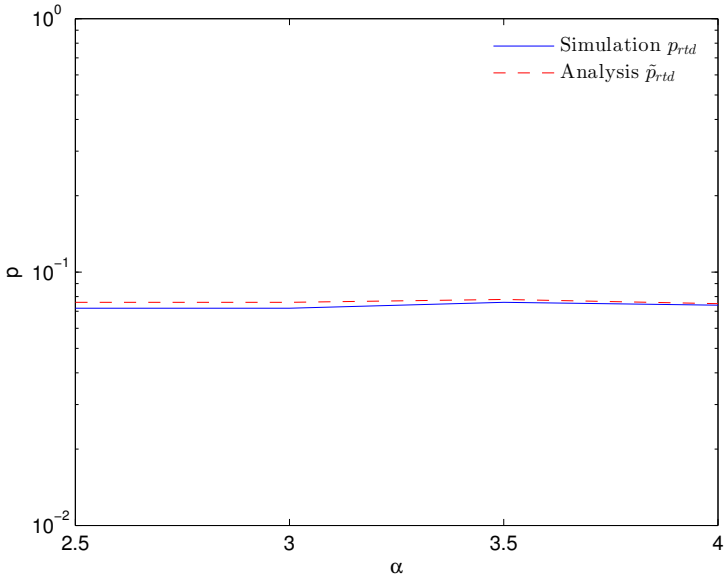

Figure 3.9: The optimal p_{rtd} and its approximation $\tilde{p}_{rtd}$ from (3.24) and (3.32) respectively plotted against the path loss exponent α at $\lambda = 1$.

3.4 Conclusion

In this chapter, we study the performance of cooperative HARQ in wireless adhoc multihop networks using the spatial ALOHA protocol. For a network with Poisson field of interference and opportunistic routing, we solve the network design problem of choosing the optimal HARQ coding rate and MAP by optimizing the transport capacity. We derive an approximate expression for expected progress based on the concept of decoding cells. Optimization of the approximate transport capacity using convex optimization methods yields close approximations to optimal HARQ coding rate and MAP. A key result of the analysis was the invariance of optimal HARQ coding rate and MAP to the node density in the network. It was noted that the analysis framework could be extended to study the performance of cooperative HARQ in power limited regime.

Extending the current line of work by studying the performance of cooperative HARQ protocol with RATC[47] as the performance metric since it accounts for

the bandwidth resources consumed by the relays when forwarding data packets is a step towards understanding the design of practical wireless multihop adhoc networks. Most of the research using stochastic geometric model for wireless networks has focused on fixed rate transmission and outage probability model[58, 59]. Studying CSIT based variable rate transmission methods would be a possible direction of work[30, 67].

3.5 Mathematical Proofs

3.5.1 Expression for $\mathbb{E}\left[|\Sigma_{ir}|\right]$

We first derive an expression for $\mathbb{P}_{\Phi^t}(\cdot)$ in (3.13) and then subsequently derive an expression for $\mathbb{E}\left[|\Sigma_{ir}|\right]$.

Expression for $\mathbb{P}_{\Phi^t}\left(I_{v,0}+I_{v,\eta_1}\geq R\right)$

From (3.12),

$$\begin{aligned} I_{v,0} &= \log_2\left(1+\mathrm{SIR}_{v,0}\right) \equiv \log_2\left(1+S|v|^{-\alpha}\right), \\ S &= \frac{|h_0|^2}{\sum_{k\in\Phi^t}|h_k|^2|v-X_k|^{-\alpha}} \end{aligned} \tag{3.35}$$

The RV S has been defined to facilitate the derivation as illustrated below.

$$\begin{aligned} &\mathbb{P}_{\Phi^t}\left(I_{v,0}+I_{v,\eta_1}\geq R\right) \\ &= \mathbb{P}\left(\log_2\left(1+S_1|v|^{-\alpha}\right)+\log_2\left(1+S_2|v-\eta_1|^{-\alpha}\right)\geq R\right) \\ &= \int_0^\infty \mathbb{P}\left(\log_2\left(1+S_2|v-\eta_1|^{-\alpha}\right)\geq \log_2\left(\frac{2^R}{1+s_1|v|^{-\alpha}}\right)\right) \\ &\quad f_{S_1}(s_1)\,\mathrm{d}s_1 \\ &= \int_0^\infty \mathbb{P}\left(S_2\geq |v-\eta_1|^\alpha\left(\frac{2^R}{1+s_1|v|^{-\alpha}}-1\right)\right) \\ &\quad f_{S_1}(s_1)\,\mathrm{d}s_1 \end{aligned} \tag{3.36}$$

From [16], the CCDF of RV S is given as

$$\mathbb{P}\left(S \geq s\right) = \begin{cases} e^{-\lambda p G(\alpha) s^{\delta}} & , s \geq 0 \\ 1 & , s < 0. \end{cases} \tag{3.37}$$

Using (3.37) and defining $A = \lambda p G\left(\alpha\right)$ and $T = 2^R - 1$, we get

$$\begin{aligned} &\mathbb{P}_{\Phi^t}\left(I_{v,0} + I_{v,\eta_1} \geq R\right) \\ &= \int_0^{T|v|^{\alpha}} e^{-A|v-\eta_1|^2\left(\frac{2^R}{1+s_1|v|^{-\alpha}}-1\right)^{\delta}} f_{S_1}\left(s_1\right) \ \mathrm{d}s_1 \\ &+ \int_{T|v|^{\alpha}}^{\infty} f_{S_1}\left(s_1\right) \mathrm{d}s_1 \\ &\overset{(a)}{=} \int_0^{T|v|^{\alpha}} e^{-A|v-\eta_1|^2\left(\frac{2^R}{1+s_1|v|^{-\alpha}}-1\right)^{\delta}} f_{S_1}\left(s_1\right) \ \mathrm{d}s_1 \\ &+ e^{-AT^{\delta}|v|^2} \qquad (3.38) \\ &\equiv P_1 + P_2 \qquad (3.39) \end{aligned}$$

where (a) follows by evaluating the tail probability of RV S_1 at $T|v|^{\alpha}$. The pdf $f_{S_1}\left(s_1\right)$ follows from (3.37) and the integral term in (3.38) is written as

$$\begin{aligned} P_1 &= \int_0^{T|v|^{\alpha}} e^{-A|v-\eta_1|^2\left(\frac{2^R}{1+s_1|v|^{-\alpha}}-1\right)^{\delta}} e^{-As_1^{\delta}} \ A \ \mathrm{d}\left(s_1^{\delta}\right) \\ &\overset{(b)}{=} A|v|^2 \int_0^{T^{\delta}} e^{-A|v-\eta_1|^2\left(\frac{2^R}{1+\tau^{1/\delta}}-1\right)^{\delta}} e^{-A|v|^2\tau} \ \mathrm{d}\tau \end{aligned} \tag{3.40}$$

where (b) follows by the substitution $\tau = |v|^{-2} s_1^{\delta}$.

Let $P_1 \equiv P_{1,a} + P_{1,b}$ with $P_{1,a}$ and $P_{1,b}$ defined as

$$\begin{aligned} P_{1,a} &= A|v|^2 \int_0^{1} e^{-A|v-\eta_1|^2\left(\frac{2^R}{1+\tau^{1/\delta}}-1\right)^{\delta}} e^{-A|v|^2\tau} \ \mathrm{d}\tau \\ &\overset{(c)}{\geq} A|v|^2 \int_0^{1} e^{-A|v-\eta_1|^2\left(2^R-1\right)^{\delta}} e^{-A|v|^2\tau} \ \mathrm{d}\tau \\ &\overset{(d)}{=} e^{-A|v-\eta_1|^2 T^{\delta}} \left(1 - e^{-A|v|^2}\right) \end{aligned} \tag{3.41}$$

where (c) is based on the fact that $e^{-A|v-\eta_1|^2\left(\frac{2^R}{1+\tau^{1/\delta}}-1\right)^{\delta}}$ is increasing in $0 \leq \tau < 1$ and (d) follows by taking the CDF of an exponential RV with parameter $A|v|^2$ at 1.

Similiar bounds yield a lower bound for the 2^{nd} half of P_1.

$$\begin{aligned} P_{1,b} &= A|v|^2 \int_1^{T^\delta} e^{-A|v-\eta_1|^2\left(\frac{2^R}{1+\tau^{1/\delta}}-1\right)^{\delta}} e^{-A|v|^2\tau}\, d\tau \\ &\geq A|v|^2 \int_1^{T^\delta} e^{-A|v-\eta_1|^2\left(2^R/2-1\right)^{\delta}} e^{-A|v|^2\tau}\, d\tau \\ &\overset{(e)}{=} e^{-A|v-\eta_1|^2\check{T}^\delta}\left(e^{-A|v|^2} - e^{-AT^\delta|v|^2}\right) \end{aligned} \tag{3.42}$$

where in (e) $\check{T} = \left(2^R/2-1\right)$.

Combining (3.41) and (3.42), (3.38) is rewritten as

$$\begin{aligned} \mathbb{P}_{\Phi^t}\left(I_{v,0} + I_{v,\eta_1} \geq R\right) \geq\ & e^{-A|v-\eta_1|^2T^\delta}\left(1 - e^{-A|v|^2}\right) \\ & + e^{-A|v-\eta_1|^2\check{T}^\delta}\left(e^{-A|v|^2} - e^{-AT^\delta|v|^2}\right) \\ & + e^{-AT^\delta|v|^2} \end{aligned} \tag{3.43}$$

Derivation of $\mathbb{E}\big[|\Sigma_{ir}|\big]$

From (3.13),

$$\begin{aligned}
\mathbb{E}\big[|\Sigma_{ir}|\big] &= \int_{\mathbb{R}^2} \mathbb{P}_{\Phi^t}\left(I_{v,0} + I_{v,\eta_1} \geq R\right)\ \mathrm{d}v \\
&\geq \int_{\mathbb{R}^2} \Big[e^{-A|v-\eta_1|^2 T^\delta}\left(1 - e^{-A|v|^2}\right) \\
&\quad + e^{-A|v-\eta_1|^2 \check{T}^\delta}\left(e^{-A|v|^2} - e^{-AT^\delta|v|^2}\right) \\
&\quad + e^{-AT^\delta|v|^2}\Big]\,\mathrm{d}v \\
&= \int_{\mathbb{R}^2} \Big[e^{-A|v-\eta_1|^2 T^\delta} - e^{-A\left(T^\delta|v-\eta_1|^2+|v|^2\right)} \\
&\quad + e^{-A\left(\check{T}^\delta|v-\eta_1|^2+|v|^2\right)} - e^{-A\left(\check{T}^\delta|v-\eta_1|^2+T|v|^2\right)} \\
&\quad + e^{-AT^\delta|v|^2}\Big]\,\mathrm{d}v \\
&\equiv H_1 - H_2 + H_3 - H_4 + H_5
\end{aligned} \tag{3.44}$$

To evaluate the 5 integrals in (3.44), first the following integral in general form is written down.

$$\begin{aligned}
H &= \int_{\mathbb{R}^2} e^{-A\left(c_1|v|^2+c_2|v-\eta_1|^2\right)}\ \mathrm{d}v \\
&= \iint e^{-A\left(c_1\left(v_1^2+v_2^2\right)+c_2(v_1-d_1)^2+c_2v_2^2\right)}\ \mathrm{d}v_1\ \mathrm{d}v_2 \\
&= \int_{-\infty}^{\infty} e^{-A\left(c_1v_1^2+c_2(v_1-d_1)^2\right)}\ \mathrm{d}v_1\ \cdot \\
&\quad \int_{-\infty}^{\infty} e^{-A(c_1+c_2)v_2^2}\ \mathrm{d}v_2
\end{aligned} \tag{3.45}$$

The exponent in the 1^{st} integral of (3.45) is rewritten by completing squares as

$$c_1v_1^2 + c_2\left(v_1 - d_1\right)^2 = (c_1+c_2)\left(v_1 - \frac{d_1c_2}{c_1+c_2}\right)^2 + \frac{d_1^2c_1c_2}{c_1+c_2} \tag{3.46}$$

Using (3.46), the integral H in (3.45) becomes

$$H = e^{-\frac{Ad_1^2 c_1 c_2}{c_1+c_2}} \int_{-\infty}^{\infty} e^{-A(c_1+c_2)\left(v_1 - \frac{d_1 c_2}{c_1+c_2}\right)^2} \, \mathrm{d}v_1 \cdot \int_{-\infty}^{\infty} e^{-A(c_1+c_2)v_2^2} \, \mathrm{d}v_2 \tag{3.47}$$

To evaluate (3.47), the following rewritten form of the standard Gaussian pdf relation is used.

$$\int_{-\infty}^{\infty} \frac{1}{\sqrt{2\pi\sigma^2}} \, e^{-(x-\mu)^2/2\sigma^2} \, \mathrm{d}x = 1$$
$$\int_{-\infty}^{\infty} e^{-b(x-\mu)^2} \, \mathrm{d}x = \sqrt{\frac{\pi}{b}} \tag{3.48}$$

where $b = \frac{1}{2\sigma^2}$.

Applying the relation (3.48) for the integral H in (3.47) twice yields

$$H = \int_{\mathbb{R}^2} e^{-A\left(c_1|v|^2 + c_2|v-\eta_1|^2\right)} \, \mathrm{d}v$$
$$= e^{-\frac{Ad_1^2 c_1 c_2}{c_1+c_2}} \, \frac{\pi}{A\,(c_1+c_2)} \tag{3.49}$$

Using the result in (3.49) to the integrals in (3.44), the lower bound for $\mathbb{E}\big[|\Sigma_{ir}|\big]$ is given as

$$\mathbb{E}\big[|\Sigma_{ir}|\big] \geq H_1 - H_2 + H_3 - H_4 + H_5$$
$$= \frac{\pi}{A}\Bigg[\frac{1}{T^\delta} - \frac{e^{-AT^\delta d_1^2/\left(1+T^\delta\right)}}{1+T^\delta} + \frac{e^{-A\check{T}^\delta d_1^2/\left(1+\check{T}^\delta\right)}}{1+\check{T}^\delta} - \frac{e^{-AT^\delta \check{T}^\delta d_1^2/\left(T^\delta+\check{T}^\delta\right)}}{T^\delta+\check{T}^\delta} + \frac{1}{T^\delta}\Bigg] \tag{3.50}$$

3.5.2 Repetition Time Diversity

Expression for $\mathbb{P}_{\Phi^t}\left(\mathrm{SIR}_{v,0}+\mathrm{SIR}_{v,\eta_1}\geq 2^R-1\right)$

Using the notation for $\mathrm{SIR}_{v,0}$ in (3.35), we have

$$\begin{aligned}
&\mathbb{P}_{\Phi^t}\left(\mathrm{SIR}_{v,0}+\mathrm{SIR}_{v,\eta_1}\geq 2^R-1\right)\\
&=\mathbb{P}\left(S_1|v|^{-\alpha}+S_2|v-\eta_1|^{-\alpha}\geq T\right)\\
&=\int_0^{\infty}\mathbb{P}\left(S_2\geq|v-\eta_1|^{\alpha}\left(T-s_1|v|^{-\alpha}\right)\right)f_{S_1}(s_1)\,\mathrm{d}s_1\\
&\overset{(a)}{=}\int_0^{T|v|^{\alpha}}e^{-A|v-\eta_1|^2\left(T-s_1|v|^{-\alpha}\right)^{\delta}}f_{S_1}(s_1)\,\mathrm{d}s_1\\
&\quad+\int_{T|v|^{\alpha}}^{\infty}f_{S_1}(s_1)\,\mathrm{d}s_1\\
&=\int_0^{T|v|^{\alpha}}e^{-A|v-\eta_1|^2T^{\delta}\left(1-\frac{s_1}{T|v|^{\alpha}}\right)^{\delta}}e^{-As_1^{\delta}}\;A\;\mathrm{d}\left(s_1^{\delta}\right)\\
&\quad+e^{-AT^{\delta}|v|^2}\\
&\overset{(b)}{=}\int_0^{1}e^{-A|v-\eta_1|^2T^{\delta}\left(1-u^{1/\delta}\right)^{\delta}}e^{-AT^{\delta}|v|^2u}\;AT^{\delta}|v|^2\;\mathrm{d}u\\
&\quad+e^{-AT^{\delta}|v|^2}\\
&\overset{(c)}{\geq}e^{-AT^{\delta}|v-\eta_1|^2}\int_0^{1}AT^{\delta}|v|^2\;e^{-AT^{\delta}|v|^2u}\mathrm{d}u\\
&\quad+e^{-AT^{\delta}|v|^2}\\
&=e^{-AT^{\delta}|v-\eta_1|^2}\left(1-e^{-AT^{\delta}|v|^2}\right)+e^{-AT^{\delta}|v|^2}
\end{aligned}\tag{3.51}$$

where (a) uses the CCDF of S_2 in (3.37), (b) follows from the previous line using the simple substitution $u=\left(\frac{s_1}{T|v|^{\alpha}}\right)^{\delta}$ and (c) uses the relation $e^{-A|v-\eta_1|^2T^{\delta}\left(1-u^{1/\delta}\right)^{\delta}}\geq e^{-A|v-\eta_1|^2T^{\delta}},\ 0\leq u\leq 1$.

Derivation of $\mathbb{E}\big[|\Sigma_{rtd}|\big]$

$$\begin{aligned}
\mathbb{E}\big[|\Sigma_{rtd}|\big] &= \int_{\mathbb{R}^2} \mathbb{P}_{\Phi^t}\left(\mathrm{SIR}_{v,0} + \mathrm{SIR}_{v,\eta_1} \geq 2^R - 1\right) \ \mathrm{d}v \\
&\geq \int_{\mathbb{R}^2} \Bigg[e^{-AT^\delta |v-\eta_1|^2} \left(1 - e^{-AT^\delta |v|^2}\right) \\
&\quad + e^{-AT^\delta |v|^2} \Bigg] \ \mathrm{d}v \\
&= \int_{\mathbb{R}^2} \Bigg[e^{-AT^\delta |v-\eta_1|^2} + e^{-AT^\delta |v|^2} \\
&\quad - e^{-AT^\delta \left(|v|^2 + |v-\eta_1|^2\right)} \Bigg] \ \mathrm{d}v \\
&\equiv H_1 + H_2 - H_3
\end{aligned} \tag{3.52}$$

The 3 integrals in (3.52) are evaluated using (3.49)

$$\begin{aligned}
\mathbb{E}\big[|\Sigma_{rtd}|\big] &\geq H_1 + H_2 - H_3 \\
&= \frac{\pi}{AT^\delta} \left(2 - \frac{e^{-AT^\delta d_1^2/2}}{2}\right)
\end{aligned} \tag{3.53}$$

Chapter 4

Multiuser Diversity in Downlink Channels

In the previous two chapters of the thesis, the focus was on the performance of continuous version of HARQ i.e., rateless codes and the block level IR- HARQ in single hop and cooperative multihop WANETs respectively. In this chapter, we shift the focus of the thesis to performance analysis of multiuser diversity scheduling in cellular networks. Multiuser diversity is a key concept in user scheduling in both downlink and uplink of cellular networks. It is widely incorporated into both mobile and WLAN standards. It is well known that multiuser diversity provides significant benefits by increasing the spectral efficiency double logarithmically with the number of users served.

In the research literature, although there has been a lot of effort studying the benefits of multiuser diversity, very little emphasis is given to the cost associated with multiuser diversity and this is precisely the focus of this chapter. The benefit of multiuser diversity is heavily dependent on the ability of the base station to acquire accurate CQI of the users, which requires significant feedback resources. The goal of this chapter is to present a cost benefit analysis of multiuser diversity. We consider two contemporary cellular systems, FDD and TDD. Two types of feedback methods are studied in this chapter namely dedicated feedback and SNR

dependent feedback. While most of the chapter focuses on single antenna users, the last part presents a study of the interaction between single user multiantenna techniques and multiuser diveristy. The research results and material presented in this chapter has been published in [68].

The remainder of the chapter is organized as follows. In section 4.1, the system model and analysis framework are introduced. In sections 4.2 and 4.3, the cost-benefit analysis of multiuser diversity in the FDD and TDD systems is performed. In section 4.4, we study the effect of single user multiantenna techniques on multiuser diversity and we conclude in Section 4.5.

4.1 System Model

We consider a single antenna broadcast channel with K users. Each of the users has identical average SNR P and fading distribution. For downlink, a Rayleigh block fading model is assumed. Throughout the chapter, we make simplifying assumptions about the uplink channel with appropriate justifications. Every coherence block has $\check{T}$ symbols, which is termed the downlink resource blocklength and is given by $\check{T} = W_c T_c$, where W_c is the coherence bandwidth and T_c is the coherence time. The BS performs single user scheduling once every coherence block and to do so the BS collects SNR information from the K users at the begining of every coherence block. Through common downlink training from the BS, users will learn their SNR and explicitly feed it back on the uplink. We assume that the SNR value received at the BS is error free and delay free. Although practical systems exhibit continuous fading, with possibly different coherence times and bandwidths for different users, we are able to get to the core insights of the problem by focusing on the simple scenario of block fading with the same block size for all users. Furthermore, the effect of feedback delay can be accounted for by choosing an appropriate effective coherence time. After learning the downlink SNR of the K users, the BS selects the user with the largest instantaneous SNR for transmission. In a practical system users will have different average SNR's, in

which case the proportionally fair scheduler [69], which chooses the user with the largest instantaneous SNR relative to its own average SNR, should be used.

4.1.1 Quantifying the benefit of multiuser diversity

In this subsection, we quantify the benefit of multiuser diversity i.e., how the spectral efficiency increases w.r.t the number of feedback users when using dedicated feedback. The spectral efficiency is

$$C_{D-df}(K) = \mathbb{E}\left[\log_2(1 + P\gamma_{df})\right] \tag{4.1}$$

where $\gamma_{df} = \max_{1\leq i\leq K} \gamma_i$ is the scheduled SNR, $\gamma_i = |h_i|^2$ and $h_i \sim \mathcal{CN}(0,1)$ are the downlink SNR and channel of the i^{th} user respectively.

The spectral efficiency in (4.1) has a closed form expression [70], $C_{D-df}(K) = \sum_{k=1}^{K} \binom{K}{k} (-1)^{k+1} e^{\frac{k}{P}} E_1\left(\frac{k}{P}\right)$, where $E_1(.)$ is the exponential integral $E_1(x) = \int_x^\infty \frac{e^{-t}}{t}\, dt$. But the closed form expression does not quantify how $C_{D-df}(K)$ increases with K. To quantify the growth rate of $C_{D-df}(K)$ with K, the following upper bound and lower bound on $C_{D-df}(K)$ are useful.

Proposition 1. *For large K, the spectral efficiency $C_{D-df}(K)$ is bounded as*

$$\log_2\left(1 + P\left(\log K - \log\log\log K\right)\right) + o(1) \leq C_{D-df}(K) \leq \log_2\left(1 + P\left(0.58 + \log K\right)\right) \tag{4.2}$$

Proof: See Appendix 4.6.1. ∎

Based on (4.2), an approximation to the spectral efficiency is defined as

$$\begin{aligned} C_{D-df}(K) \approx \tilde{C}_{D-df}(K) &= \log_2\left(1 + P\log K\right) \\ &= O\left(\log\log K\right) \end{aligned} \tag{4.3}$$

In Fig.4.1, the average scheduled SNR $\mathbb{E}[\gamma_{df}]$ in dB scale is plotted against the number of feedback users[1] . From Fig.4.1, it is seen that the scheduled SNR increases quickly for the first few users, but afterwards the rate of increase slows down dramatically.

[1] $10\log_{10}\mathbb{E}[\gamma_{df}]$ is plotted against K. Also, γ_{df} is defined at the begining of section 4.1.1.

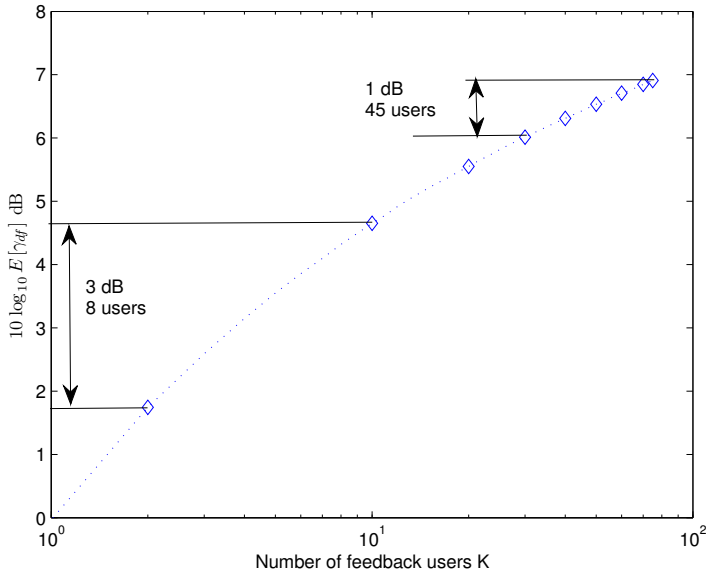

Figure 4.1: Average scheduled SNR in dB scale plotted against the number of feedback users.

4.1.2 FDD System

In Frequency Divison Duplexing (FDD) systems, the uplink and downlink have separate bandwidths. Fig.4.2.a shows the structure of the uplink and downlink bandwidths in a FDD system. The downlink bandwidth is used only for downlink data whereas the uplink bandwidth is used for SNR feedback, to aid downlink, and uplink data. During every coherence block, the uplink bandwidth is split into two pieces, the first one used for SNR feedback and the second one used for data transmission. At the begining of each uplink bandwidth, K users feedback SNR to the BS. Let $\check{W}_{U-fb}(K)$ be the number of symbols used for SNR feedback on the uplink. $\check{W}_{U-fb}(K)$ will be defined separately for each of the two types of SNR feedback methods in the later sections. The remaining $\check{T} - \check{W}_{U-fb}(K)$ symbols are used for uplink data. The uplink rate is determined by the uplink data bandwidth and uplink spectral efficiency. The uplink data bandwidth $W_{U-data}(K)$,

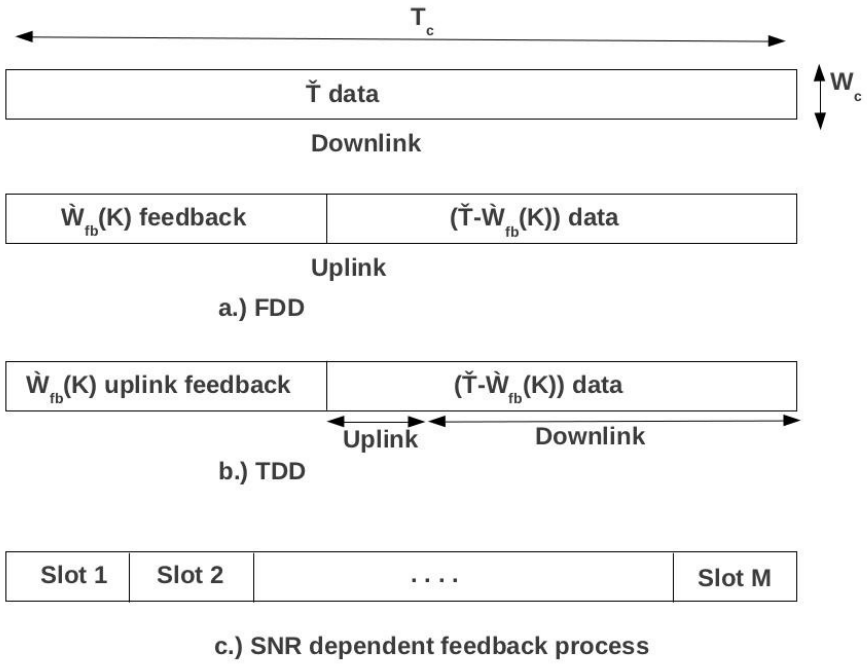

Figure 4.2: a.) Separate uplink and downlink bandwidths in the FDD system. b.) Common bandwidth for uplink and downlink in the TDD system. c.) Feedback bandwith in the SNR dependent feedback process.

normalized to the total uplink bandwidth $\check{T}$, is

$$W_{U-data}(K) = 1 - \frac{\check{W}_{U-fb}(K)}{\check{T}} \tag{4.4}$$

We model the uplink channel as an AWGN channel with SNR P, and hence the uplink spectral efficiency is

$$C_U = \log_2(1+P) \tag{4.5}$$

Therefore, the uplink rate is

$$\begin{aligned} R_U(K) &= W_{U-data}(K) \cdot C_U \\ &= \left(1 - \frac{\check{W}_{U-fb}(K)}{\check{T}}\right) \log_2(1+P) \end{aligned} \tag{4.6}$$

On the uplink, orthogonal multiple access and superposition decoding are the two multiple access methods used for both control and data signalling[69]. It is a standard result that orthogonal multiple access achieves the capacity at one point in the multiple access capacity region. For Rayleigh fading, the per user rate of orthogonal multiple access can be upper bounded using Jensen's inequality for concave functions and is given as $\frac{1}{K}\sum_{i=1}^{K}\mathbb{E}\left[\log_2(1+P\sigma_i)\right] \leq \log_2(1+P)$. Hence assuming the uplink to be an AWGN channel helps to simplify the mathematical analysis without changing the cost-benefit tradeoff of multiuser diversity. On the downlink $W_{D-data}(K) = 1$, since the downlink bandwidth is only used for data. The downlink spectral efficiency is

$$C_D(K) = \mathbb{E}\left[\log_2(1+P\gamma_{sch})\right] \tag{4.7}$$

where γ_{sch} is the scheduled SNR, expression for which depends on the type of SNR feedback method. Therefore, the downlink rate is

$$R_D(K) = W_{D-data}(K) \cdot C_D(K) = \mathbb{E}\left[\log_2(1+P\gamma_{sch})\right] \tag{4.8}$$

Increasing the number of feedback users increases the downlink rate but decreases the uplink data bandwidth and thus, decreases the uplink rate. Clearly there

exists a tradeoff between the uplink and downlink rates. A balance between the two rates can be achieved by considering the maximization of the weighted sum of the uplink and downlink rates.

$$\max_{K} \left[\lambda_R R_D\left(K\right) + R_U\left(K\right)\right] \tag{4.9}$$

where λ_R is the weight factor, specifying the preference of the downlink rate over the uplink rate. Thus, our fundamental objective is to determine the optimal number of feedback users as function of the system parameters, blocklength, average SNR and weight factor.

If the total number of users in the system is K_t, our objective is to find the number of feedback users K from among K_t which achieves an optimal balance between the uplink and downlink rates.

4.1.3 TDD System

Time Divison Duplexing (TDD) systems differ from the FDD systems in that, one common bandwidth is used for both the uplink and downlink. Fig.4.2.b shows the structure of the common bandwidth for both the uplink and downlink in a TDD system. During every coherence block, the bandwidth is split into 3 pieces, the first one used for SNR feedback on the uplink, the second one used for uplink data and the third one used for downlink data. (In TDD systems employing dedicated feedback, the users can alternatively send uplink pilots to allow the BS to estimate the per-user SNR. Although we don't explicitly refer to this mode of operation in the chapter, it is straightforward to see that it fits into our framework.)

At the begining of each bandwidth, users feedback SNR to the BS on the uplink using $\check{W}_{U-fb}(K)$ symbols. Let us assume that a fraction α of the data bandwidth $\left(1 - \frac{\check{W}_{U-fb}(K)}{\check{T}}\right)$ is used for uplink data and the remaining for downlink data. The

uplink and downlink rates are

$$\begin{aligned} R_U(K) &= W_{U-data}(K) \cdot C_U \\ &= \alpha \left(1 - \frac{\check{W}_{U-fb}(K)}{\check{T}}\right) \log_2 (1+P) \qquad (4.10) \\ R_D(K) &= W_{D-data}(K) \cdot C_D\,(K) \\ &= (1-\alpha) \left(1 - \frac{\check{W}_{U-fb}(K)}{\check{T}}\right) \mathbb{E}\left[\log_2(1+P\gamma_{sch})\right] \qquad (4.11) \end{aligned}$$

The weighted sum of the uplink and downlink rates is written as

$$\begin{aligned} &\lambda_R R_D\,(K) + R_U\,(K) = \\ &\lambda_R(1-\alpha) \left(1 - \frac{\check{W}_{U-fb}(K)}{\check{T}}\right) \mathbb{E}\big[\log_2 D\,(1+P\gamma_{sch})\big] \qquad (4.12) \end{aligned}$$

where $\log_2 D = \frac{\alpha}{\lambda_R(1-\alpha)} \log_2 (1+P)$. See appendix 4.6.2 for details. From (4.11) and (4.12), the downlink rate and the weighted sum rate have the same tradeoff with the number of feedback users, since the downlink spectral efficiency increases and the data bandwidth decreases with K. Hence without changing the cost-benefit tradeoff of multiuser diversity in the TDD system, we simplify the analysis by assuming $\alpha = 0$ and focus only on the downlink rate. Thus, our fundamental objective is to determine the optimal number of feedback users, in terms of maximizing the downlink rate achieveing a balance between the data bandwidth and spectral efficiency, as function of the system parameters, blocklength and average SNR.

4.2 FDD System

In this section, a cost-benefit analysis of multiuser diversity in a FDD system is executed. As outlined in the section 4.1.2, we determine the optimal number of feedback users as a function of the system parameters for both dedicated feedback and SNR dependent feedback respectively.

4.2.1 Dedicated Feedback

In dedicated feedback, each user is allocated orthogonal feedback resources per coherence block i.e., a fixed number of symbols on the uplink for SNR feedback. Each user uses L_{fb} bits for SNR feedback. The number of feedback symbols per user will be $\frac{L_{fb}}{\log_2(1+P)}$. So the feedback bandwidth in (4.4) is $\check{W}_{U-fb}(K) = \frac{KL_{fb}}{\log_2(1+P)} = O(K)$ and the uplink rate of the FDD system is

$$\begin{aligned} R_U(K) &= \left(1 - \frac{KL_{fb}}{\check{T}\log_2(1+P)}\right)\log_2(1+P) \\ &= \log_2(1+P) - \frac{K}{T} \end{aligned} \tag{4.13}$$

where $T = \frac{\check{T}}{L_{fb}}$ is the effective blocklength. The downlink rate of a FDD system is $R_D(K) = \mathbb{E}[\log_2(1+P\gamma_{df})]$. We ignore the effect of L_{fb} bit quantization of the SNR value at the user and assume that the feedback channel is error free. These simplifications simplify the analysis yet capturing the cost-benefit tradeoff of multiuser diversity which is primarily quantified in terms of the number of feedback users. These simplications are reasonable enough since L_{fb} is large enough such that the high precision quantized SNR value very closely approximates the unquantized SNR value, the effect of errors in the feedback channel can be made very small by using standard QAM methods [71].

The cost of an additional feedback user is $\frac{dR_U}{dK} = \frac{-1}{T}$ and it specifies the decrease in the uplink rate. The benefit of an additional feedback user is $\frac{dR_D}{dK} = O\left(\frac{1}{K\log K}\right)$ since $R_D(K) = O(\log\log K)$ from (4.3) and it specifies the marginal increase in the downlink rate. The tradeoff between the uplink and downlink rates is more clearly illustrated in Fig.4.3, which plots $R_U(K)$ in (4.13) against $R_D(K)$, just defined above. From the figure, it is very clear that an optimized system should operate in region C which achieves a better tradeoff between the uplink and downlink rates than the regions A and B. The optimal operating point on the tradeoff curve can be quantified by solving the optimization problem in (4.9),

$$K_{op}^{df} = \arg\max_K \left[\lambda_R\, \mathbb{E}[\log_2(1+P\gamma_{df})] + \log_2(1+P) - \frac{K}{T}\right] \tag{4.14}$$

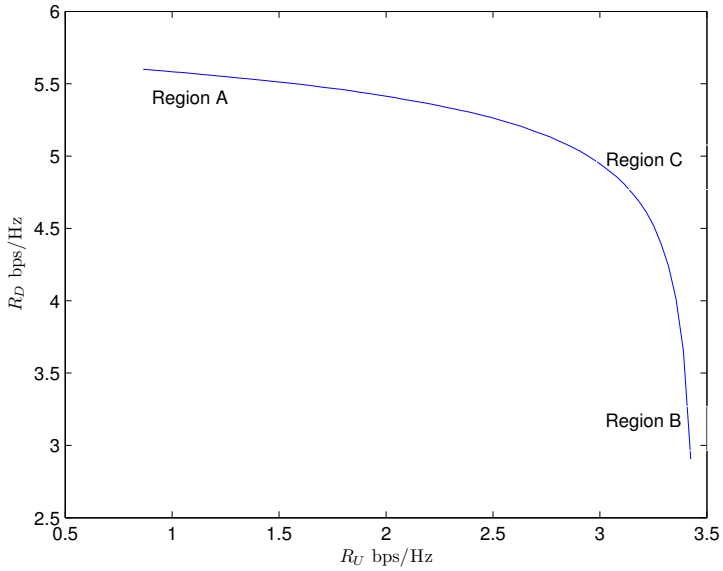

Figure 4.3: A plot of the downlink rate against the uplink rate in the FDD system at 10 dB.

The objective function in (4.14) is concave and at the optimal operating point, the benefit of an additional feedback user on the downlink will equal the cost of an additional feedback user on the uplink i.e., $\frac{dR_D}{dK} = \frac{-1}{\lambda_R}\frac{dR_U}{dK}$. It is very difficult to obtain a closed form expression for K_{op}^{df}. In an effort to get an expression for K_{op}^{df}, we define a tight approximation to the downlink rate based on the upper and lower bounds in (4.2), $R_D(K) \approx \tilde{R}_D(K) = \log_2(1 + P\log K)$. The optimization problem is defined for the approximation

$$K_{ap}^{df} = \arg\max_K \left[\lambda_R \log_2(1 + P\log K) + \log_2(1+P) - \frac{K}{T}\right] \tag{4.15}$$

The solution to the above optimization problem is given in the following theorem.

Theorem 5. *In a FDD single antenna broadcast channel using dedicated feedback, the number of feedback users K_{ap}^{df} which maximize the approximate weighted sum*

rate as per (4.15) is

$$K_{ap}^{df} = \frac{\lambda_R T}{\mathcal{W}\left[e^{\frac{1}{P}\lambda_R T}\right]} \approx \frac{\lambda_R T}{\frac{1}{P} + \log \lambda_R T - \log\left(\frac{1}{P} + \log \lambda_R T\right)} \tag{4.16}$$

where $\mathcal{W}(\cdot)$ is the Lambert-W function.

Proof: See Appendix 4.6.3. ■

Scaling of K_{ap}^{df} w.r.t T

From (4.16), it is easily seen that $K_{ap}^{df} = O\left(\frac{T}{\log T}\right)$. As T increases, the uplink bandwidth increases and hence an optimized system should increase the number of feedback users. To see why K_{ap}^{df} does not scale linearly with T, let us consider how the weighted sum rate in (4.15) grows as $T \to \infty$. The weighted sum rate for $K = O(T)$ and $K = O\left(\frac{T}{\log T}\right)$ are given below

$$K = cT, 0 < c < 1 : \lambda_R R_D + R_U \approx \lambda_R \log\log T + (1 + \lambda_R)\log P - c. \tag{4.17}$$

$$K = O\left(\frac{T}{\log T}\right) : \lambda_R R_D + R_U \approx \lambda_R \log\log T + (1 + \lambda_R)\log P - \frac{1}{\log T}. \tag{4.18}$$

From (4.17) and (4.18), it is clear why $K_{ap}^{df} \neq O(T)$.

Before giving the numerical results, the simulation setup is briefly described. The chosen system parameters are $T_c = 1$ms, W_c has the range $100 - 300$kHz which corresponds to the blocklength $\check{T} = 100 - 300$, $L_{fb} = 5$ and $\lambda_R = 0.5$. The number of users in the system is 75. In Fig.4.4, K_{op}^{df} in (4.14) and K_{ap}^{df} in (4.16) are plotted against the blocklength at 10 and 0 dB. The scaling of both K_{op}^{df} and K_{ap}^{df} w.r.t T is very similiar. It is seen that for a FDD 75 user single antenna broadcast channel using dedicated feedback, it is wiser to collect SNR only from a few users, more specifically around 8-25 users. For example, $K_{op}^{df} = 8$ for $\check{T} = 100$ and 0 dB, $K_{op}^{df} = 25$ for $\check{T} = 300$ and 10 dB. The number of feedback

users in an optimized system should be selected very conservatively because the feedback cost in dedicated feedback is $O(K)$, in contrast to the benefit which is only $O(\log \log K)$, and this limits the amount of multiuser diversity that can be used.

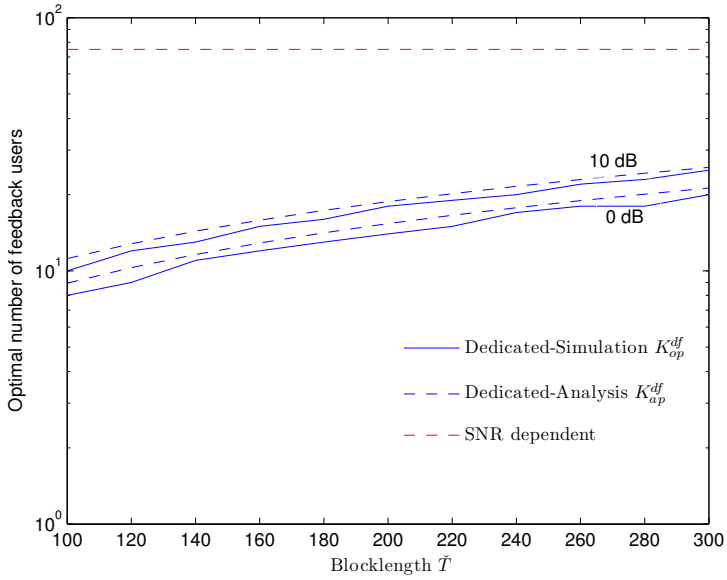

Figure 4.4: Optimal number of feedback users against the blocklength in the FDD system for the two SNR feedback methods .

Scaling of K_{ap}^{df} w.r.t P

From (4.16), it is easily seen that $K_{ap}^{df} = O(1)$ w.r.t P. Fig.4.5 shows a plot of K_{ap}^{df} in (4.16) against P. As the average SNR increases, the per user feedback bandwidth decreases. Hence, initially as P increases, the number of feedback users increases in an optimized system, but as $P \to \infty$, the multiuser diversity benefit diminishes and $O(1)$ scaling is seen.

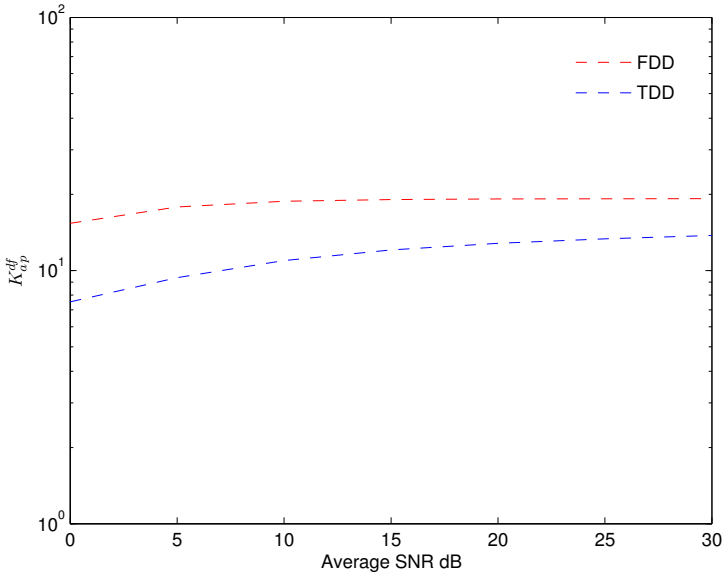

Figure 4.5: K_{ap}^{df} in both the FDD and TDD systems plotted against the average SNR.

4.2.2 SNR dependent feedback

SNR dependent feedback introduced in [25] has the basic idea that since only the good users (those with a large instantaneous SNR) will be scheduled, feedback bandwidth can be reduced significantly by asking only the good users to feedback SNR. Users with good SNR are differentiated from users with bad SNR by a SNR threshold γ_{th}. The SNR independent feedback method considered in the previous subsection wastes bandwidth since users with bad SNR also feedback SNR. User i compares its SNR γ_i to a predetermined γ_{th} and only if $\gamma_i \geq \gamma_{th}$, SNR is fedback on a random access channel. The choice of γ_{th} determines how many users feedback SNR and thus the feedback bandwidth. The feedback random access channel can be implemented as a slotted ALOHA channel [23, 26] or CDMA channel [27].

We have considered the slotted ALOHA like random access channel introduced in [26]. The random access channel has M slots [2] as illustrated in Fig.4.2.c. A

[2] In this chapter, a slot refers to a fixed number of symbols grouped together.

user is eligible to feedback SNR only if $\gamma_i \geq \gamma_{th} = \log\left(\frac{K}{M}\right)$. An eligible user will select one of the M slots with probability $\frac{1}{M}$ to feedback its SNR and user ID. Each user feeds back L_{fb} bits of SNR value and $\log_2 K$ bits of user ID. The number of feedback symbols required for a user is $\frac{L_{fb}+\log_2 K}{\log_2(1+P)}$. These many symbols are grouped into one feedback slot. A feedback attempt by a user is successful (hereafter referred to as user being captured) only if that user is the only one to attempt feedback in its selected slot, because a collision occurs when multiple users select the same slot. After M slots of SNR feedback, the BS selects the user with the best downlink SNR from amongst the captured users. A more generalized SNR feedback algorithm is given in [23], although it is very complex. The uplink rate is given by

$$\begin{aligned} R_U(K) &= W_{U-data}(K) \cdot C_U \\ &= \left[1 - \left(\frac{L_{fb} + \log_2 K}{\log_2(1+P)}\right)\frac{M}{\check{T}}\right]\log_2(1+P) \end{aligned} \tag{4.19}$$

The downlink rate is

$$R_D(K) = P(X \geq 1)\ \mathbb{E}[\log_2(1 + P\gamma_{sdf})] \tag{4.20}$$

$\gamma_{sdf} = \max_{1\leq m\leq X} \gamma_{m|\gamma_{th}}$ is the scheduled SNR, $\gamma_{m|\gamma_{th}}$ is the SNR of the m^{th} captured user and X is the number of captured users. An expression for $P(X \geq 1)$ is given in Appendix 4.6.4. The two parameters which determine the cost-benefit tradeoff of multiuser diversity in SNR dependent feedback are K and M. The uplink and downlink rates in (4.19) and (4.20) are decreasing and increasing functions of K and M respectively. The cost of an additional feedback user and an additional feedback slot are $\frac{\partial R_U}{\partial K} = \frac{-M}{K\check{T}}$ and $\frac{\partial R_U}{\partial M} = \frac{-(L_{fb}+\log_2 K)}{\check{T}}$ respectively. Although it is hard to quantify the rate of increase of $R_D(K)$ w.r.t K and M, it is easy to see that both $P(X \geq 1)$ and γ_{sdf} increase when both K and M are increased simultaneously. Values of K and M which achieve an optimal balance between the cost and benefit of multiuser diversity can be found by solving the weighted sum optimization,

$$\langle K, M\rangle_{op}^{sdf} = \arg\max_{K,M}\left[\lambda_R R_D(K) + R_U(K)\right] \tag{4.21}$$

Based on the expression for $P(X \geq 1)$ in Appendix 4.6.4, it is easily seen that the optimization in (4.21) does not have a closed form solution and has to be solved numerically. Intuitively, the value of K_{op}^{sdf} can be easily understood. The feedback bandwidth in SNR dependent feedback (4.19) is $O(\log K)$, unlike $O(K)$ in dedicated feedback, and this literally allows for all of the available multiuser diversity to be used i.e., $K_{op}^{sdf} = K_{total}$ and all users in the system can participate in the feedback process. In Fig.4.4, K_{op}^{sdf} in (4.21) is plotted against the blocklength at 10 and 0 dB. Both K_{op}^{sdf} and M_{op}^{sdf} are found by exhaustive search. It is seen that all the 75 users in the system can participate in the feedback process.

The key finding of this section is that the cost-benefit tradeoff of multiuser diversity for dedicated feedback is completely different from that for SNR dependent feedback. For dedicated feedback, due to the significant feedback cost, the number of feedback users has to be very carefully selected, where as for SNR dependent feedback, due to the relatively much smaller feedback cost, all the users in the system can participate in the feedback process. This is summarized in Fig.4.6 which plots the weighted sum rates of both dedicated feedback from (4.14) and SNR dependent feedback from (4.21) against the number of feedback users.

4.3 TDD System

In this section, a cost-benefit analysis of multiuser diversity in a TDD system is performed. As outlined in the section 4.1.3, we determine the optimal number of feedback users as a function of the system parameters for both dedicated feedback and SNR dependent feedback respectively.

4.3.1 Dedicated Feedback

The feedback process in the TDD system is the same as in the FDD system except that it consumes bandwidth common to both the uplink and downlink.

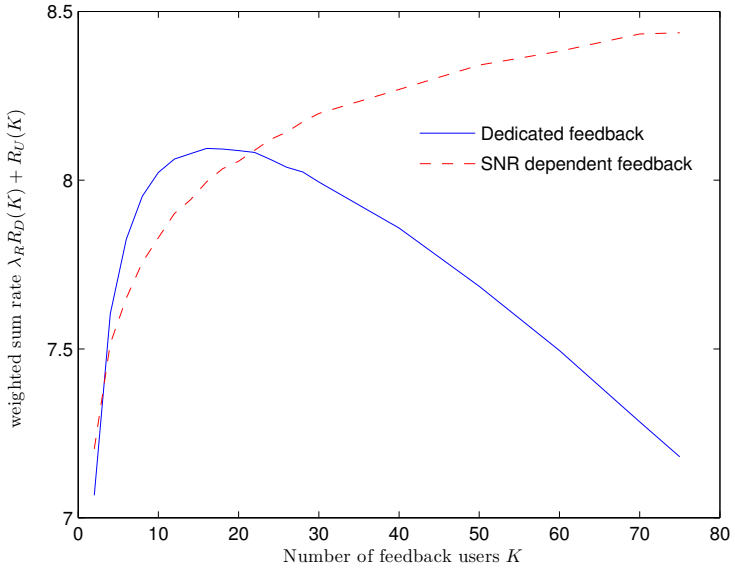

Figure 4.6: Weighted sum rates of both the feedback methods against the number of feedback users in the FDD system .

The downlink rate of the TDD system is

$$\begin{aligned} R_D(K) &= W_{D-data}(K) \cdot C_{D-df}(K) \\ &= \left(1 - \frac{KL_{fb}}{\check{T}\log_2(1+P)}\right) \mathbb{E}\left[\log_2(1+P\gamma_{df})\right] \end{aligned} \tag{4.22}$$

In the TDD system, the cost of an additional feedback user is $\frac{L_{fb}}{\log_2(1+P)}$ downlink symbols. The benefit of an additional feedback user is the increase in spectral efficiency quantified by $\frac{dC_{D-df}}{dK} = O\left(\frac{1}{K\log K}\right)$. This tradeoff can be better understood from Fig.4.7, which shows a plot of the spectral efficiency and the downlink rate, both in (4.22), against the number of feedback users at 10 dB. Based on this plot, it is very clear that beyond a certain point, the knee region in the spectral efficiency curve, the benefit from feedback is too small, not worth increasing the feedback cost. So for an optimized system, the intuition is to operate around the knee region achieving an optimal balance between the spectral efficiency benefit and the feedback cost. The knee region can be quantified

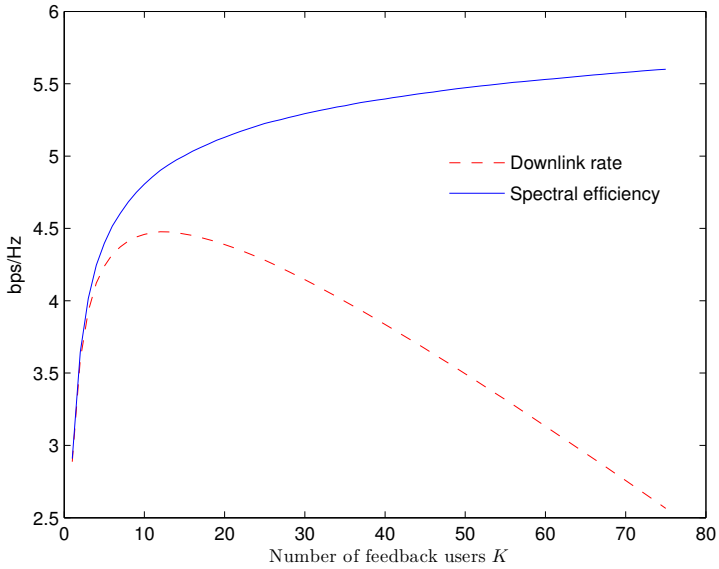

Figure 4.7: Spectral efficiency and downlink rate plotted against the number of feedback users at 10 dB in the TDD system.

by solving the optimization problem

$$K_{op}^{df} = \arg\max_{K} \left(1 - \frac{K}{T \log_2 (1+P)}\right) \mathbb{E}\left[\log_2 (1 + P\gamma_{df})\right] \tag{4.23}$$

It is very difficult to quantify K_{op}^{df} in closed form. In an effort to get an expression for K_{op}^{df}, an approximation to the downlink rate based on (4.2) is used, $R_D(K) \approx \tilde{R}_D(K) = \left(1 - \frac{K}{T \log_2(1+P)}\right) \log_2 (1 + P \log K)$. The optimization problem for the approximation is

$$K_{ap}^{df} = \arg\max_{K} \left(1 - \frac{K}{T \log_2 (1+P)}\right) \log_2 (1 + P \log K) \tag{4.24}$$

The objective function is concave and the following theorem quantifies the scaling of K_{ap}^{df} w.r.t T.

Theorem 6. *In a TDD single antenna broadcast channel using dedicated feedback, the number of feedback users K_{ap}^{df} which maximize the approximate downlink rate*

as in (4.24) scales with the blocklength T as

$$K_{ap}^{df} = O\left(\frac{T}{\log T \cdot \log\log T}\right) \tag{4.25}$$

Proof: See Appendix 4.6.5, where the following expression for K_{ap}^{df} is derived. Defining

$$\begin{aligned} T_1 &= T\log_2(1+P), \;\; K_1 = \frac{T_1}{\mathcal{W}\left[e^{\frac{1}{P}}T_1\right]}, \\ T_2 &= \frac{T_1 - K_1}{\log(1+P\log K_1)}, \;\; \text{then } K_{ap}^{df} \approx \frac{T_2}{\mathcal{W}\left[e^{\frac{1}{P}}T_2\right]} \end{aligned} \tag{4.26}$$

■

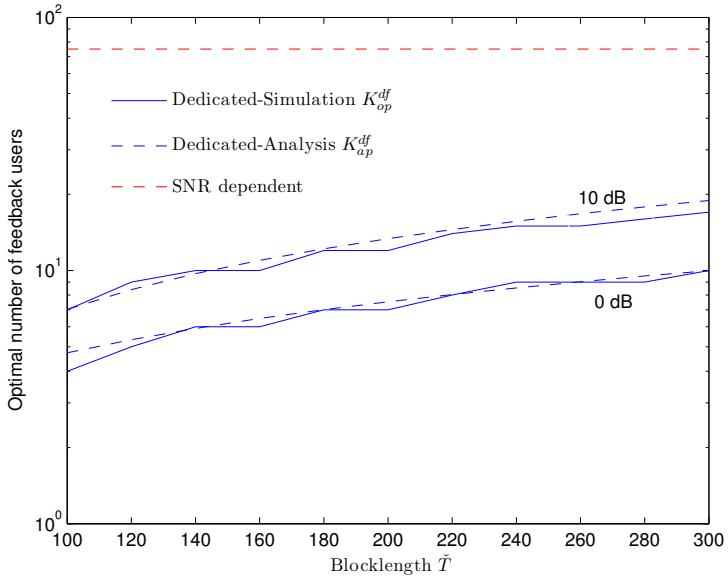

Figure 4.8: Optimal number of feedback users against the blocklength in the TDD system for the two SNR feedback methods .

In Fig.4.8, K_{op}^{df} in (4.23) and K_{ap}^{df} in (4.26) are plotted against the blocklength at 10 and 0 dB. The simulation setup is the same as in the FDD section. As in the FDD system, the scaling of both K_{op}^{df} and K_{ap}^{df} w.r.t T is very similiar. It

is seen that in a TDD 75 user single antenna broadcast channel using dedicated feedback, it is strictly advisable to collect SNR only from a few users around 4-18 users. For example, $K_{op}^{df} = 4$ for $\check{T} = 100$ and 0 dB, $K_{op}^{df} = 18$ for $\check{T} = 300$ and 10 dB. In the TDD system, the feedback bandwidth affects the downlink rate unlike the FDD system, where the feedback bandwidth only affects the uplink rate and hence the scaling of K_{ap}^{df} in the TDD system in (4.25) is more conservative than that of the FDD system in 4.2.1.

Scaling of K_{ap}^{df} w.r.t P

It can be seen that $K_{ap}^{df} = O(1)$ after some high SNR analysis in (4.26) [3] . K_{ap}^{df} in (4.26) is plotted against P in Fig.4.5 and $O(1)$ scaling is observed. The intuition behind the scaling is the same as in the FDD section.

4.3.2 SNR dependent feedback

The SNR dependent feedback process in the TDD system is the same as described in the subsection 4.2.2 for the FDD system except that it consumes the common bandwidth. The downlink rate in the TDD system when using SNR dependent feedback is given by

$$R_D(K) = \left[1 - \left(\frac{L_{fb} + \log_2 K}{\log_2(1+P)}\right)\frac{M}{\check{T}}\right] \cdot P\left(X \geq 1\right)\ \mathbb{E}[\log_2(1 + P\gamma_{sdf})] \tag{4.27}$$

In the TDD system, similiar to the FDD system, both K and M are the two parameters which determine the cost-benefit tradeoff of multiuser diversity. Similar to the appendix 4.6.2, it can be shown that the weighted sum rate and the downlink rate scale w.r.t both K and M in the same way. Optimal choices of K and M are found by optimizing the downlink rate.

$$\langle K, M\rangle_{op}^{sdf} = \arg\max_{K,M} R_D(K) \tag{4.28}$$

[3] Mathematical details are omitted due to space limitations.

In Fig.4.8, K_{op}^{sdf} in (4.28) is plotted against the blocklength at 10 and 0 dB. The optimization is solved numerically by exhaustive search. Similiar to the FDD system, all the 75 users in the system can participate in the feedback process. The interpretation of the scaling of K_{op}^{sdf} is the same as in the FDD system.

Similiar to the FDD system, in the TDD system the cost-benefit tradeoff of multiuser diversity for dedicated feedback is completely different from that for SNR dependent feedback and is summarized in Fig.4.9, which shows a plot of the downlink rates of both dedicated feedback from (4.23) and SNR dependent feedback from (4.27).

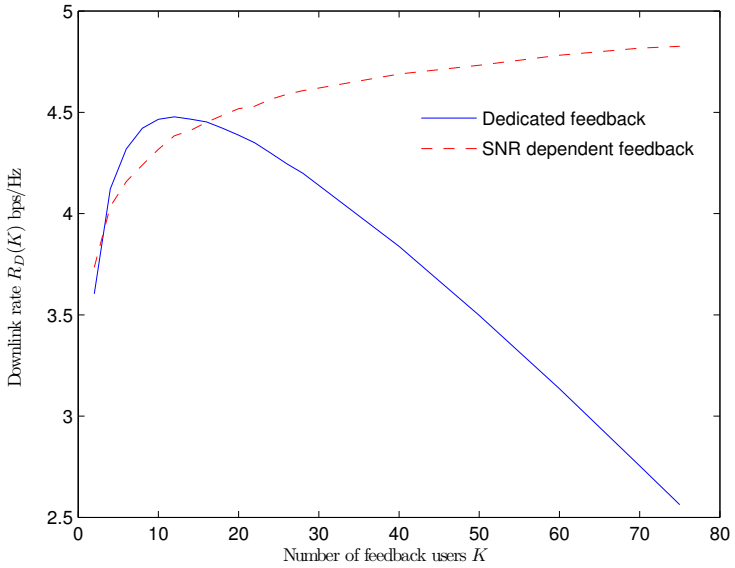

Figure 4.9: Downlink rates of both the feedback methods against the number of feedback users in the TDD system .

4.4 Single user multiantenna techniques and multiuser diversity

Multiuser diversity makes use of SNR variation among users. The previous two sections quantify the optimal number of feedback users in single antenna broadcast channels using dedicated feedback. But when single user multiantenna techniques are employed at BS and/or users, the SNR or mutual information variation tends to cease with the spatial dimension [72, 73], which suggests that the optimal number of feedback users in dedicated feedback should decrease with the spatial dimension. This effect of single user multiantenna techniques on multiuser diversity order in a broadcast channel using dedicated feedback is studied in the next two subsections, specifically for MIMO spatial multiplexing and SIMO. We consider only the TDD system studied in the previous section since the intuition should extend to the FDD system.

4.4.1 MIMO

In this subsection, we study a broadcast channel where the BS uses single user MIMO spatial multiplexing, more specifically V-BLAST, as the signalling technique. The BS has N transmitter antennas and each user has N receiver antennas. The spectral efficiency of i^{th} user is

$$C_i = \log_2 \left| \mathbf{I} + \frac{P}{N} \mathbf{H}_i \mathbf{H}_i^{\dagger} \right| \tag{4.29}$$

where $\mathbf{H}_i = [h_{i-kj}]_{k,j=1}^{N}$ is the i^{th} user $N \times N$ MIMO channel. Each user feedsback its instantaneous mutual information (MI) to the BS using $\frac{L_{fb}}{\log_2(1+P)}$ symbols on the uplink. With multiple antennas at the users, the uplink control channel can use transmit diversity techniques 2×1, 4×1 SFBC or FSTD[24]. Hence we assume a single antenna AWGN uplink control channel to keep the analysis simple without changing the essence of the problem. The BS selects the user with the largest MI

for downlink transmission. The downlink rate is

$$R_D(K) = W_{D-data}(K) \cdot C_D(K) = \left(1 - \frac{KL_{fb}}{\breve{T}\log_2(1+P)}\right) \mathbb{E}\left[\max_{1\le i\le K} \log_2\left|\mathbf{I} + \frac{P}{N}\mathbf{H}_i\mathbf{H}_i^\dagger\right|\right] \tag{4.30}$$

Similiar to the section 4.3, we assume that there is no uplink data. Even if the uplink data is present, the weighted sum of the uplink and downlink rates can be shown to scale w.r.t N and K in the same way as the downlink rate in (4.30). See appendix 4.6.6 for details.

The optimal number of feedback users is $K_{op}^{df} = \arg\max_K R_D(K)$. It is difficult to quantify K_{op}^{df} in closed form and hence in order to get an approximate expression for K_{op}^{df}, the following Gaussian approximation to the mutual information (4.29) is used [74].

$$\log_2\left|\mathbf{I} + \frac{P}{N}\mathbf{H}_i\mathbf{H}_i^\dagger\right| \sim \mathcal{N}(\mu, \sigma^2),$$
$$\mu = N\log_2\left(\frac{P}{e}\right),\ \sigma^2 = (\log_2 e)^2\left[\log N + 1.58\right] \tag{4.31}$$

Using a standard result about order statistics of Gaussian distribution from [75], the downlink rate in (4.30) is approximated as

$$R_D(K) \approx \tilde{R}_D(K) = \left(1 - \frac{K}{T\log_2(1+P)}\right)\left[\mu + \sigma\sqrt{2\log K}\right] \tag{4.32}$$

The downlink rate approximation in (4.32) is concave and thus, the approximation to the optimal number of feedback users, $K_{ap}^{df} = \arg\max_K \tilde{R}_D(K)$, is easily given below. Defining

$$K_1 = \frac{T\log_2(1+P)}{2\mathcal{W}\left[\frac{T\log_2(1+P)}{2}\right]},\ \log D = 0.5\left[1 + \frac{\mu}{\sigma}\sqrt{2\log K_1}\right],$$
$$\text{then } K_{ap}^{df} \approx \frac{T\log_2(1+P)}{2\mathcal{W}\left[\frac{D\ T\log_2(1+P)}{2}\right]} \tag{4.33}$$

See appendix 4.6.7 for derivation. It is easily seen from (4.33) that $K_{ap}^{df} = O\left(\frac{\sqrt{\log N}}{N}\right)$. Fig.4.10 shows a plot of both K_{op}^{df}, as defined above, and K_{ap}^{df} in (4.33) against N. It is seen that both K_{op}^{df} and K_{ap}^{df} decrease with N.

Fig.4.10 includes a plot for MI dependent feedback. Although not explicitly discussed, the theory of MI dependent feedback is the same as SNR dependent feedback. Similiar to the results in the SNR dependent feedback, all the users in the system can participate in the feedback process in the MI dependent feedback, although the number of slots M in the random access channel should decrease with the spatial dimension.

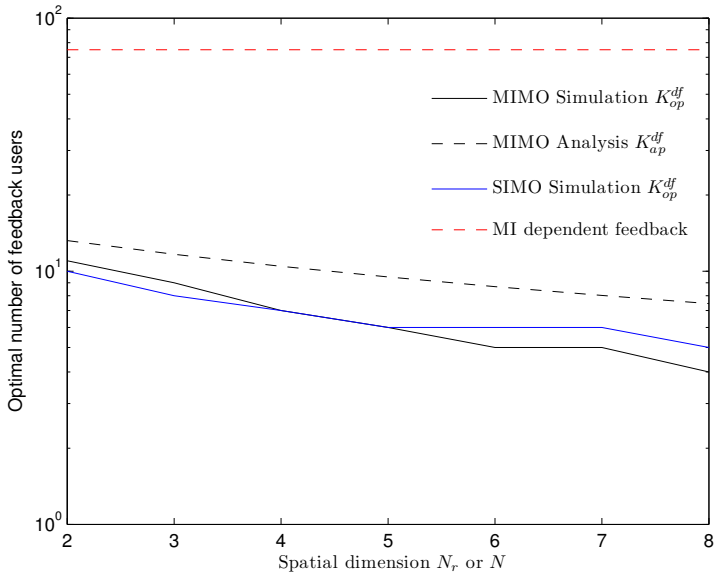

Figure 4.10: Optimal number of feedback users against the spatial dimension in a broadcast channel using single user multiantenna techniques and dedicated feedback.

4.4.2 SIMO

In this subsection, we study a broadcast channel where the users have multiple receiver antennas. Each user has N_r receiver antennas. The i^{th} user downlink channel is $\vec{\mathbf{h}}_i = [h_{i1}, h_{i2}, \cdots, h_{iN_r}]$ and the downlink SNR is $\gamma_i = \sum_{j=1}^{N_r} |h_{ij}|^2$. The downlink spectral efficiency is given by $C_{D-df}(K) = \mathbb{E}[\log_2(1+P\gamma_{df})]$, where $\gamma_{df} = \max_{1 \le i \le K} \gamma_i$. The downlink rate is $R_D(K) = \left(1 - \frac{KL_{fb}}{\tilde{T}\log_2(1+P)}\right) \mathbb{E}[\log_2(1+P\gamma_{df})]$.

The users can use $N_r \times 1$ transmit diversity SFBC or FSTD on the uplink data channel. Hence we assume the uplink data channel to be AWGN and ignore the uplink data to keep the analysis simple without changing the main part of the problem. The optimal number of feedback users is $K_{op}^{df} = \arg\max_K \ R_D(K)$. In Fig.4.10, shows a plot of K_{op}^{df} against N_r. Similiar to the MIMO case, K_{op}^{df} decreases with N_r.

The key finding of this section is that a broadcast channel using single user multiantenna techniques and dedicated feedback should decrease the multiuser diversity order with the spatial dimension, which agrees with the findings in [71].

4.5 Summary

The cost-benefit analysis of multiuser diversity in single antenna broadcast channels using both dedicated and SNR dependent feedback methods was worked out. A single antenna broadcast channel using dedicated feedback due to the significant feedback cost has to very carefully select the number of feedback users. A single antenna broadcast channel using SNR dependent feedback due to the relatively much smaller feedback cost can have all the users in the system participate in the feedback process i.e., all of the available multiuser diversity can be used. The effect of single user multiantenna techniques on the multiuser diversity order in a broadcast channel using dedicated feedback was studied. A broadcast channel using single user multiantenna techniques and dedicated feedback should decrease the multiuser diversity order with the spatial dimension, since the single user multiantenna techniques decrease the SNR or MI variation with the spatial dimension.

4.6 Mathematical Proofs

4.6.1 Proof of Proposition 1

Jensen's upper bound for $C_{D-df}(K)$ is $\mathbb{E}\left[\log_2\left(1+P\gamma_{df}\right)\right] \leq \log_2\left(1+P\mathbb{E}[\gamma_{df}]\right)$. From [75], it is known that $\mathbb{E}[\gamma_{df}] = \sum_{i=1}^{K}\frac{1}{i}$. From [57], $\sum_{i=1}^{K}\frac{1}{i} \approx 0.58 + \log K$. Thus, $C_{D-df}(K)$ is upper bounded as $C_{D-df}(K) \leq \log_2\left(1+P\left(0.58+\log K\right)\right)$. Applying Markov Inequality (For a non-negative RV X, $\mathbb{E}[X] \geq P(X \geq \delta)\delta$, for any $\delta > 0$) to $C_{D-df}(K)$, we get

$$\mathbb{E}\left[\log_2\left(1+P\gamma_{df}\right)\right] \geq \log_2\left(1+P\delta\right)P\left(\gamma_{df} \geq \delta\right). \tag{4.34}$$

Picking $P\left(\gamma_{df} \geq \delta\right) = 1-\frac{1}{(\log K)^s},\ s>0$, a corresponding value of δ can be choosen

$$\begin{aligned} P\left(\gamma_{df} \geq \delta\right) &= 1 - \frac{1}{(\log K)^s} = 1 - \left(1-e^{-\delta}\right)^K \\ \Rightarrow\ \delta &= \log K - \log\left(s\log\log K\right) \end{aligned} \tag{4.35}$$

Letting $s=1$, we get a lower bound for $C_{D-df}(K)$

$$\begin{aligned} C_{D-df}(K) &\geq \left(1-\frac{1}{\log K}\right)\log_2\left(1+P\left(\log K - \log\log\log K\right)\right) \\ &= \log_2\left(1+P\left(\log K - \log\log\log K\right)\right) + o(1) \end{aligned} \tag{4.36}$$

Thus $C_{D-df}(K)$ is bounded as

$$\begin{aligned} &\log_2\left(1+P\left(\log K - \log\log\log K\right)\right) + o(1) \leq C_{D-df}(K) \leq \\ &\log_2\left(1+P\left(0.58+\log K\right)\right) \end{aligned} \tag{4.37}$$

4.6.2 Weighted sum rate in the TDD system rewritten in the same form as (4.11)

The weighted sum of the uplink and downlink rates is

$$\begin{aligned}
&\lambda_R R_D\left(K\right) + R_U\left(K\right) \\
&= \left(1 - \frac{\check{W}_{U-fb}(K)}{\check{T}}\right)\Big[\lambda_R(1-\alpha)\ \mathbb{E}\left[\log_2\left(1+P\gamma_{sch}\right)\right] + \\
&\quad \alpha \log_2\left(1+P\right)\Big] \\
&= \lambda_R(1-\alpha)\left(1 - \frac{\check{W}_{U-fb}(K)}{\check{T}}\right)\Big[\mathbb{E}\left[\log_2\left(1+P\gamma_{sch}\right)\right] + \\
&\quad \frac{\alpha}{\lambda_R(1-\alpha)} \log_2\left(1+P\right)\Big] \qquad (4.38)
\end{aligned}$$

Define $\log_2 D = \frac{\alpha}{\lambda_R(1-\alpha)} \log_2\left(1+P\right)$, then (4.38) can be rewritten as

$$\begin{aligned}
&\frac{\lambda_R R_D\left(K\right) + R_U\left(K\right)}{\lambda_R(1-\alpha)} = \\
&\left(1 - \frac{\check{W}_{U-fb}(K)}{\check{T}}\right)\mathbb{E}\big[\log_2 D\left(1+P\gamma_{sch}\right)\big] \qquad (4.39)
\end{aligned}$$

The scaling of the weighted sum rate in (4.39) and the downlink rate in (4.11) w.r.t K is the same.

4.6.3 Proof of Theorem 1

The objective function in (4.15) is concave. K_{ap}^{df} is easily found by setting the derivative to zero.

$$\frac{\lambda_R P}{K\left(1+P\log K\right)} - \frac{1}{T} = 0 \ \Rightarrow\ K\left(\frac{1}{P} + \log K\right) = \lambda_R T \qquad (4.40)$$

Let $B = e^{\frac{1}{P}}$, (4.40) can be rewritten as

$$\begin{aligned}
&K \log BK = \lambda_R T \Rightarrow K_{ap}^{df} = \frac{\lambda_R T}{\mathcal{W}\left[e^{\frac{1}{P}}\lambda_R T\right]} \\
&K_{ap}^{df} \approx \frac{\lambda_R T}{\frac{1}{P} + \log \lambda_R T - \log\left(\frac{1}{P} + \log \lambda_R T\right)} \qquad (4.41)
\end{aligned}$$

(4.41) is obtained using $\mathcal{W}(x) = \log x - \log\log x + o(1)$ from [76].

4.6.4 Proof of $P(X \geq 1)$ in (4.20)

X represents the number of captured SNR's. Let L represent the number of SNR's above the threshold. It is easily seen that $L \sim \text{Binomial}(K, p)$, where $p = \frac{M}{K}$ since $\gamma_{th} = \log\left(\frac{K}{M}\right)$. An expression for $P(X \geq 1)$ is derived below.

$$\begin{aligned} P(X \geq 1) &= 1 - P(X = 0) \\ P(X = 0) &= \sum_{l=1}^{K} P(X = 0|L = l)\, P(L = l) \\ &= \sum_{l=1}^{K} P(X = 0|L = l) \binom{K}{l} p^l (1-p)^{K-l} \\ &= \sum_{l=1}^{K} P(X = 0|L = l) \binom{K}{l} \frac{M^l}{K^K} (K - M)^{K-l} \end{aligned} \tag{4.42}$$

$P(X = 0|L = l)$ represents the probability that each of the M slots is accessed by multiple feedback users (> 1).

$$\begin{aligned} P(X = 0|L = l) = \Bigg[& M + \sum_{i=2}^{\lfloor \frac{l}{2} \rfloor} M(M-1)\cdots(M-(i-1)) \\ & !l \sum_{j=1}^{|S_i|} \Phi\left(S_i^j\right) \prod_{k=1}^{i} \frac{1}{!S_i^j(k)} \Bigg] \frac{1}{l^M} \end{aligned} \tag{4.43}$$

where

S_i: Set of all i-tuples s.t all elements of a tuple add upto M,

S_i^j: j^{th} $i-$tuple in S_i,

$S_i^j(k)$: k^{th} element of S_i^j and $\sum_{k=1}^{i} S_i^j(k) = M$,

$\Phi\left(S_i^j\right) = \frac{1}{!m_1!m_2\cdots!m_i}$ where $m_j \in [1, i], 1 \leq j \leq i$ represents the number of repetitions of an element in the i-tuple.

The distribution of X can be written down completely, but is omitted here due to space limitations. The distribution of γ_{sdf} in (4.20) is difficult to write out.

4.6.5 Proof of Theorem 2

The objective function in (4.24) is concave. Define $T_1 = T\log_2(1+P)$ and $\log B = \frac{1}{P}$, then

$$\tilde{R}'_D(K) = \frac{\frac{1}{K} - \frac{1}{T_1}}{\frac{1}{P} + \log K} - \frac{\log(1+P\log K)}{T_1} = 0$$
$$\frac{T_1}{K} - 1 = \log(1+P\log K)\cdot\log BK$$
$$K\log BK\cdot\log(1+P\log K) + K = T_1 \tag{4.44}$$

It is difficult to solve (4.44) in closed form and hence, a step by step heuristic solution is developed. Dropping the linear term and the $\log\log(\ )$ factor in (4.44), a I^{st} order solution to K_{ap}^{df}, say K_1, is given below

$$K\log BK = T_1 \Rightarrow K_1 = \frac{T_1}{\mathcal{W}[BT_1]} \tag{4.45}$$

Using K_1 back in (4.44), a 2^{nd} order solution is obtained.

$$K\log BK = \frac{T_1 - K_1}{\log(1+P\log K_1)} = T_2 \tag{4.46}$$
$$\Rightarrow K_{ap}^{df} \approx \frac{T_2}{\mathcal{W}[BT_2]} = O\left(\frac{T_2}{\log T_2}\right) = O\left(\frac{T}{\log T\cdot\log\log T}\right) \tag{4.47}$$

In (4.47) we have used $T_2 = O\left(\frac{T}{\log\log T}\right)$ from (4.46).

4.6.6 Scaling of the weighted sum rate and the downlink rate in the section 4.4.1

Using the expression in (4.38), the weighted sum rate for the broadcast channel in the section 4.4.1, excluding the pre-log factor and assuming the uplink data

channel uses MIMO spatial multiplexing, is

$$\mathbb{E}\left[\max_{1\leq i\leq K}\log_2\left|\mathbf{I}+\frac{P}{N}\mathbf{H}_i\mathbf{H}_i^{\dagger}\right|\right]+\frac{\alpha}{\lambda_R(1-\alpha)}\cdot$$
$$\mathbb{E}\left[\log_2\left|\mathbf{I}+\frac{P}{N}\mathbf{H}\mathbf{H}^{\dagger}\right|\right]$$
$$=\mathbb{E}\left[\max_{1\leq i\leq K}\sum_{j=1}^{N}\log_2\left(1+P\lambda_{i,j}\right)\right]+N\cdot\frac{\alpha}{\lambda_R(1-\alpha)}\cdot$$
$$\mathbb{E}\left[\log_2\left(1+P\lambda\right)\right] \tag{4.48}$$

where $\mathbf{H}=[h_{kj}]_{k,j=1}^{N}$ is the $N\times N$ MIMO uplink data channel and $\lambda_{i,j}$ is the j^{th} eigenvalue of the Wishart matrix $\frac{1}{N}\mathbf{H}_i\mathbf{H}_i^{H}$. The first term is $O(N)$ since the $\sum$ term is $O(N)$ [74], both the max() and $\mathbb{E}()$ operations preserve the linearity. The second term is also $O(N)$. Hence the weighted sum rate and downlink rate in the section 4.4.1 scale w.r.t N and K in the same way.

4.6.7 Proof of (4.33)

The approximation in (4.32) is concave. K_{ap}^{df} is easily found by setting the derivative to zero.

$$\tilde{R}_D'(K)=\left(1-\frac{K}{T\log_2(1+P)}\right)\frac{\sigma}{K\sqrt{2\log K}}-$$
$$\frac{\left[\mu+\sigma\sqrt{2\log K}\right]}{T\log_2(1+P)}=0\ \Rightarrow$$
$$K\left[1+\frac{\mu\sqrt{2\log K}}{\sigma}+2\log K\right]=T\log_2(1+P) \tag{4.49}$$

Similiar to appendix 4.6.5, it is difficult to solve (4.49) in closed form and hence, a step by step heuristic solution is developed. Dropping the linear term and the $\sqrt{\log(\ )}$ term in (4.49), I^{st} order solution to (4.49), say K_1, is given by

$$K\log K=\frac{T\log_2(1+P)}{2}\ \Rightarrow K_1=\frac{T\log_2(1+P)}{2\mathcal{W}\left[\frac{T\log_2(1+P)}{2}\right]} \tag{4.50}$$

Using (4.50) back in (4.49) and defining $\log D = 0.5\left[1 + \frac{\mu\sqrt{2\log K_1}}{\sigma}\right]$, a 2^{nd} order solution is given below.

$$K\left[1 + \frac{\mu\sqrt{2\log K_1}}{\sigma} + 2\log K\right] = T\log_2(1+P)$$
$$K\log DK = \frac{T\log_2(1+P)}{2} \;\Rightarrow K_{ap}^{df} \approx \frac{T\log_2(1+P)}{2\mathcal{W}\left[\frac{DT\log_2(1+P)}{2}\right]} \tag{4.51}$$

Chapter 5

Conclusion

In this thesis, we present a performance analysis of two cross layer protocols, one is the joint error correction and retransmission protocol namely HARQ and the second is multiuser diversity opportunistic scheduling in random wireless networks.

A study of the performance of continuous version of HARQ i.e., rateless codes in a single hop WANET was presented. It was shown that rateless codes can achieve near ERD performance with substantially shorter delays. An immediate consequence of this result is that even for delay constrained traffic such as voice and video, attaining near ERD performance is feasible. The instantaneous rate in a WANET employing rateless codes is random and its distribution is essential for studying the queue sizes and network congestion. The dynamic variations of the packet transmission time in a WANET employing rateless codes was characterized by deriving an accurate upper bound to the CCDF of the packet transmission time.

The block level IR-HARQ protocol was incorporated into a cooperative multihop WANET. The information is transported from source to destination via intermediate relays. The codeword of an information packet is split into punctured blocks and sequentially transmitted from source and relay(s) to the destination. A convex approximation to the transport capacity was derived using the concept of decoding cells. Based on the convex approximation, the coding rate and medium access probability of the IR-HARQ protocol were optimized to operate

the WANET at maximal transport capacity.

The concept of multiuser diversity opportunistic scheduling as applied to downlink transmission in cellular networks was studied. While it is widely known that multiuser diversity provides significant benefits in terms of increase in spectral efficiency with the number of users, very little emphasis is placed on the cost associated with the multiuser diversity. The focus of the thesis is to present the cost of multiuser diversity in terms of the feedback resources for acquiring user CQI at the base station. The cost benefit tradeoff of multiuser diversity is quantified. Multiuser diversity order which balances the tradeoff between cost and benefit is characterized. The effect of increase in spatial dimension of multiple antenna transmission techniques on the multiuser diversity order was studied.

It would be interesting to study the achievability of ERD using rateless codes in MIMO WANETs since multiple antenna techniques provide degrees of freedom to cancel interference and achieve robustness against poor fading states[77, 78, 79]. The effect of increase in spatial dimension on the dynamic variations of the packet transmission time is worth investigating.

An interesting future work would be to optimize the rate density as a function of delay constraint D and transmit density λ. Optimal choice of D balances the tradeoff between the rate and outage probability. Optimal λ balances the tradeoff between transmit density and rate. A possible direction of work would involve obtaining analysis results for channel thresholding. Analytical bounds on the CCDF of packet transmission time would help in optimizing the rate density as function of channel threshold β without relying on exhaustive monte carlo simulations.

In the performance evaluation of rateless codes in chapter 2, we focus on slow fading scenario. It would be worth pursuing the effect of fast fading on the achievability of ERD using rateless codes. Since the fading diversity is easier to achieve in a fast fading scenario, its effect on the ERD achievability is worth pursuing.

The thesis studies the performance of rateless codes in a single hop WANET.

In a multihop WANET, information is transported from source to destination and the time delay in doing so must be accounted for in the capacity or throughput analysis. Rateless codes have a good fit for relay networks [13]. It would be interesting to incorporate rateless codes into a multihop WANET and quantify the throughput, optimize it w.r.t delay and outage, and study its behavior.

The concept of multiuser diversity will be integrated with HARQ in a wireless system. The interaction between HARQ and multiuser diversity, for example, the effect of the number of retransmission rounds on the order of multiuser diversity subject to average delay constraints of traffic is a potential topic to be pursued. Since rateless codes provide robustness against no or incomplete CSIT transmission, it would be worth investigating the effect of using rateless codes on the demanding requirements of the CQI acquisition channel inherent in multiuser diversity.

Bibliography

[1] R. Comroe and D. Costello Jr. Arq schemes for data transmission in mobile radio systems. *IEEE Jour. Sel. Areas Commun.*, 2(4):472 481, 1984.

[2] D. Mandelbaum. An adaptive-feedback coding scheme using incremental redundancy. *Information Theory, IEEE Transactions on*, 20(3):388 –389, 1974.

[3] H. Holma and A. Toskala. *Hsdpa/Hsupa for UMTS*. Wiley Online Library, 2006.

[4] F. Wang, A. Ghosh, C. Sankaran, P. Fleming, F. Hsieh, , and S. Benes. Mobile wimax systems: performance and evolution. *IEEE Communications Magazine*, 46(10):41 –49, 2008.

[5] J. G. Andrews, A. Ghosh, and R. Muhamed. *Fundamentals of Wimax: Understanding Broadband Wireless Networking*. Prentice Hall PTR, 2007.

[6] S. Sesia, I. Toufik, , and M. Baker. *LTE-the UMTS Long Term Evolution: From Theory to Practice*. Wiley, 2 ed edition, 2011.

[7] M. Luby. Lt codes. In *43rd Annual IEEE Symp. on the Found. of Comp. Sci.*, pages 271 – 280, 2002.

[8] A. Shokrollahi. Raptor codes. In *Proc IEEE Int. Symp. on Inform. Theory*, page 36, 2004.

[9] R. Palanki and J.S. Yedidia. Rateless codes on noisy channels. In *Proc IEEE Int. Symp. on Inform. Theory*, page 37, 2004.

[10] O Etesami, M Molkaraie, and A. Shokrollahi. Raptor codes on symmetric channels. In *Proc IEEE Int. Symp. on Inform. Theory*, page 38, 2004.

[11] J. Castura and Yongyi Mao. Rateless coding over fading channels. *IEEE Communications Letters*, 10(1):46–48, 2006.

[12] N. Bonello, Yuli Yang, S. Aissa, and L. Hanzo. Myths and realities of rateless coding. *IEEE Communications Magazine*, 49(8):143–151, 2011.

[13] J. Castura and Yongyi Mao. Rateless coding and relay networks. *IEEE Signal Processing Magazine*, pages 27 –35, September 2007.

[14] U. Erez, M.D. Trott, and Gregory W. Wornell. Rateless coding for gaussian channels. *Information Theory, IEEE Transactions on*, 58(2):530–547, Feb 2012.

[15] Bin Zhao and M.C. Valenti. Practical relay networks: a generalization of hybrid- arq. *Selected Areas in Communications, IEEE Journal on*, 23(1):7 – 18, Jan. 2005.

[16] F. Baccelli, B. Blaszczyszyn, and P. Muhlethaler. An aloha protocol for multihop mobile wireless networks. *Information Theory, IEEE Transactions on*, 52(2):421 – 436, Feb. 2006.

[17] P.A. Anghel and M. Kaveh. On the performance of selection cooperation arq. In *Communications, 2009. IEEE International Conference on*, pages 1 –6, June 2009.

[18] S. Weber, J.G. Andrews, and N. Jindal. An overview of the transmission capacity of wireless networks. *Communications, IEEE Transactions on*, 58(12):3593 –3604, December 2010.

[19] J. Blomer and N. Jindal. Opportunistic routing in ad hoc networks: How many relays should there be? what rate should nodes use? In *Proc. of IEEE Global Commun. Conf.*, pages 1–5, Dec 2010.

[20] J.G. Andrews, R.K. Ganti, M. Haenggi, N. Jindal, and S. Weber. A primer on spatial modeling and analysis in wireless networks. *Communications Magazine, IEEE*, 48(11):156 –163, November 2010.

[21] R. Knopp and P. Humblet. Information capacity and power control in single user cell multiuser communications. In *Proc. Int. Conf. Commun*, volume 1, pages 331–335, Seatle,WA, June 1995.

[22] P. Vishwanath, D. N. C. Tse, and R. Laroia. Opportunistic Beamforming using dumb antennas. *IEEE Trans. Inf. Theory*, 48(6):1277–1294, June 2002.

[23] J. So and J. M. Cioffi. Feedback reduction scheme for downlink multiuser diversity. *IEEE Trans. Wireless. Commun.*, 8(2):668–672, Feb 2009.

[24] Matthew Baker. Lte advanced physical layer. In *REV-090003r1 IMT-Advanced Evaluation Workshop*, Bejing, Dec 17-18 2009.

[25] D. Gesbert and M. S. Alouini. How much feedback is multi-user diversity really worth? In *Proc. Int. Conf. Commun*, pages 234–238, Paris,France, June 2004.

[26] T. Tang and R. W. Heath. Opportunistic feedback for downlink multiuser diversity. *IEEE Commun. Lett.*, 9(10):948–950, Oct 2005.

[27] Seung Young Park, Daeyoung Park, and D. J. Love. On scheduling for multiple-antenna wireless networks using contention-based feedback. *Communications, IEEE Transactions on*, 55(6):1174–1190, 2007.

[28] J. Chen, R.Berry, and M.Honig. Limited feedback schemes for downlink ofdma based on sub-channel groups. *IEEE Journal on Selected Areas in Communications*, 26(8):1451–1461, Oct 2008.

[29] M. Dohler, R. W. Heath Jr, A. Lozano, C. Papadias, and R. A. Valenzuela. Is the phy layer dead? *IEEE Communications Magazine*, 49(4):159–165, April 2011.

[30] Y. George, I. Bergel, and E. Zehavi. The ergodic rate density of aloha wireless ad-hoc networks. *IEEE Transactions on Wireless Communications*, 12(12):6340–6351, Dec. 2013.

[31] Y. George, I. Bergel, and E. Zehavi. Upper bound on the ergodic rate density of aloha wireless ad-hoc networks. *submitted IEEE Transactions on Wireless Communications*, pages 1–26, Apr. 2014.

[32] G. Caire and D. Tuninetti. The throughput of hybrid- arq protocols for the gaussian collision channel. *Information Theory, IEEE Transactions on*, 47(5):1971 –1988, Jul 2001.

[33] R. Wolff. *Stochastic Modelling and the Theory of Queues*. Prentice Hall, 1989.

[34] K. Stamatiou, J.G. Proakis, and J.R. Zeidler. Channel diversity in random wireless networks. *Wireless Communications, IEEE Transactions on*, 9(7):2280–2289, 2010.

[35] Haichuan Ding, Shaodan Ma, Chengwen Xing, and Zesong Fei. Performance analysis of incremental redundancy hybrid arq in mobile ad hoc networks. In *Communications (ICC), 2014 IEEE International Conference on*, pages 5759–5764, June 2014.

[36] W.C Ao and K.C. Chen. Error Control for Local Broadcasting in Heterogeneous Wireless Ad Hoc Networks. *Communications, IEEE Transactions on*, 61(4), Apr 2013.

[37] P.H.J. Nardelli, M. Kaynia, P. Cardieri, and M. Latva-aho. Optimal Transmission Capacity of Ad Hoc Networks with Packet Retransmissions. *Wireless Communications, IEEE Transactions on*, 11(8):2760–2766, August 2012.

[38] A. Rajanna and M. Kaveh. Analysis of cooperative harq with opportunistic routing. In *Proc. of 2013 IEEE 14th Workshop on Signal Processing Advances in Wireless Communications (SPAWC)*, pages 71–75, June 2013.

[39] Y. Li, M.C. Gursoy, and S. Velipasalar. On the throughput of hybrid-arq under statistical queuing constraints. *Vehicular Technology, IEEE Transactions on*, PP(99):1–1, 2014.

[40] R.K. Ganti and M. Haenggi. Spatial analysis of opportunistic downlink relaying in a two-hop cellular system. *Communications, IEEE Transactions on*, 60(5):1443–1450, May 2012.

[41] N. Ravindran, Peng Wu, J. Blomer, and N. Jindal. Optimized multi-antenna communication in ad-hoc networks with opportunistic routing. In *Signals, Systems and Computers (ASILOMAR), 2010 Conference Record of the Forty Fourth Asilomar Conference on*, pages 1593 –1597, Nov. 2010.

[42] N. Jindal, J. Andrews, and S. Weber. Bandwidth partitioning in decentralized wireless networks. *Wireless Communications, IEEE Transactions on*, 7(12):5408 –5419, December 2008.

[43] J. Blomer and N. Jindal. Transmission capacity of wireless ad hoc networks: Successive interference cancellation vs. joint detection. In *Communications, 2009. ICC '09. IEEE International Conference on*, pages 1 –5, June 2009.

[44] N. Jindal, J.G. Andrews, and S. Weber. Multi-antenna communication in ad hoc networks: Achieving mimo gains with simo transmission. *Communications, IEEE Transactions on*, 59(2):529 –540, February 2011.

[45] R. Vaze and R.W. Heath. Transmission capacity of ad-hoc networks with multiple antennas using transmit stream adaptation and interference cancellation. *Information Theory, IEEE Transactions on*, 58(2):780 –792, Feb. 2012.

[46] R. H. Y. Louie, M. R. McKay, N. Jindal, and I. B. Collings. Spatial multiplexing with mmse receivers: Single-stream optimality in ad hoc networks. In *Proc. of IEEE Global Commun. Conf.*, Dec 2010.

[47] J.G. Andrews, S. Weber, M. Kountouris, and M. Haenggi. Random access transport capacity. *Wireless Communications, IEEE Transactions on*, 9(6):2101 –2111, June 2010.

[48] R. Vaze. Throughput-delay-reliability tradeoff with arq in wireless ad hoc networks. *Wireless Communications, IEEE Transactions on*, 10(7):2142 – 2149, July 2011.

[49] Y. Ko, S.A. Vorobyov, and M. Ardakani. How much multiuser diversity is required for energy limited multiuser systems? *IEEE Trans. Signal Processing*, 58(8):4367–4378, Aug 2010.

[50] J.G. Andrews, N. Jindal, M. Haenggi, R. Berry, S. Jafar, D. Guo, S. Shakkottai, R.W. Heath Jr., M. Neely, S.Weber, and A. Yener. Rethinking information theory for mobile ad hoc networks. *IEEE Communications Magazine*, pages 94 –101, December 2008.

[51] F. Baccelli, B. Blaszczyszyn, and P. Muhlethaler. Timespace opportunistic routing in wireless ad hoc networks: Algorithms and performance optimization by stochastic geometry. *The Computer Journal*, 53(5):592 – 609, 2010.

[52] S.C. Draper, B.J. Frey, and F.R. Kschischang. Efficient variable length channel coding for unknown dmcs. In *Proc IEEE Int. Symp. on Inform. Theory*, page 379, 2004.

[53] A. Rajanna, I.Bergel, and M. Kaveh. Analysis of Rateless Codes Performance in an ALOHA WANET. In *submitted 2015 IEEE ICC*, June 2015.

[54] A. Rajanna, I. Bergel, and M. Kaveh. Performance Analysis of Rateless Codes in an ALOHA WANET. *submitted IEEE Transactions on Wireless Communication*, Nov 2014.

[55] B. Blaszczyszyn and P. Muhlethaler. Stochastic analysis of non-slotted aloha wireless ad-hoc networks. In *Proc. of IEEE INFOCOM*, pages 1–9, 2010.

[56] A. Lapidoth. Nearest neighbor decoding for additive non-gaussian noise channels. *Information Theory, IEEE Transactions on*, 42(5):1520 – 1529, Sept 1996.

[57] I. S. Gradshteyn and I. M. Ryzhik. *Table of Integrals, Series and Products*. Academic Press, San Diego, CA, 6 edition, 2000.

[58] S. Weber and J.G Andrews. *Transmission capacity of wireless networks*. Now Publishing, 2011.

[59] R.K. Ganti. *A Stochastic Geometry Approach to the Interference and Outage Characterization of Large Wireless Networks*. PhD thesis, University of Notre Dame, 2009.

[60] Luis López-Oliveros and Sidney I Resnick. Extremal dependence analysis of network sessions. *Extremes*, 14(1):1–28, 2011.

[61] Y. George and I. Bergel. The spectral efficiency of slotted csma adhoc networks with directional antennas. *IEEE Transactions on Wireless Communication*, 11(10):3799 3809, 2012.

[62] J. Venkataraman, M. Haenggi, , and O. Collins. Shot noise models for outage and throughput analyses in wireless ad hoc networks. In *Proc IEEE Military Communication Conference (MILCOM)*, pages 1 – 7, 2006.

[63] A. Rajanna and M. Kaveh. Analysis of Cooperative HARQ with Poisson Interference and Opportunistic Routing. *submitted to IEEE Transactions on Wireless Communication*, Jul 2013.

[64] F. Baccelli and B. Blaszczyszyn. *Stochastic Geometry and Wireless Networks, Volume I: Theory*. Now Publishing, 2009.

[65] D. Stoyan, W. Kendall, and J. Mecke. *Stochastic Geometry and its Applications*. John Wiley and Sons, 2 edition, 1996.

[66] M. Haenggi. On distances in uniformly random networks. *Information Theory, IEEE Transactions on*, 51(10):3584 –3586, Oct. 2005.

[67] M. Haenggi. Outage, local throughput, and capacity of random wireless networks. *Wireless Communications, IEEE Transactions on*, 8(8):4350 – 4359, 2009.

[68] A. Rajanna and N. Jindal. Multiuser diversity in downlink channels: When does the feedback cost outweigh the spectral efficiency benefit? *Wireless Communications, IEEE Transactions on*, 11(1):408 –418, January 2012.

[69] David Tse and Pramod Vishwanath. *Fundamentals of wireless communication*. Cambridge University Press, 2005.

[70] C. J. Chen and L. C. Wang. A unified capacity analysis for wireless systems with joint multiuser scheduling and antenna diversity in Nakagami fading channels. *IEEE Trans. Commun.*, 54(3):469–478, March 2006.

[71] M. Kobayashi, N. Jindal, and G. Caire. Training and feedback optimization for multiuser mimo downlink. *IEEE Trans. Communications*, Dec 2009. submitted.

[72] E. G. Larsson. On the combination of spatial diversity and multiuser diversity. *Communications Letters, IEEE*, 8(8):517–519, Aug 2004.

[73] Q. Zhou and H. Dai. Asymptotic analysis on the interaction between spatial diversity and multiuser diversity in wireless networks. *IEEE Trans. Sig. Processing*, 55(8):4271–4283, August 2007.

[74] B. M. Hochwald, T. L. Marzetta, and V. Tarokh. Multiple-antenna channel hardening and its implications for rate feedback and scheduling. *IEEE Trans. Inf. Theory*, 50(9):1893–1909, Sept 2004.

[75] H. A. David and H. N. Nagaraja. *Order Statistics*. John Wiley and Sons, New York, 3 edition, 2003.

[76] R. M. Corless et al. On the Lambert W function. *Advances in Computational Mathematics*, 5(1):329–359, 1996.

[77] U. Erez, G. W. Wornell, and M. D. Trott. Rateless space-time coding. In *Proc IEEE Int. Symp. on Inform. Theory*, page 1937 1941, Sept 2005.

[78] M. Shanechi, U. Erez, G. W. Wornell, and K. P. Boyle. Time-invariant rateless codes for mimo channels. In *Proc IEEE Int. Symp. on Inform. Theory*, July 2008.

[79] M. Shanechi, U. Erez, and G. W. Wornell. Rateless coding for mimo channels. In *Proc. Int. Global Commun. Conf. (GLOBECOM)*, Nov 2008.

Appendix A

Glossary and Acronyms

Care has been taken in this thesis to minimize the use of jargon and acronyms, but this cannot always be achieved. This appendix defines jargon terms in a glossary, and contains a table of acronyms with their meaning.

A.1 Acronyms

Table A.1: Acronyms

Acronym	Meaning
CCDF	Complementary Cumulative Distribution Function
WANET	Wireless Adhoc Network
ERD	Ergodic Rate Density
ORD	Outage Rate Density
CQI	Channel Quality Information
SNR	Signal to Noise Ratio
TDD	Time Divison Duplexing
FDD	Frequency Divison Duplexing

Continued on next page

Table A.1 – continued from previous page

Acronym	Meaning
MIMO	Multiple Input Multiple Output
PPP	Poisson Point Process
DMC	Discrete Memoryless Channel
KKT	Karush Kahn Tucker
CSIT	Channel State Information at Transmitter
HARQ	Hybrid Automatic Repeat reQuest
SIMO	Single Input Multiple Output
SINR	Signal to Interference and Noise Ratio
MI	Mutual Information
STBC	Space Time Block Coding
MAC	Medium Access Control
BS	Base Station
CSI	Channel State Information
IR	Incremental Redundancy

A.2 Glossary

- **Multiuser Diversity** – A user scheduling protocol in which the user with best channel quality to the base station from among many is scheduled for transmission.

- **Transport Capacity** – The number of information bits in b/sec weighted by the distance over which it is communicated reliably per unit area of the network.

- **Ergodic Rate Density** – The maximum achievable area spectral efficiency in the network.

- **Area Spectral Efficiency** – The number of information bits in b/sec/Hz communicated reliably per unit area of the network.